Supplement to NASA Technical Paper 3132 - Suppl

April 1992

Comparison of a Two-Dimensional Adaptive-Wall Technique With Analytical Wall Interference Correction Techniques

Raymond E. Mineck

NASA

Supplement to NASA Technical Paper 3132

1992

Comparison of a Two-Dimensional Adaptive-Wall Technique With Analytical Wall Interference Correction Techniques

Raymond E. Mineck
Langley Research Center
Hampton, Virginia

NASA
National Aeronautics and Space Administration
Office of Management
Scientific and Technical Information Program

Introduction

A two-dimensional airfoil model has been tested in the adaptive-wall test section of the Langley 0.3-Meter Transonic Cryogenic Tunnel (0.3-m TCT) and in the ventilated test section of the Two-Dimensional High Reynolds Number Facility (HRNF) at the National Aeronautical Establishment (NAE) in Canada. The primary goal of the tests was to compare two different techniques to account for wall interference: adaptive test section walls and classical analytical corrections. Tests were conducted over a Mach number range from 0.3 to 0.8 at chord Reynolds numbers of 10×10^6, 15×10^6, and 20×10^6. The angle of attack was varied from about $-2°$ up to stall. This supplement presents comparisons of the published or baseline chordwise pressure distributions from the 0.3-m TCT and the HRNF.

Symbols

C_p	pressure coefficient
c	model chord, in.
c_n	section normal-force coefficient
M_∞	free-stream Mach number
R_c	free-stream Reynolds number based on model chord
x	chordwise position, measured aft from the leading edge, in.
y	spanwise position, measured from tunnel centerline, in.
z	normal position, measured from airfoil reference line, in.
α	geometric angle of attack, deg

Model

The model used in these tests has a 9-in. chord and a CAST 10-2/DOA 2 airfoil section. This early supercritical airfoil section is nominally 12 percent thick and has a design lift coefficient of about 0.6 at a Mach number of 0.765. A sketch of the airfoil shape is presented in the top of figure 1. The model chord is defined as the line passing through the center of the leading and trailing edges. This line is rotated 0.88° nose up relative to the reference line used to define the airfoil shape. For these tests, the angle of attack is referenced to the model chord line, not the airfoil reference line.

The model has 45 static pressure orifices in a chordwise row on the upper surface and 23 in a chordwise row on the lower surface. A sketch of the orifice layout is shown in figure 1. The orifices are staggered about the model centerline to minimize interference on the neighboring orifices. The orifice diameter is 0.014 in. for all orifices except those on the forward 22 percent of the airfoil, where the diameter is 0.010 in. The smaller diameter orifices will reduce any orifice size effects where the pressure gradients could be large.

Presentation of Results

The following chart lists the figures that present the comparisons of the results at the same nominal normal-force coefficient, Mach number, and Reynolds number:

	Figure number for R_c of		
M_∞	10×10^6	15×10^6	20×10^6
0.600			13
.700			14
.730	2	8	15
.750	3	9	16
.765	4	10	17
.780	5	11	18
.790	6		
.800	7	12	19

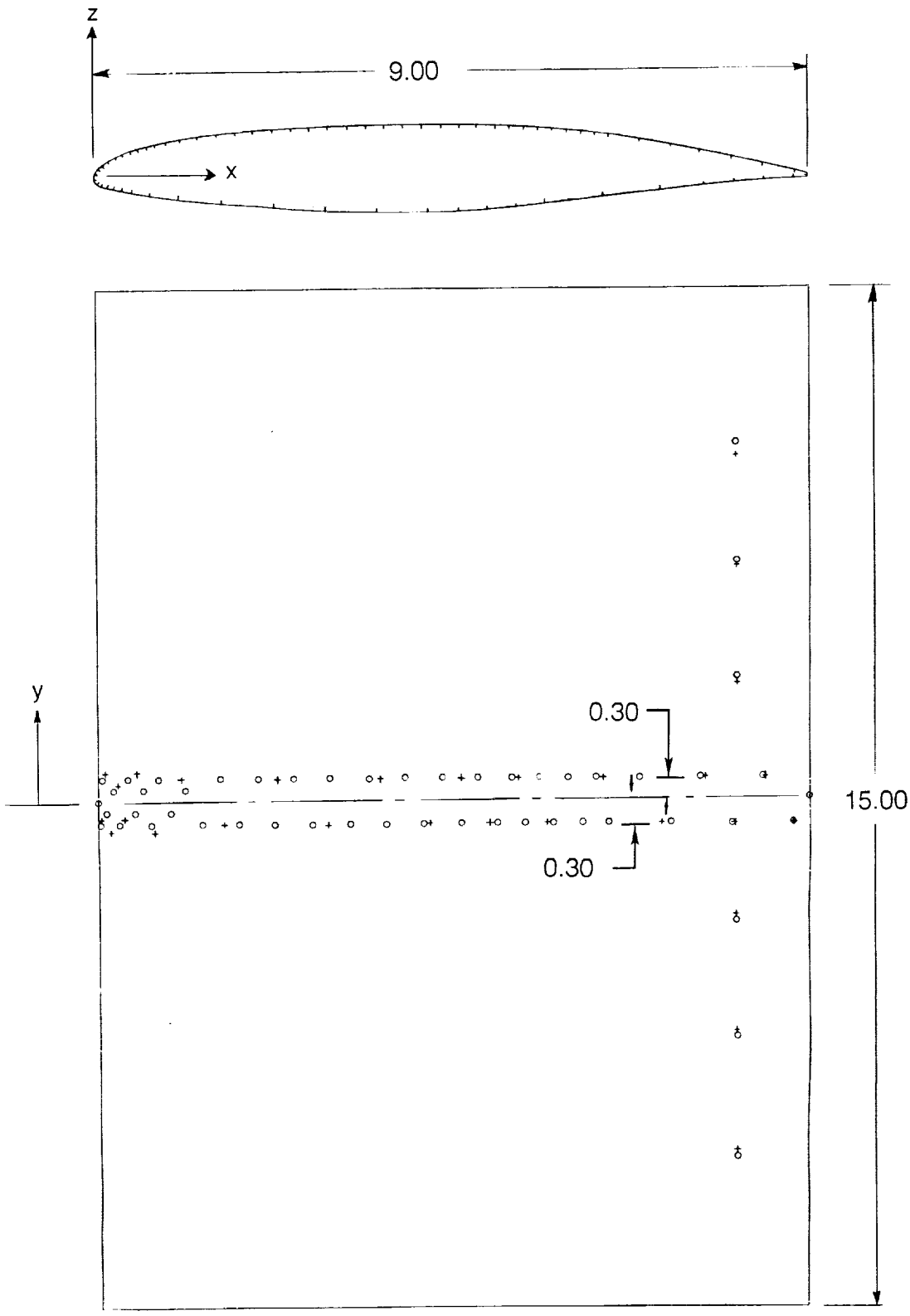

Figure 1. Layout of pressure orifice locations. All dimensions are in inches. Open symbols denote upper surface; "+" denotes lower surface.

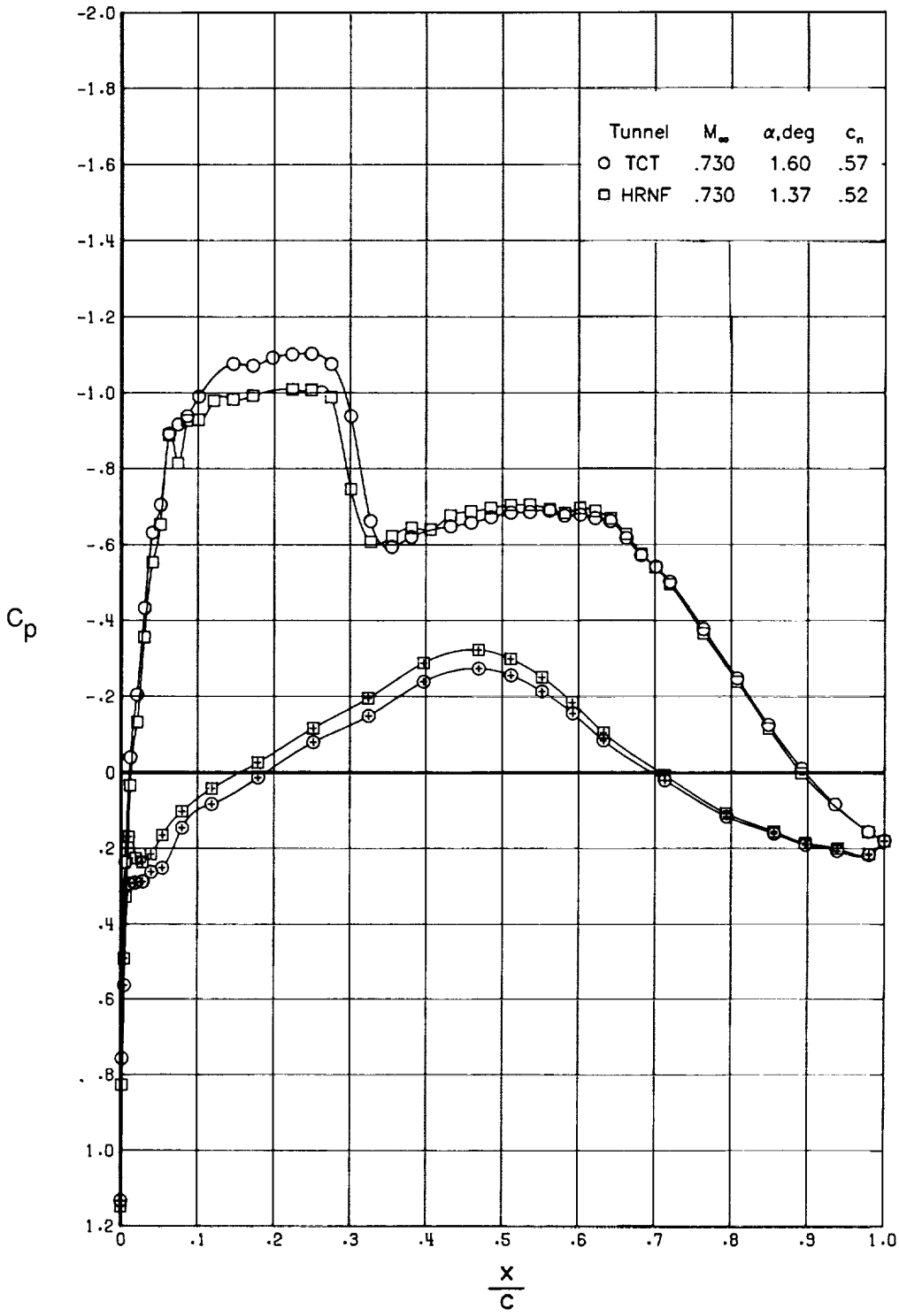

(a) $c_n \approx 0.54$.

Figure 2. Comparison of chordwise pressure distributions for $R_c = 10 \times 10^6$ and $M_\infty = 0.730$.

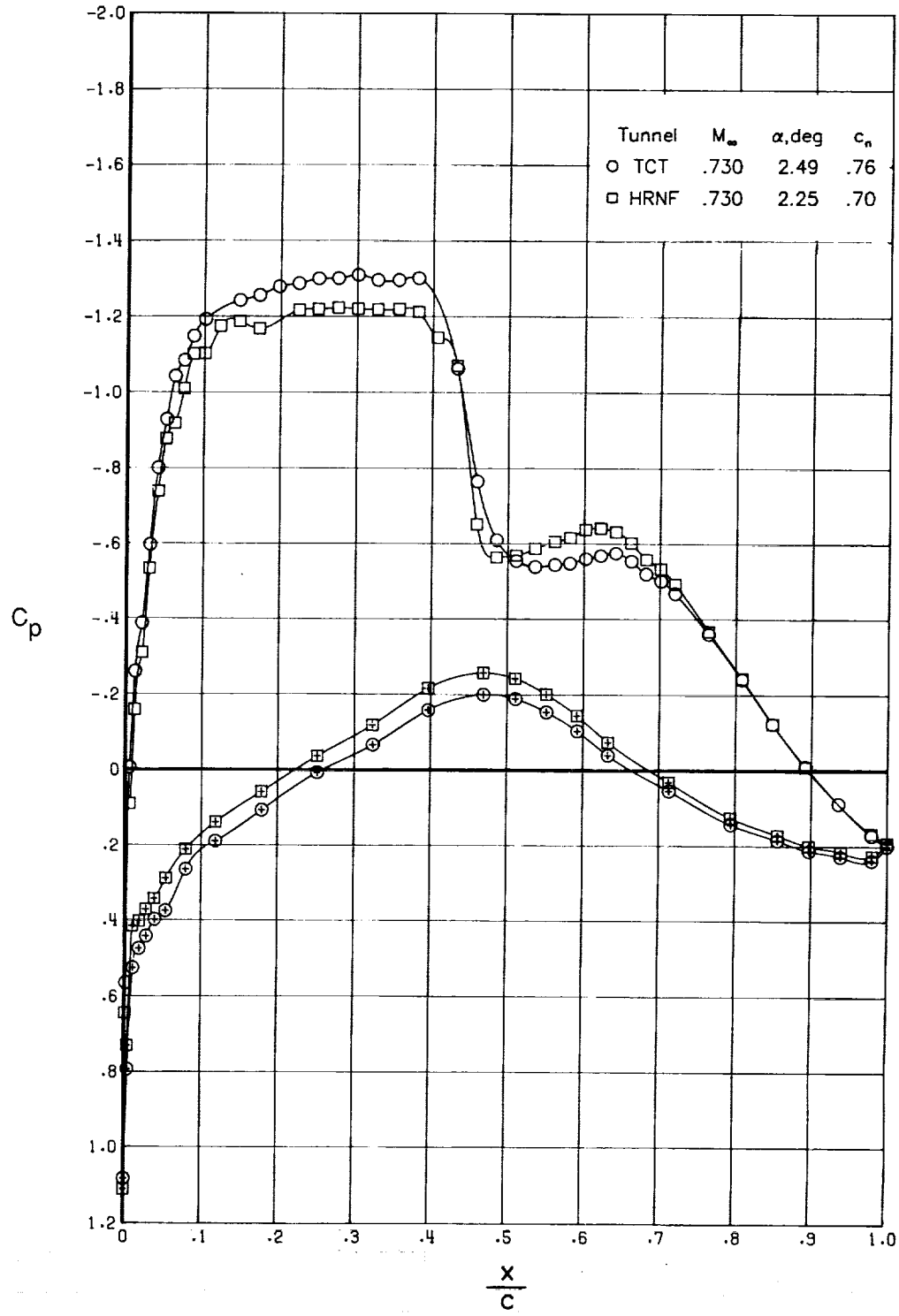

(b) $c_n \approx 0.73$.

Figure 2. Continued.

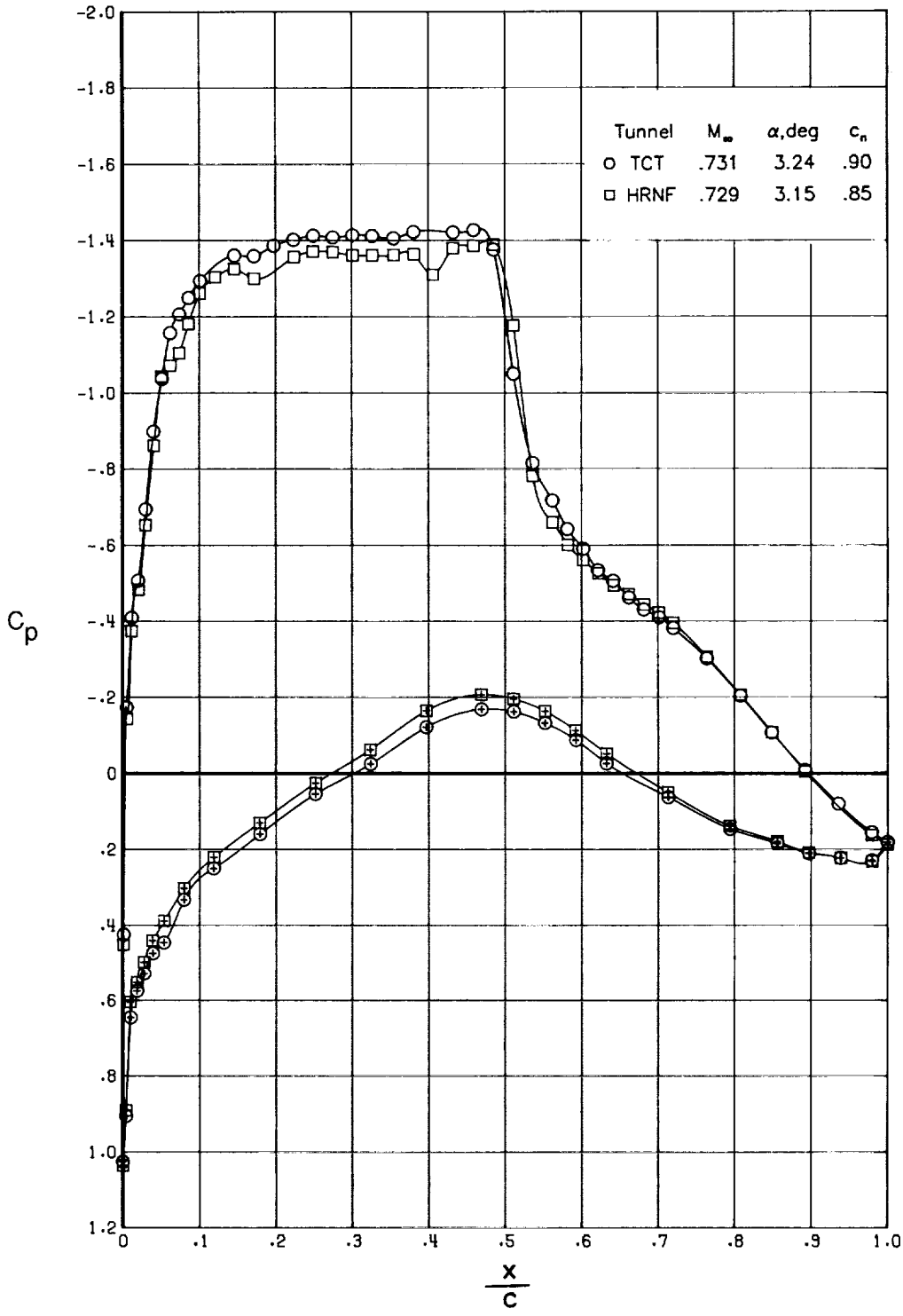

(c) $c_n \approx 0.87$.

Figure 2. Concluded.

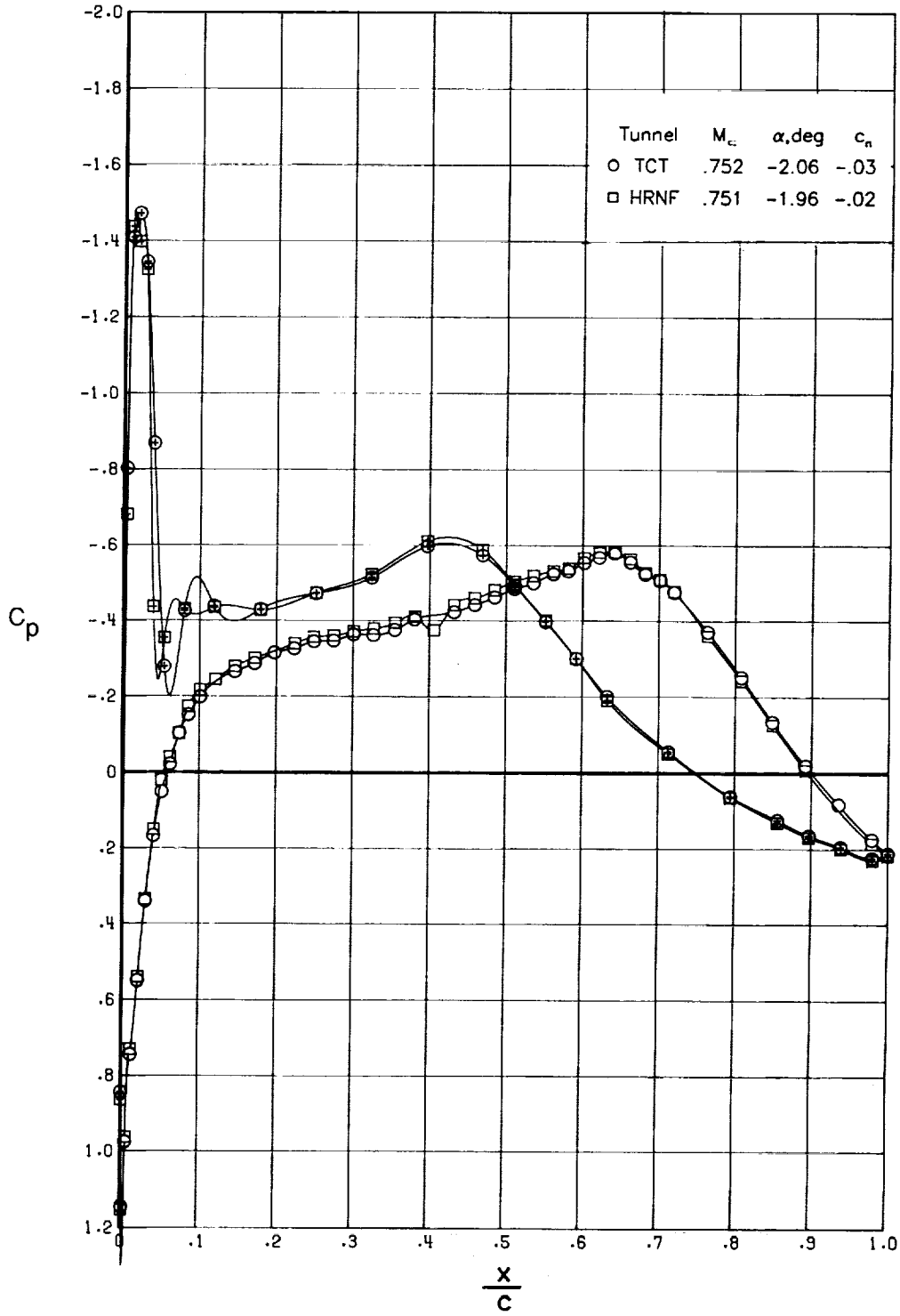

(a) $c_n \approx -0.02$.

Figure 3. Comparison of chordwise pressure distributions for $R_c = 10 \times 10^6$ and $M_\infty = 0.752$.

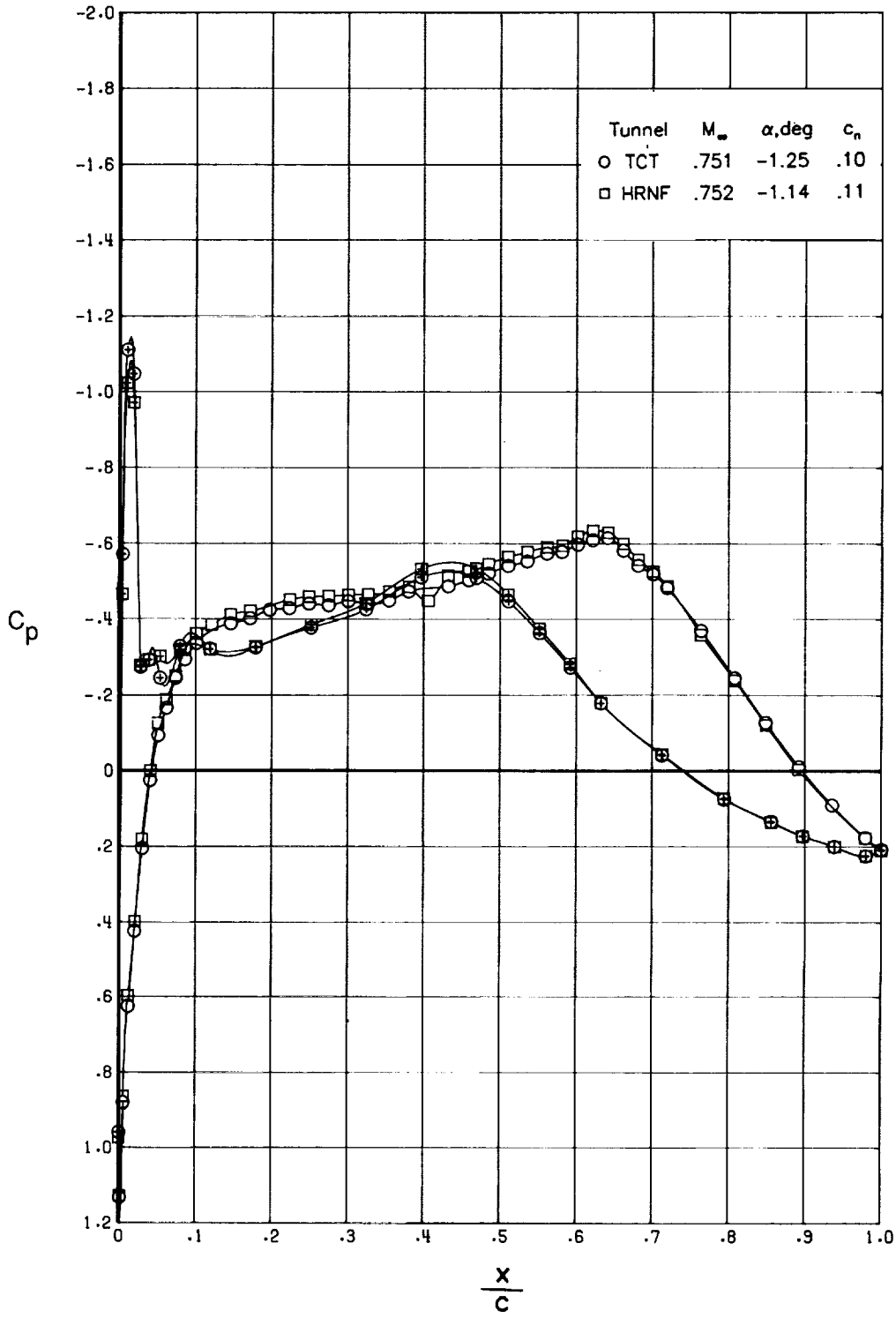

(b) $c_n \approx 0.10$.

Figure 3. Continued.

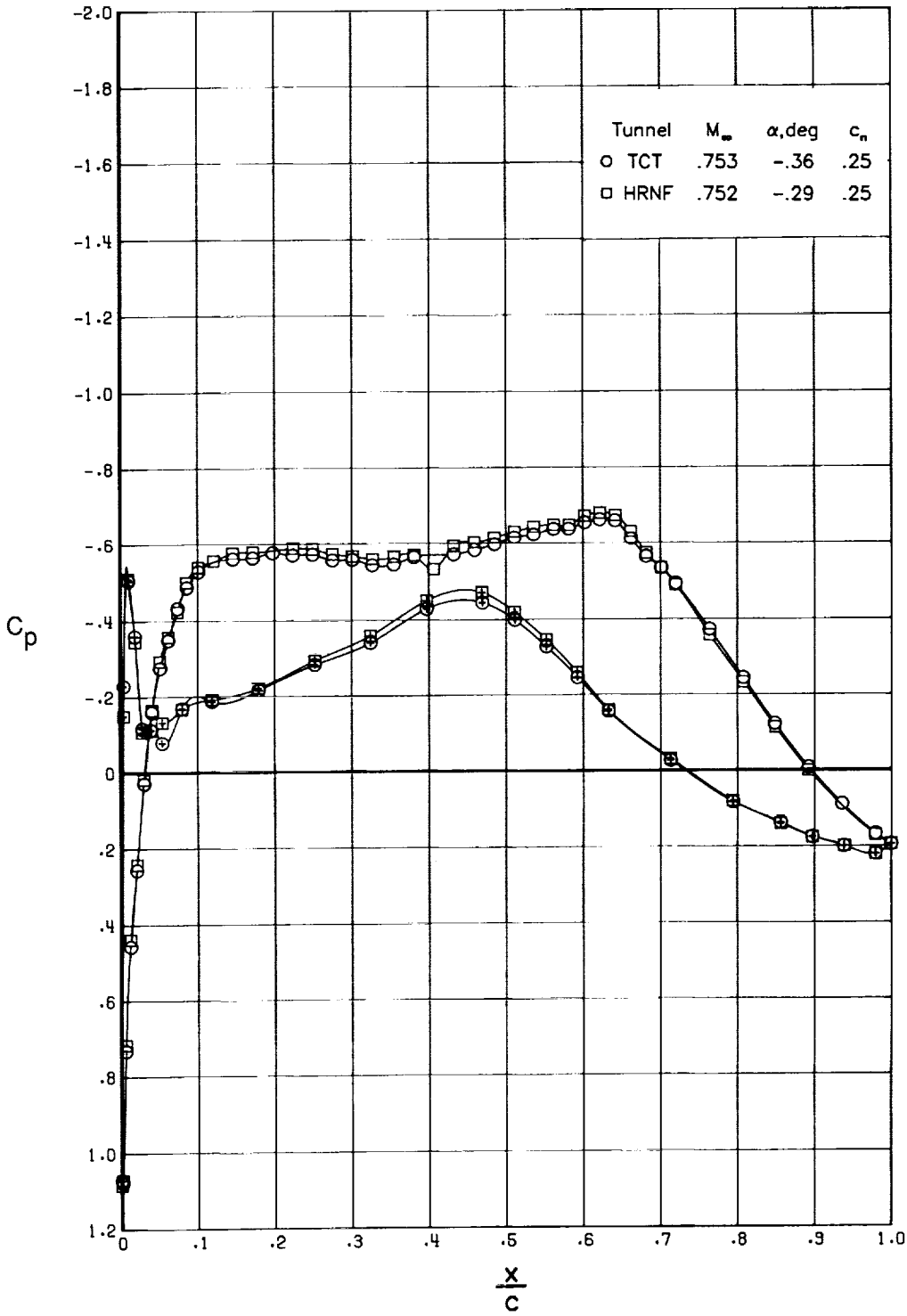

(c) $c_n \approx 0.25$.

Figure 3. Continued.

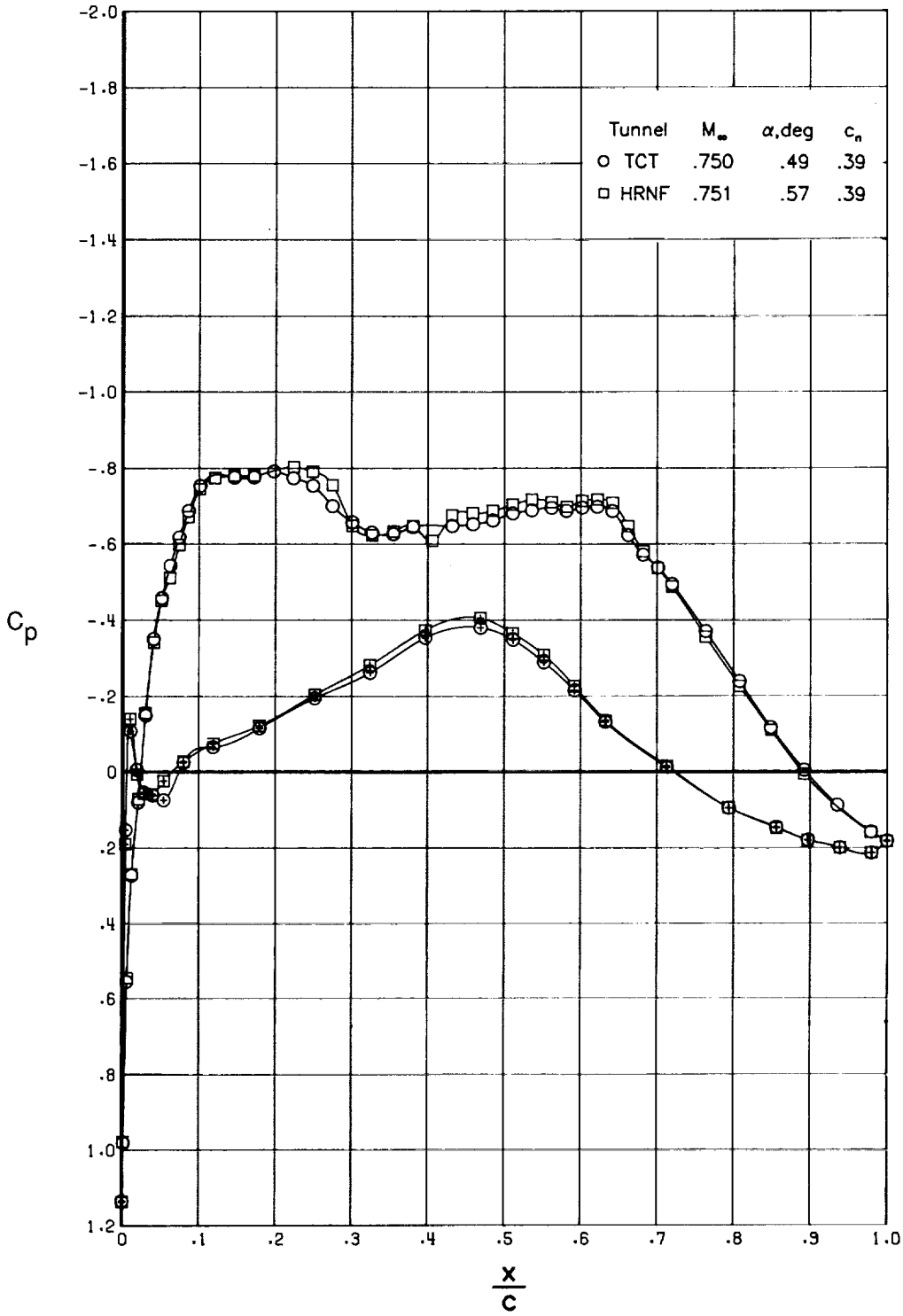

(d) $c_n \approx 0.39$.

Figure 3. Continued.

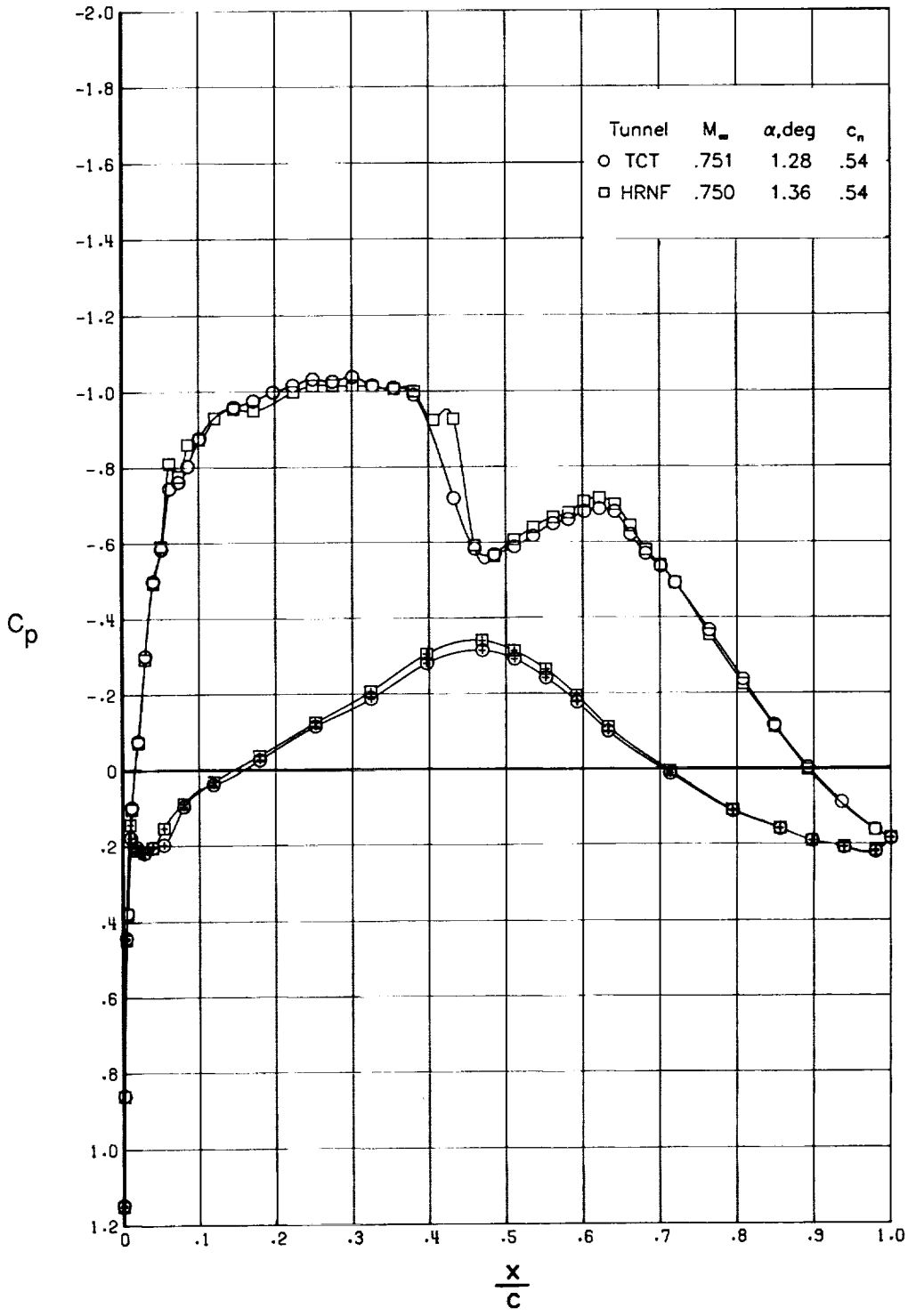

(c) $c_n \approx 0.54$.

Figure 3. Continued.

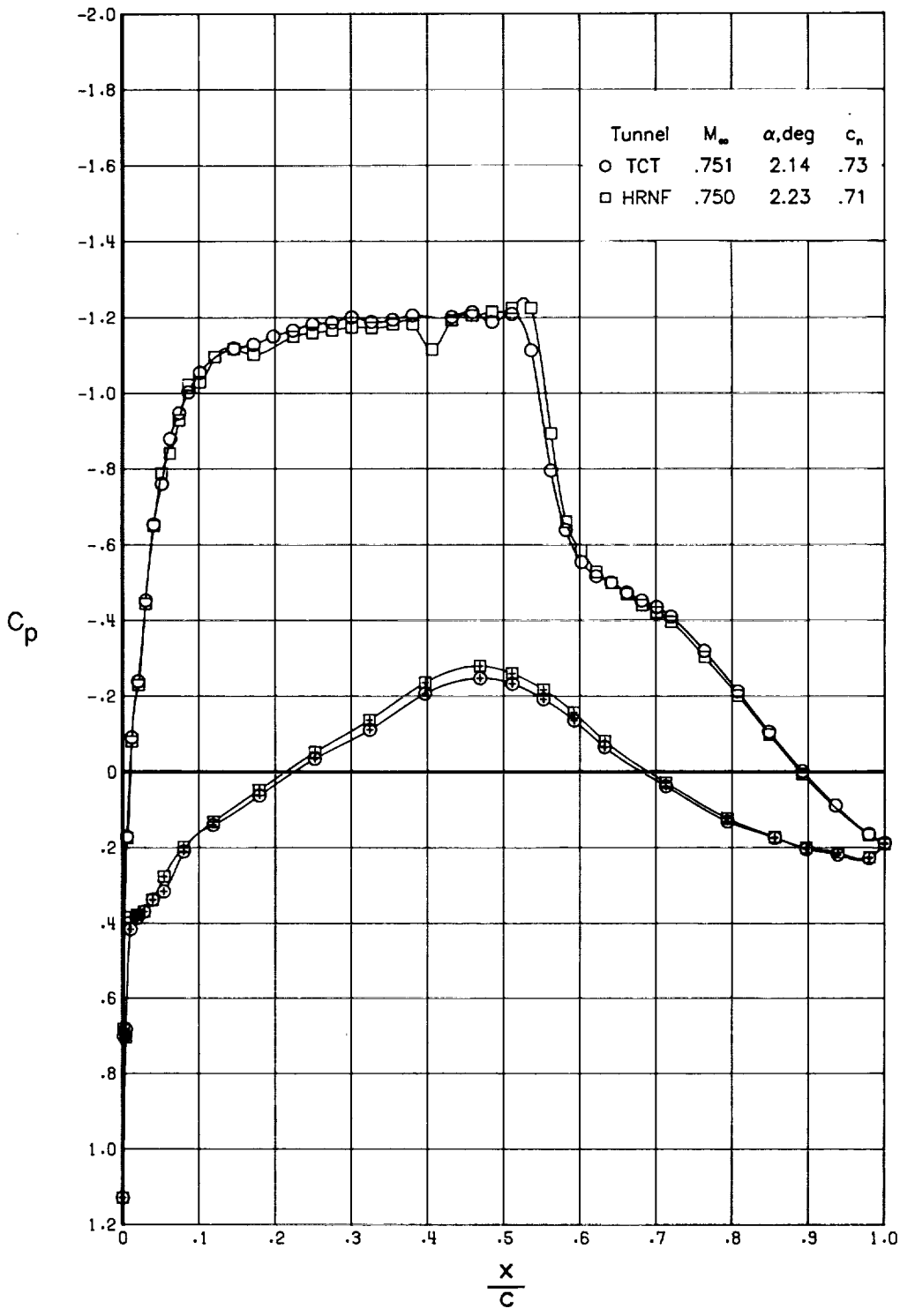

(f) $c_n \approx 0.72$.

Figure 3. Continued.

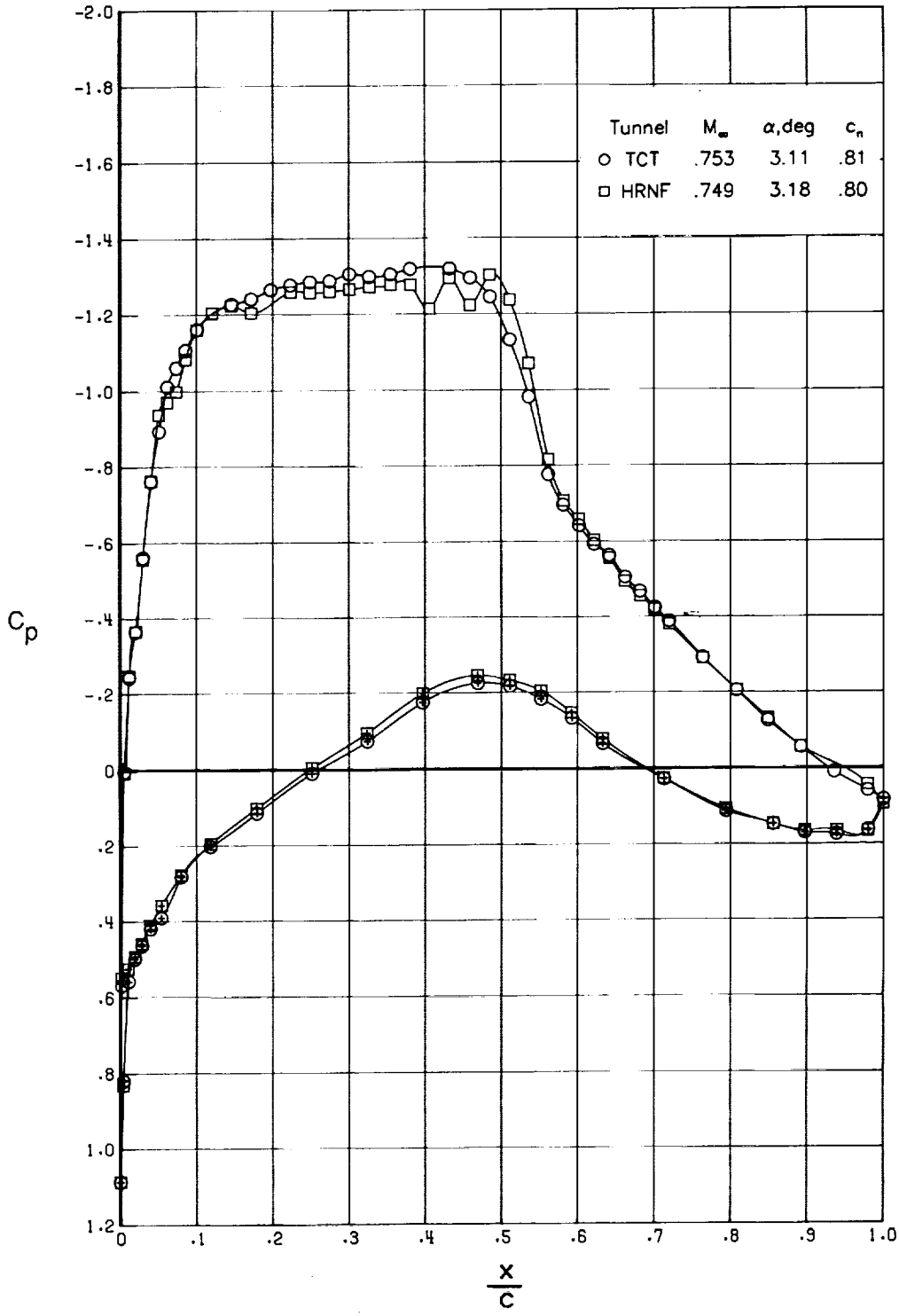

(g) $c_n \approx 0.80$.

Figure 3. Concluded.

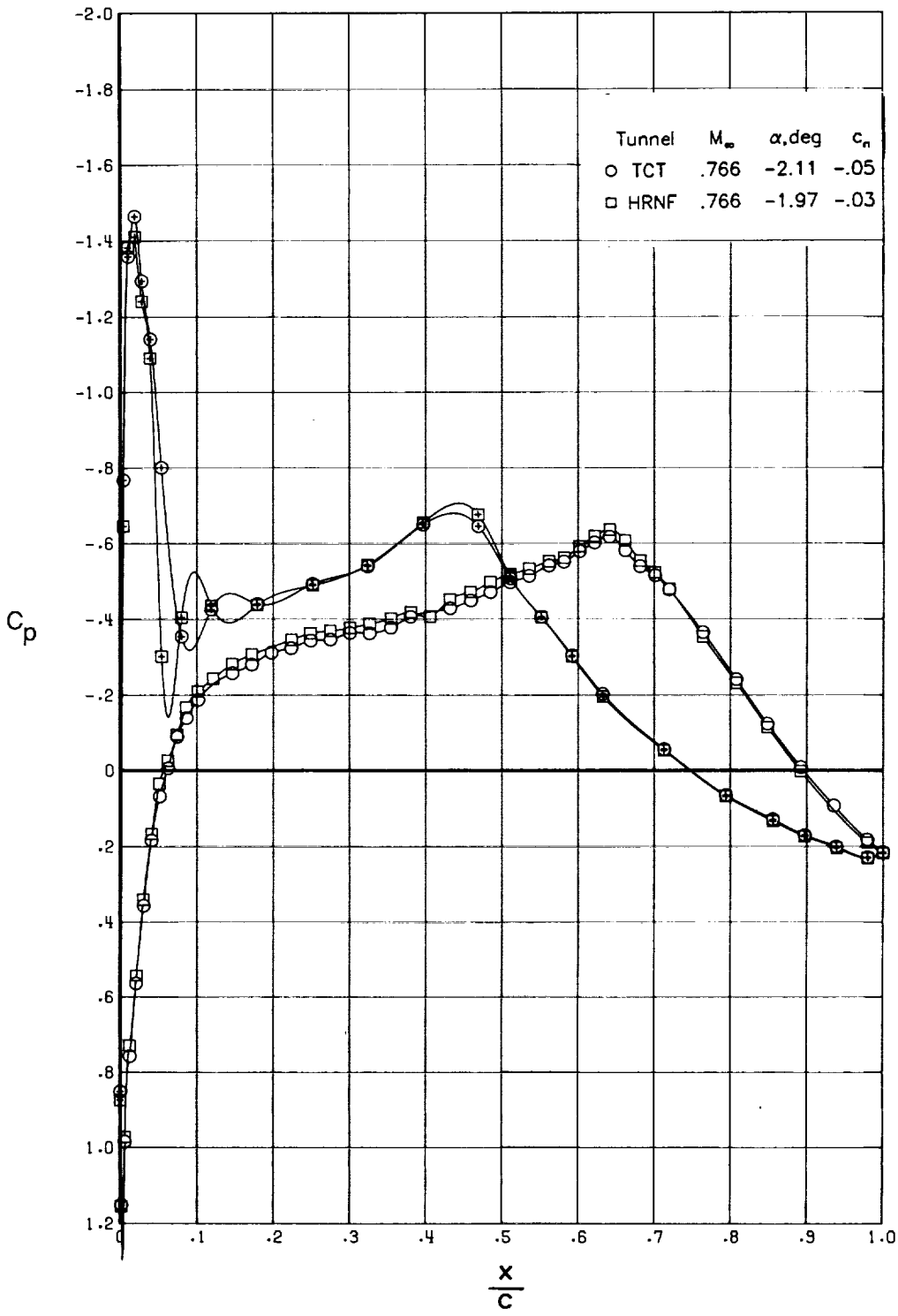

(a) $c_n \approx -0.04$.

Figure 4. Comparison of chordwise pressure distributions for $R_c = 10 \times 10^6$ and $M_\infty = 0.766$.

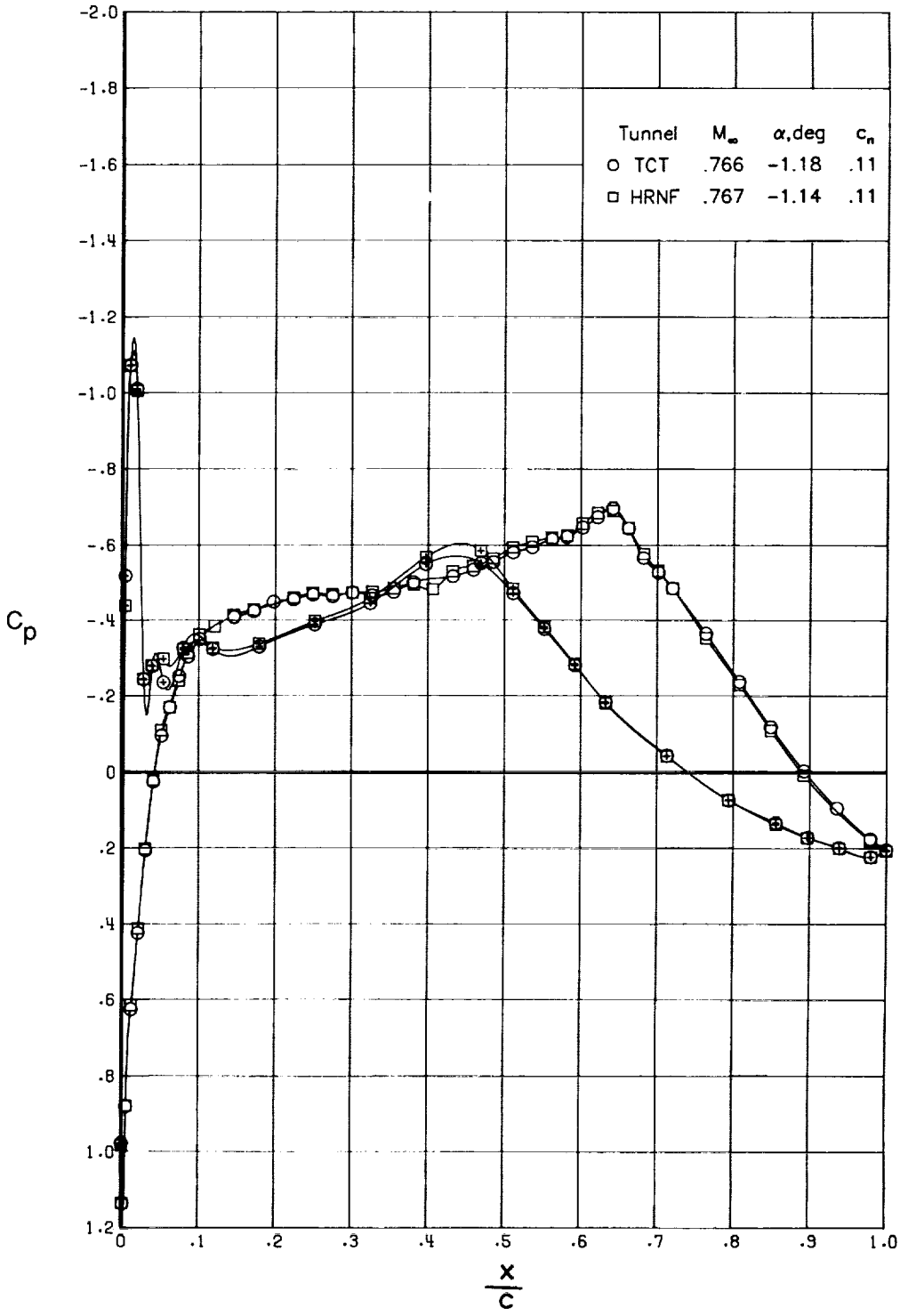

(b) $c_n \approx 0.11$.

Figure 4. Continued.

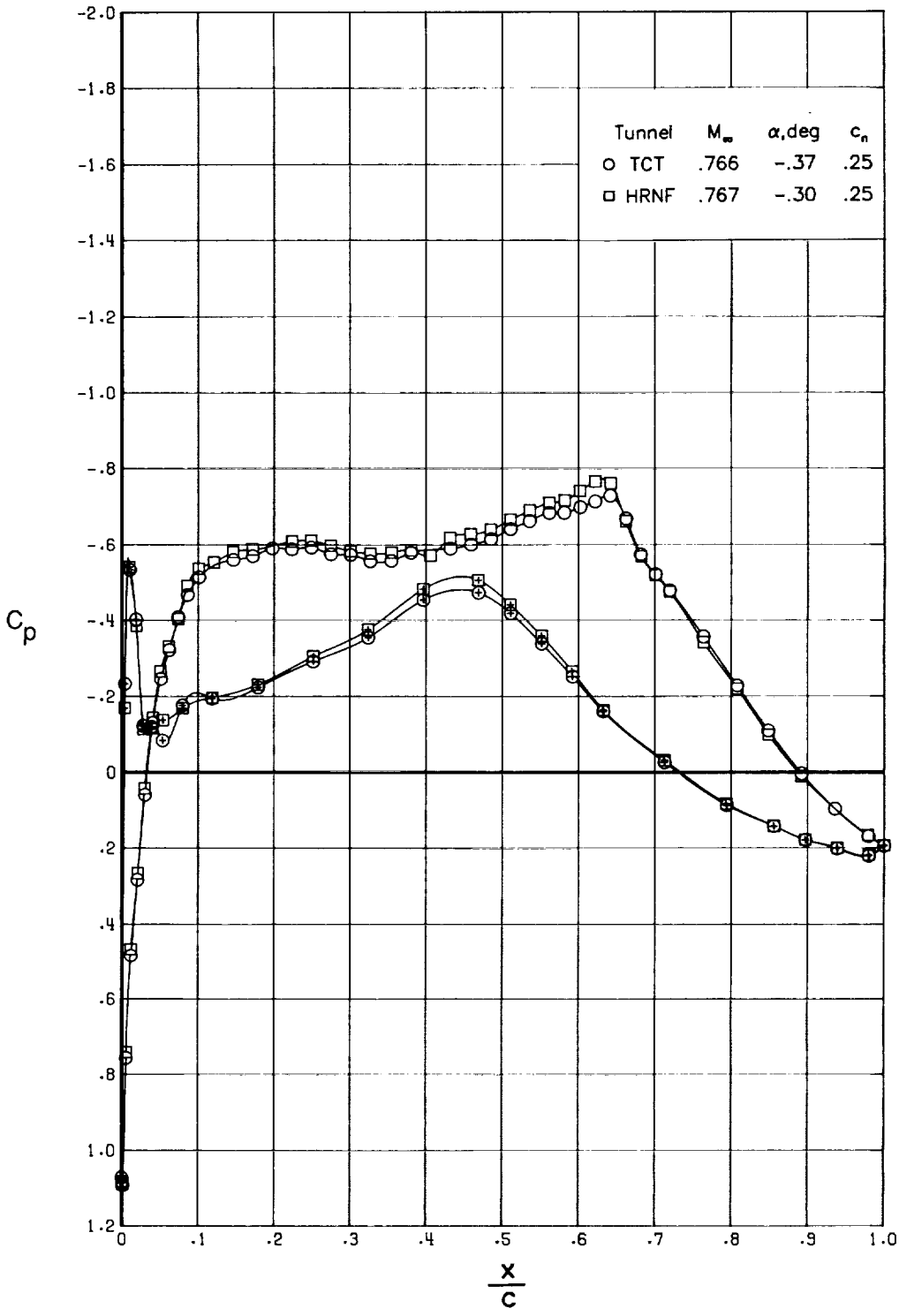

(c) $c_n \approx 0.25$.

Figure 4. Continued.

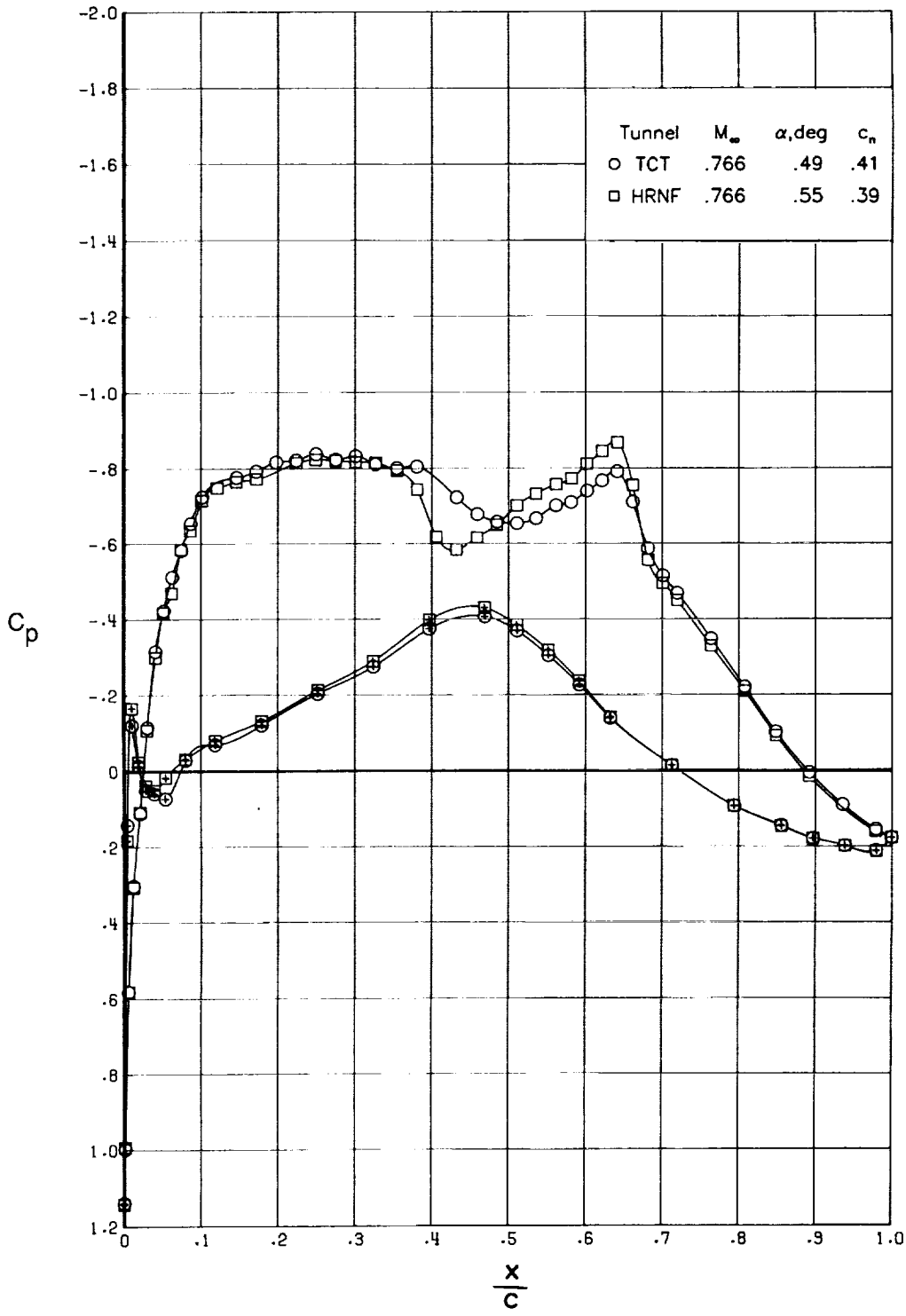

(d) $c_n \approx 0.40$.

Figure 4. Continued.

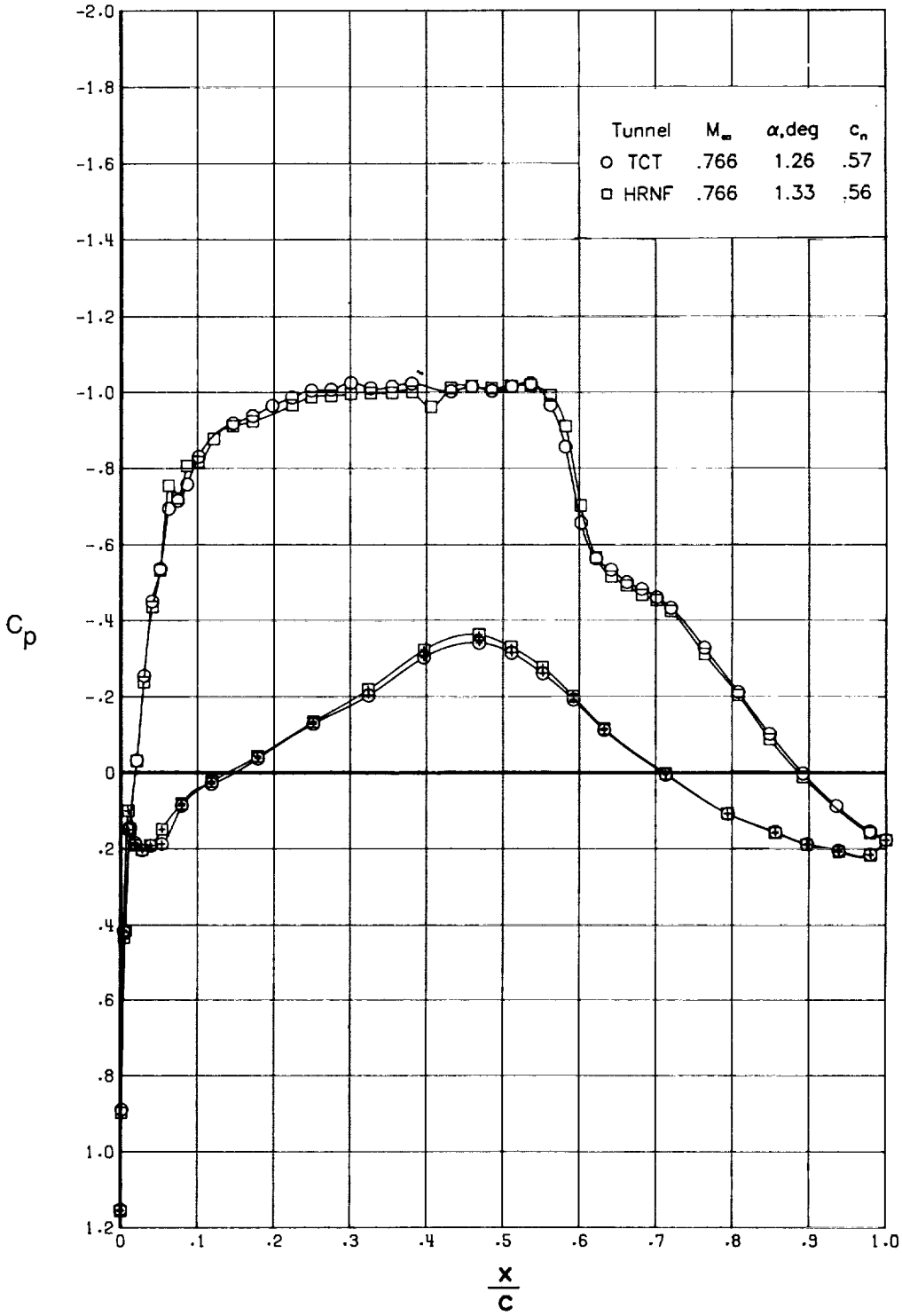

(c) $c_n \approx 0.56$.

Figure 4. Continued.

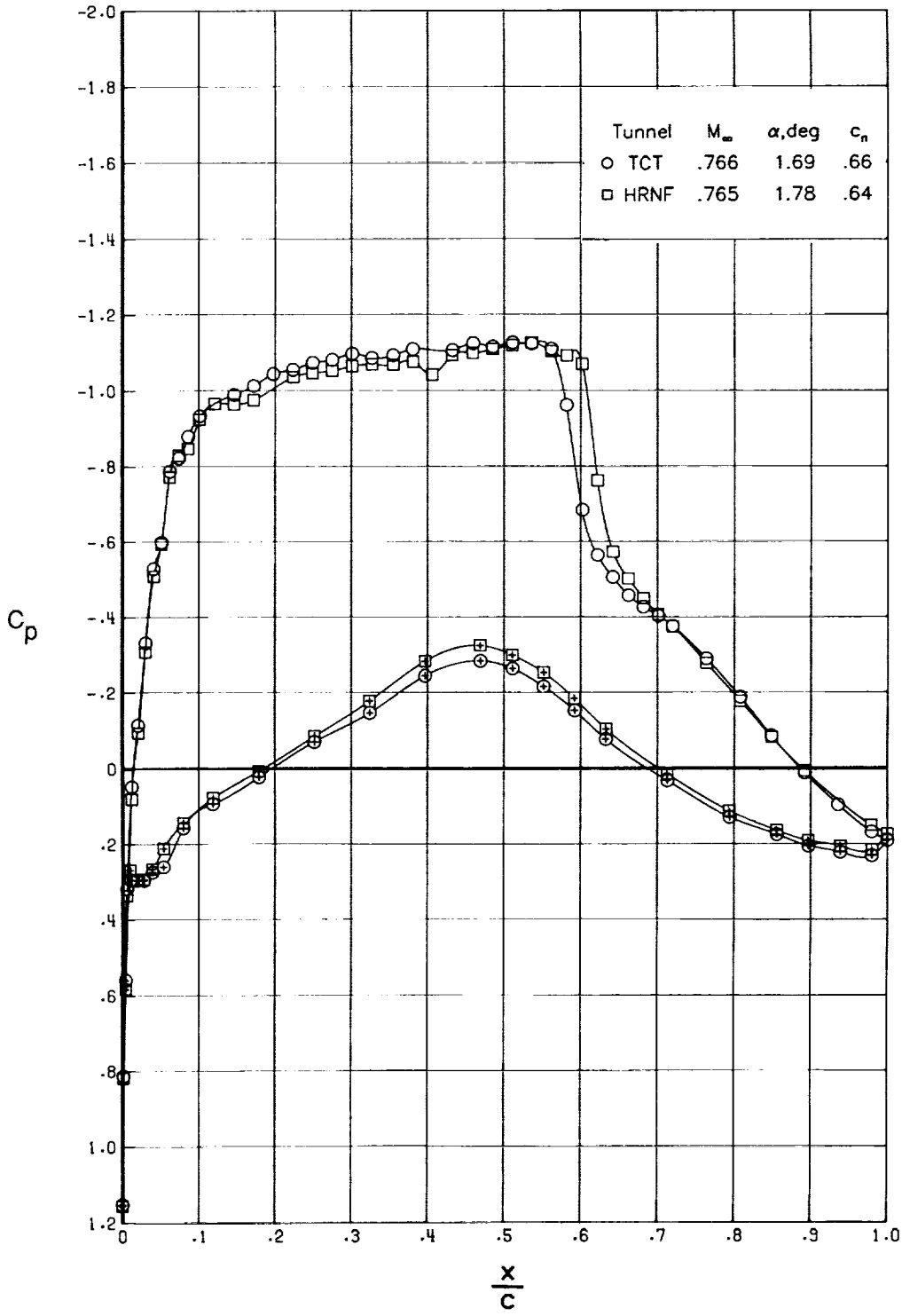

(f) $c_n \approx 0.65$.

Figure 4. Continued.

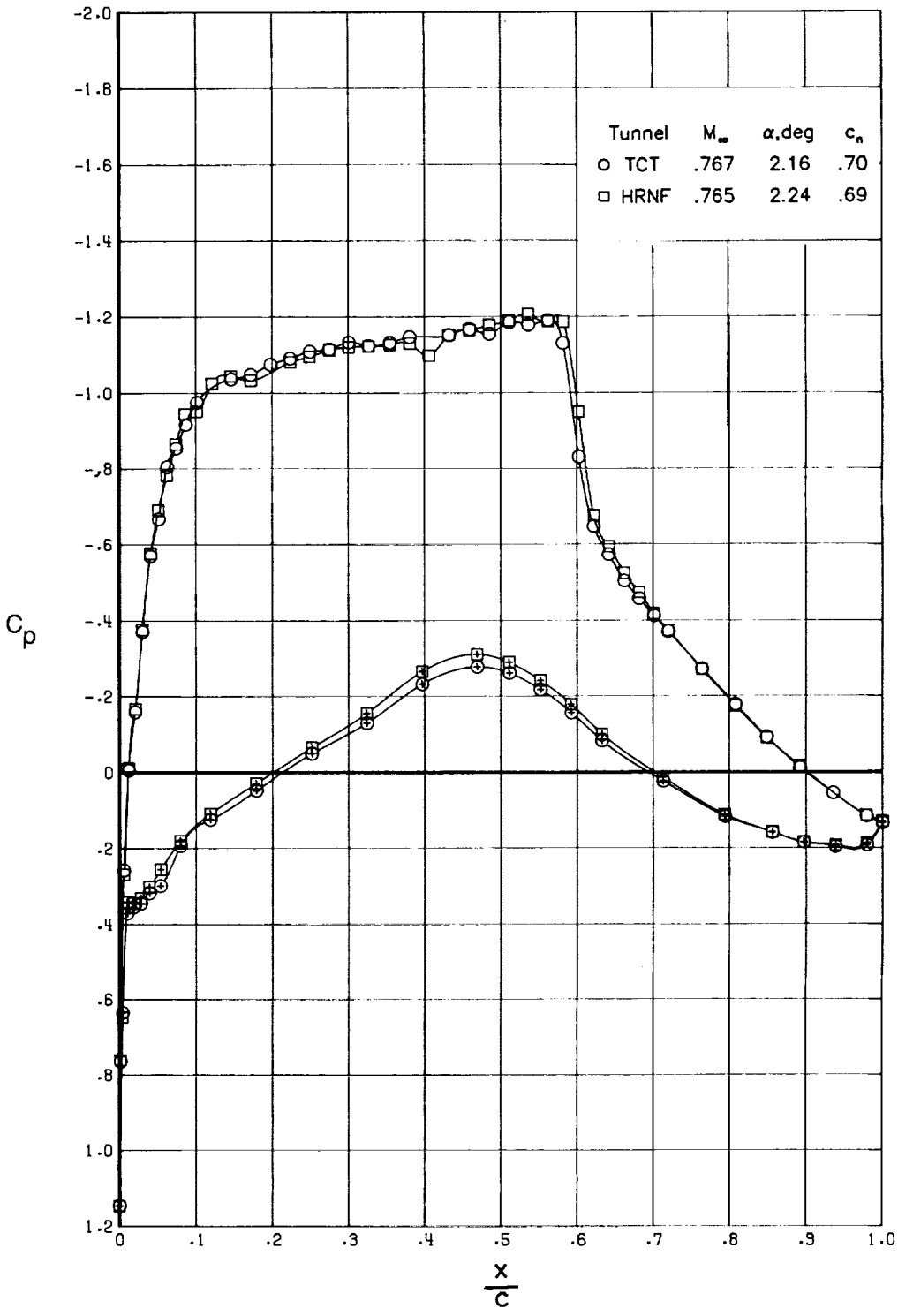

(g) $c_n \approx 0.70$.

Figure 4. Concluded.

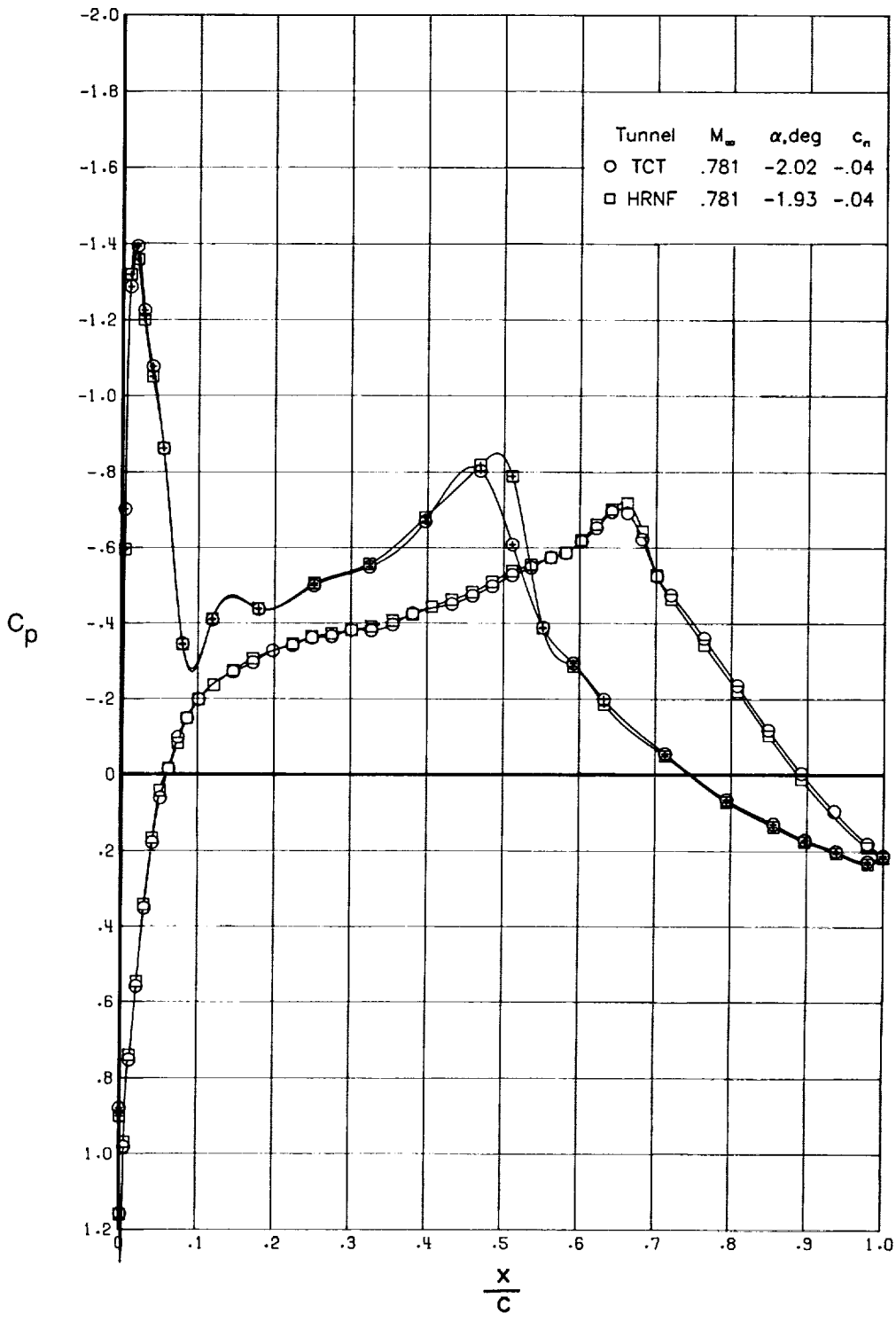

(a) $c_n \approx -0.04$.

Figure 5. Comparison of chordwise pressure distributions for $R_c = 10 \times 10^6$ and $M_\infty = 0.781$.

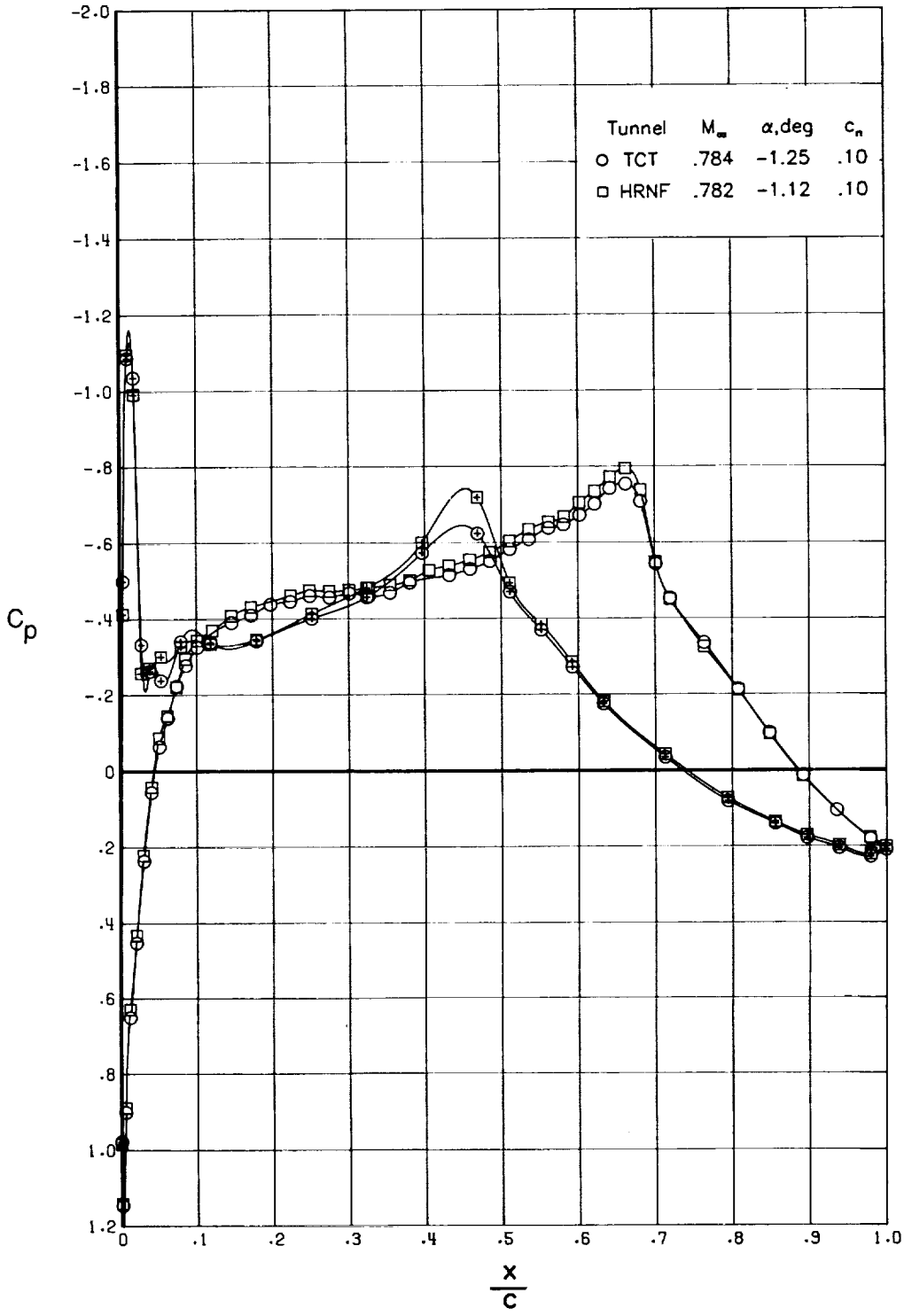

(b) $c_n \approx 0.10$.

Figure 5. Continued.

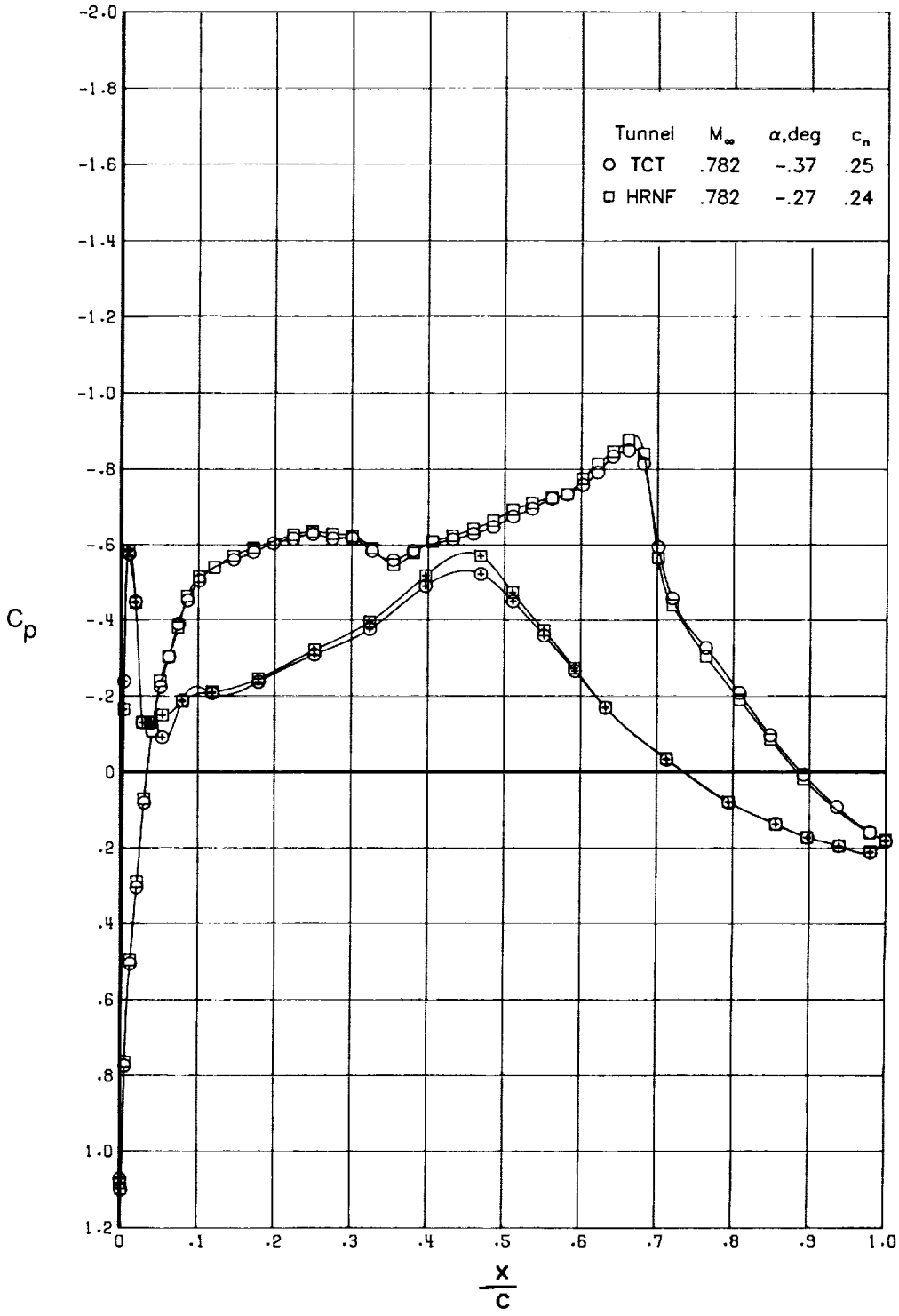

(c) $c_n \approx 0.25$.

Figure 5. Continued.

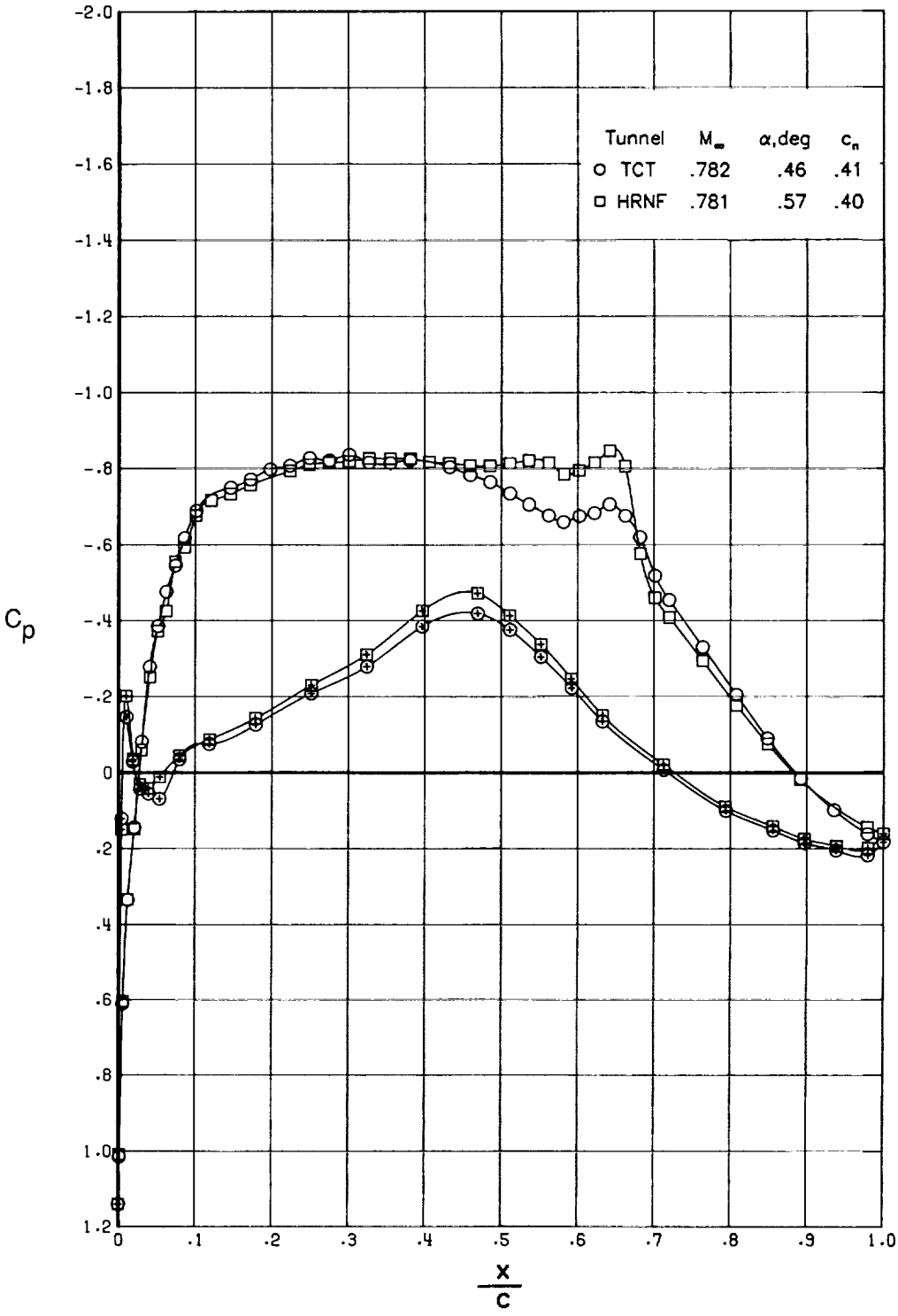

(d) $c_n \approx 0.40$.

Figure 5. Continued.

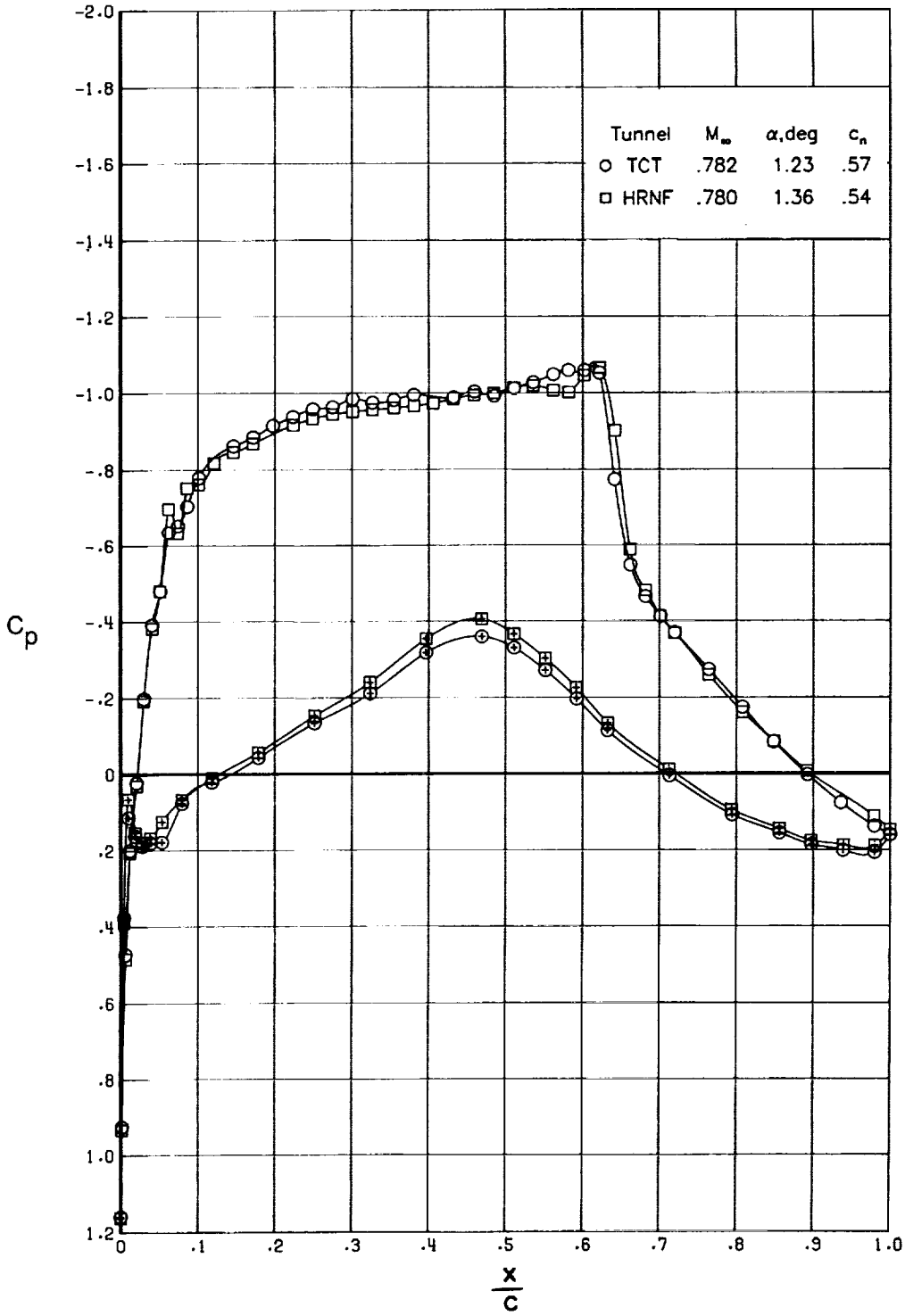

(e) $c_n \approx 0.55$.

Figure 5. Concluded.

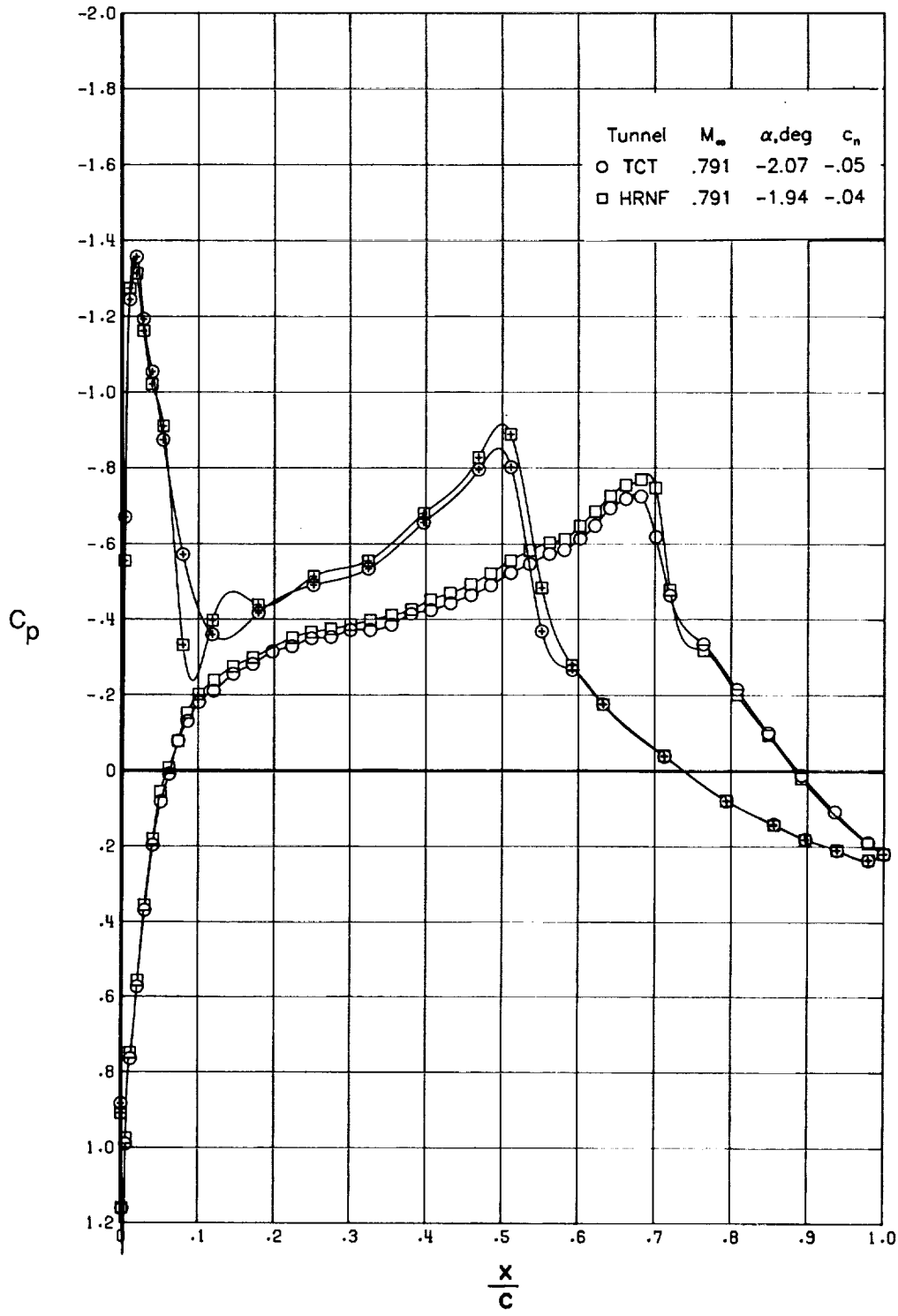

(a) $c_n \approx -0.04$.

Figure 6. Comparison of chordwise pressure distributions for $R_c = 10 \times 10^6$ and $M_\infty = 0.791$.

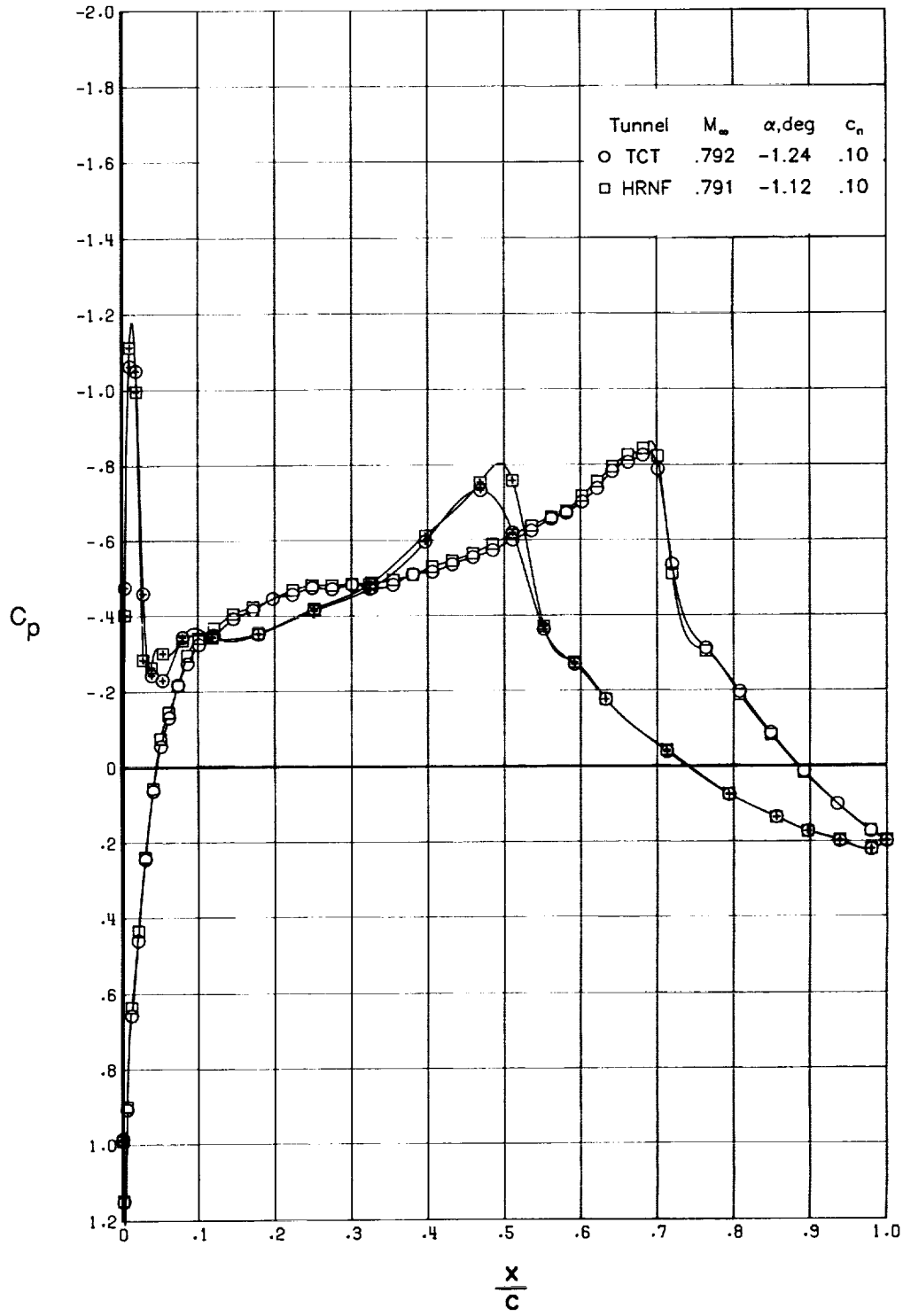

(b) $c_n \approx 0.10$.

Figure 6. Continued.

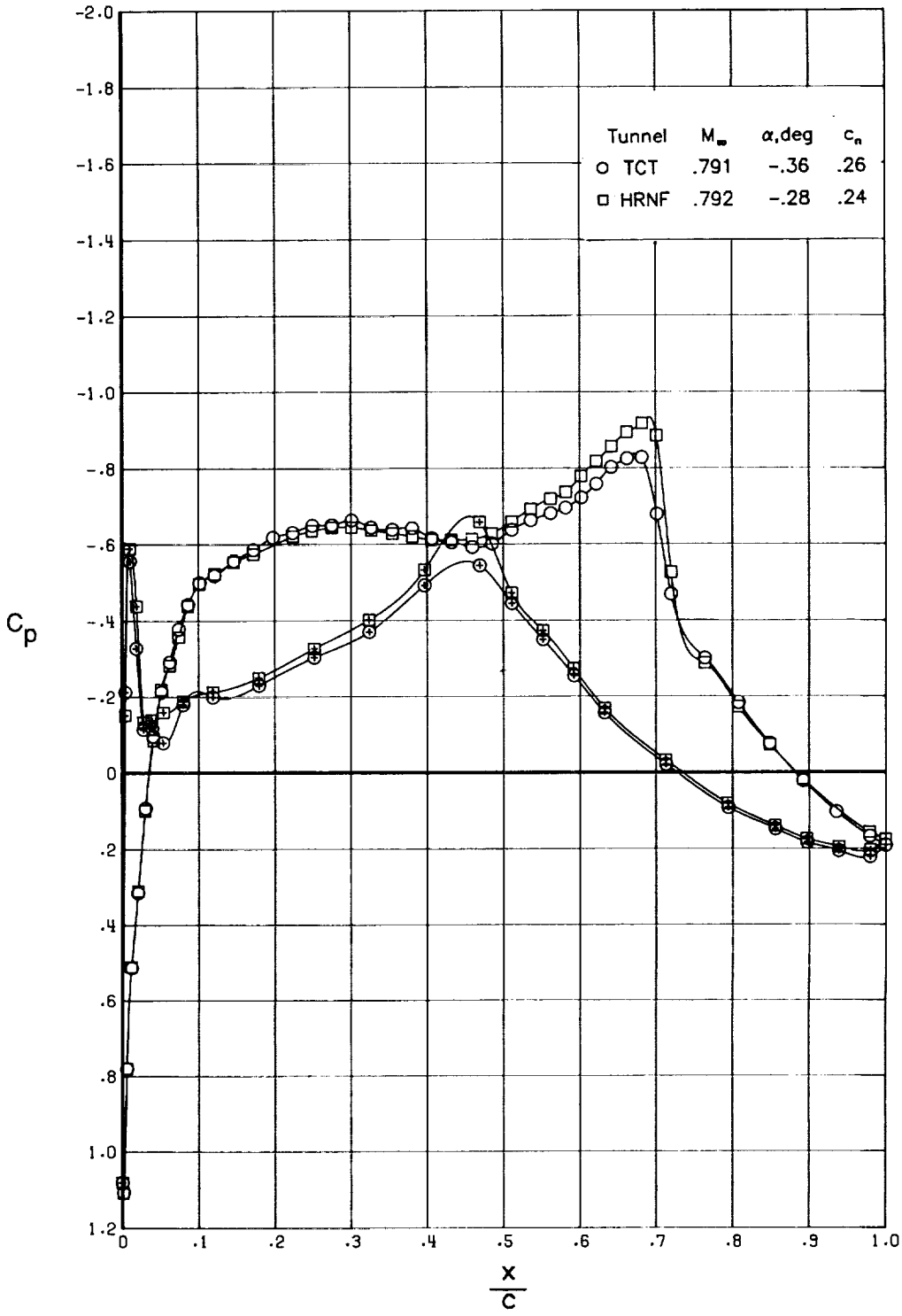

(c) $c_n \approx 0.25$.

Figure 6. Continued.

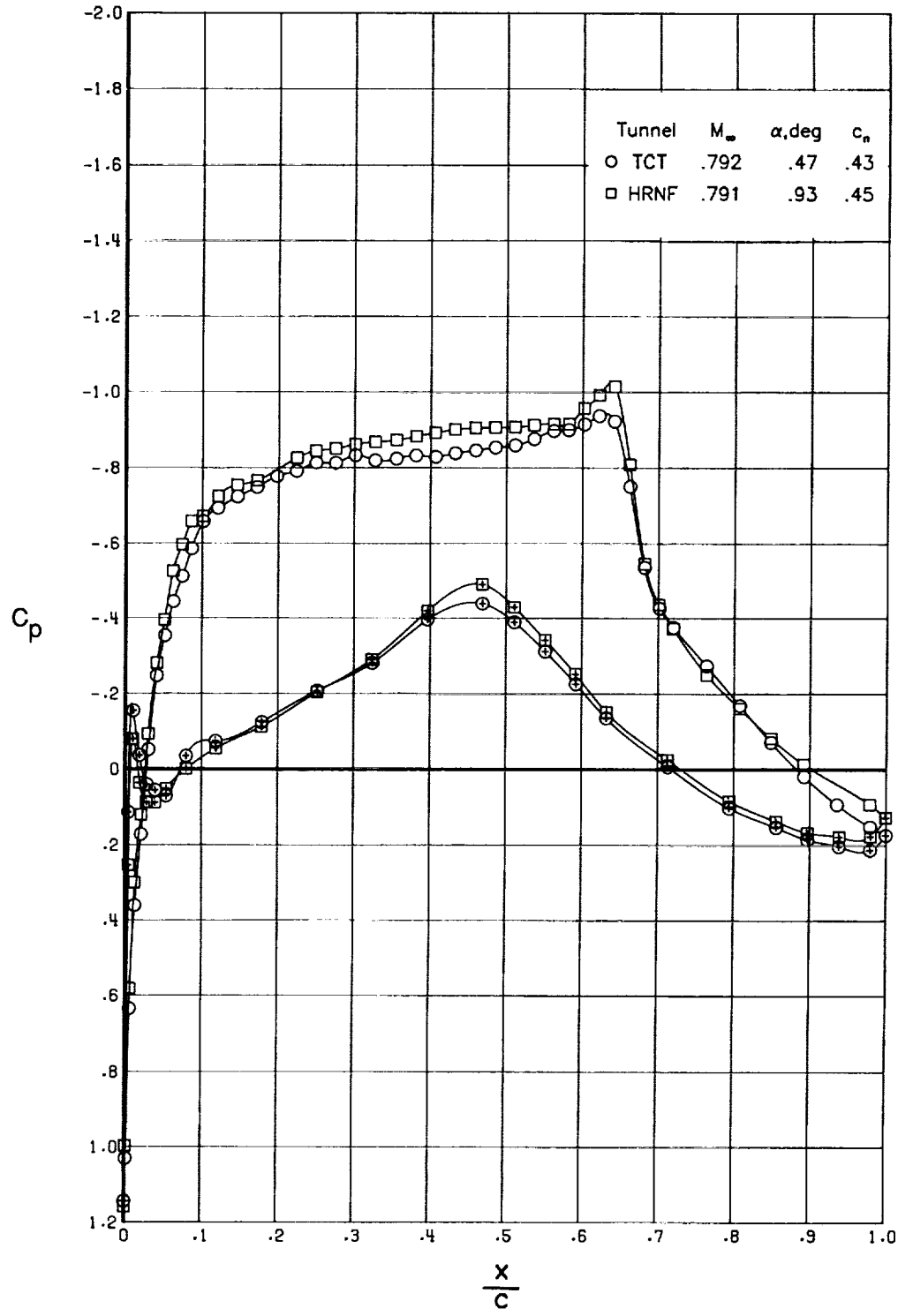

(d) $c_n \approx 0.44$.

Figure 6. Continued.

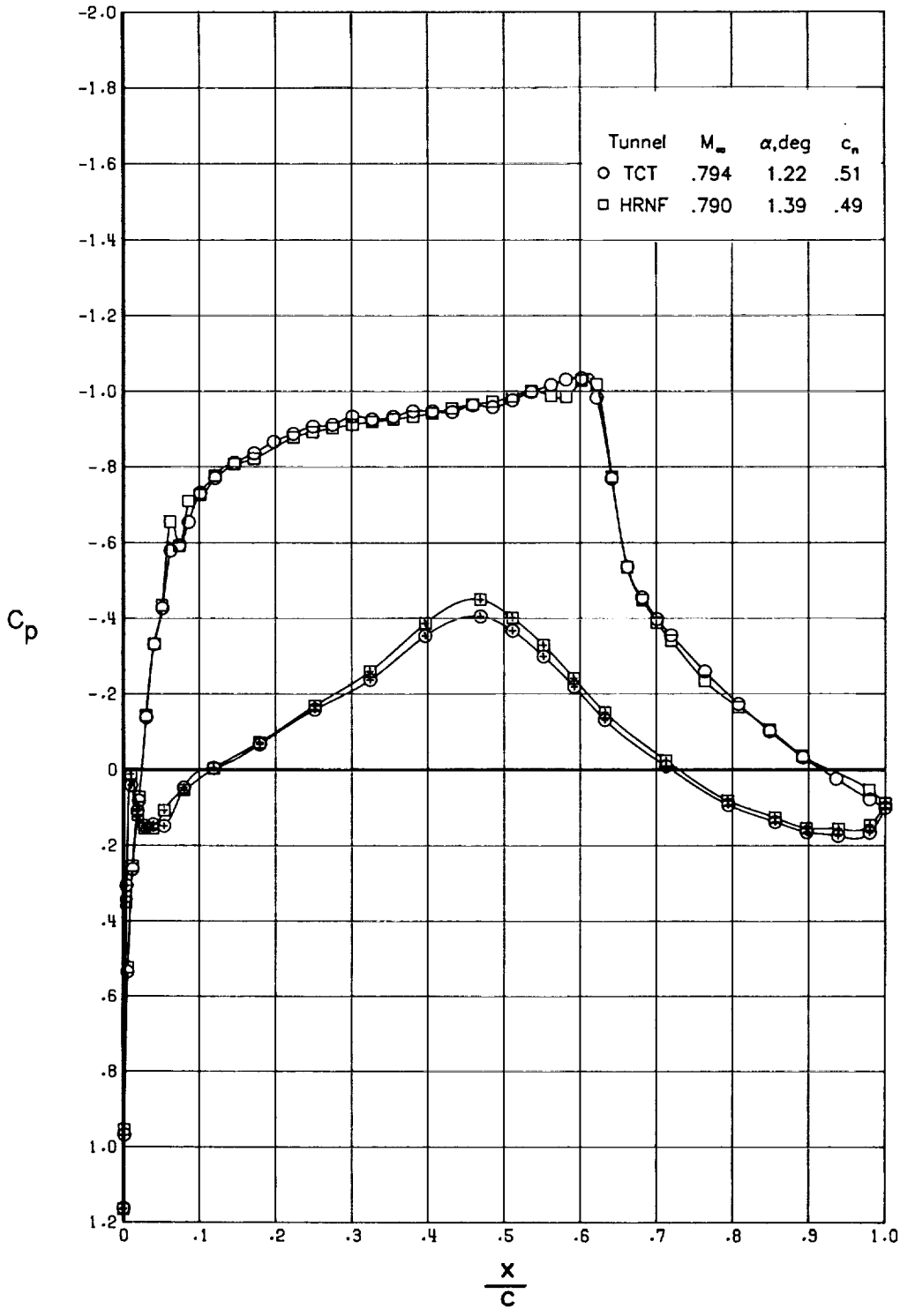

(c) $c_n \approx 0.50$.

Figure 6. Concluded.

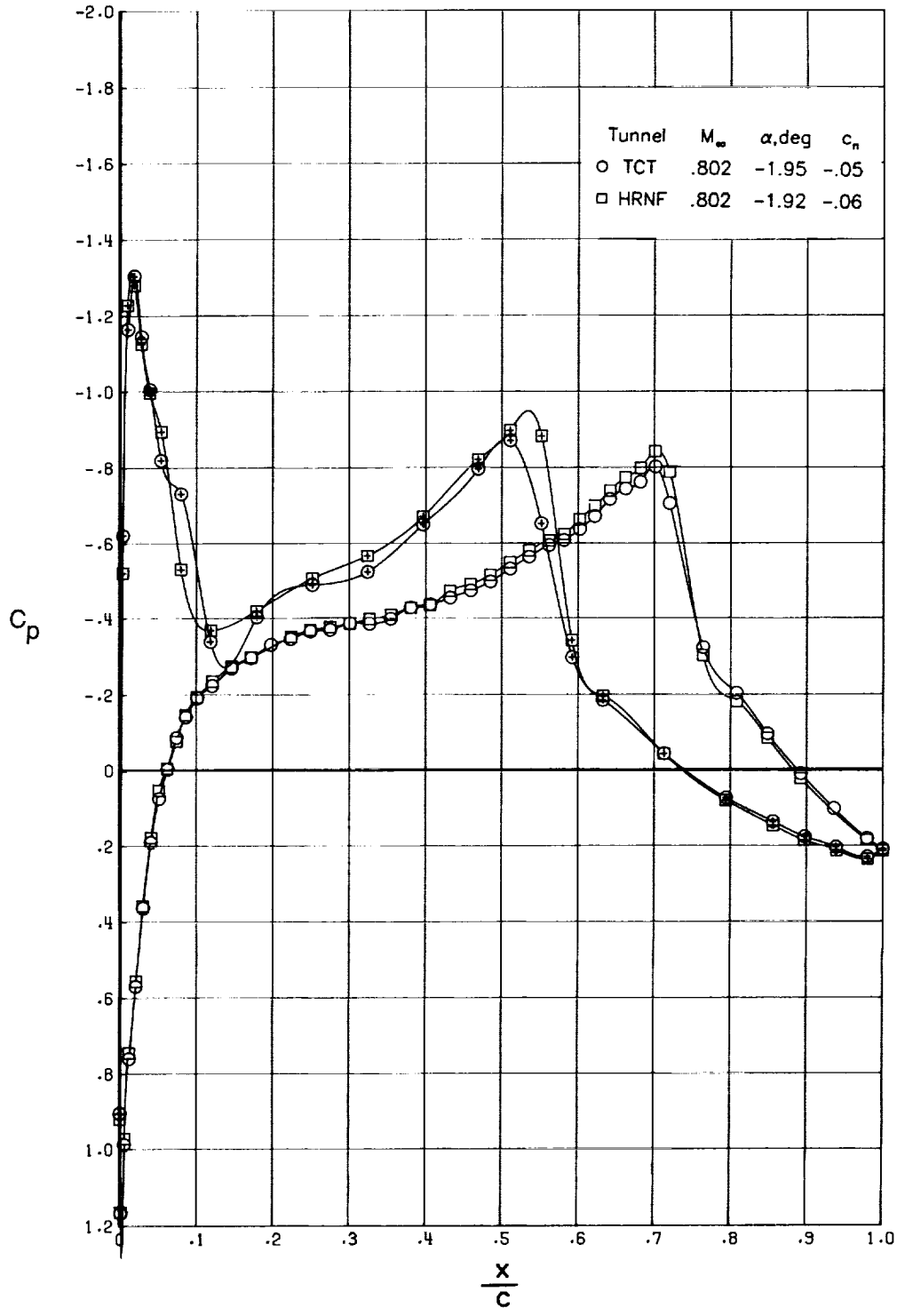

(a) $c_n \approx -0.05$.

Figure 7. Comparison of chordwise pressure distributions for $R_c = 10 \times 10^6$ and $M_\infty = 0.802$.

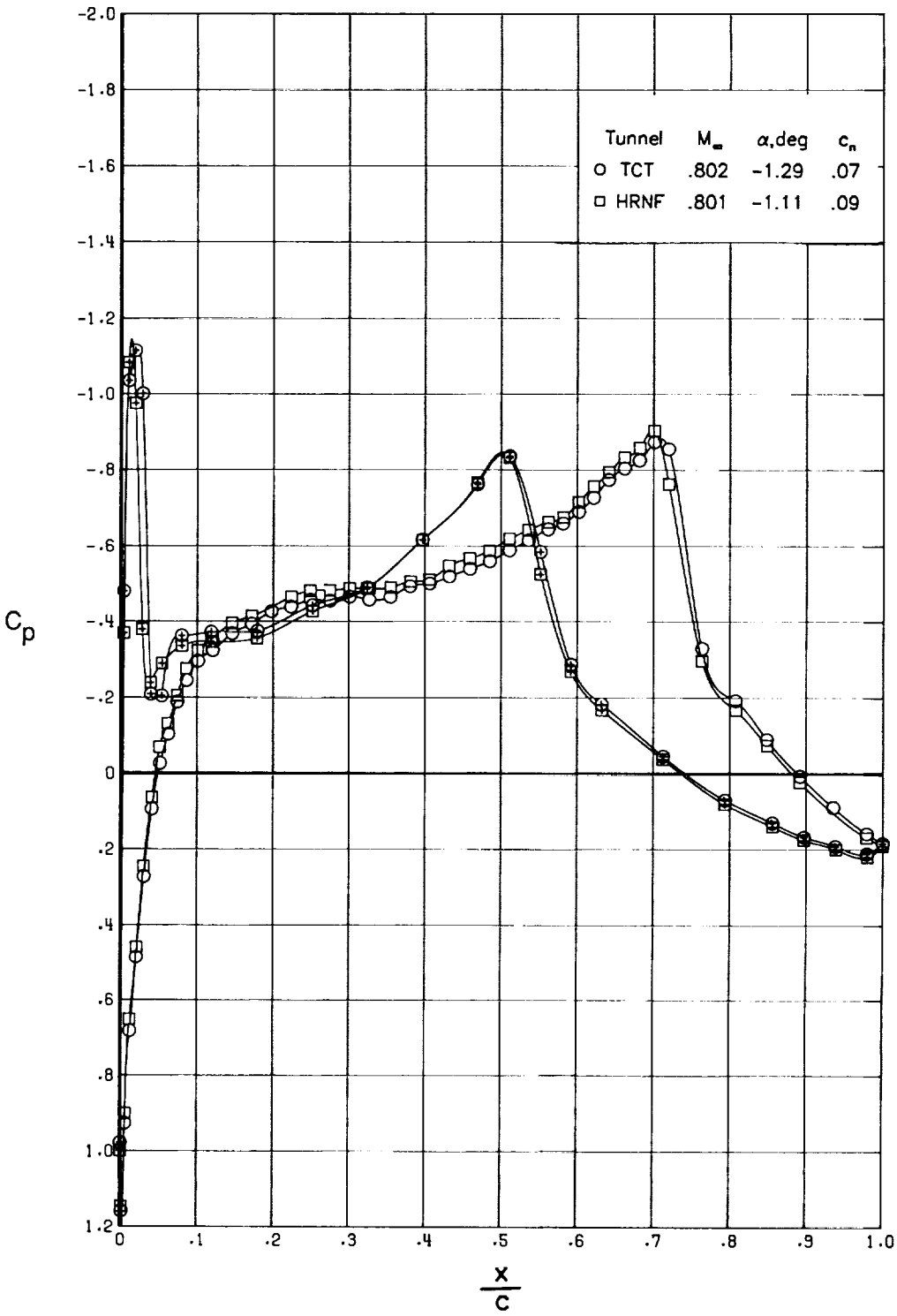

(b) $c_n \approx 0.08$.

Figure 7. Continued.

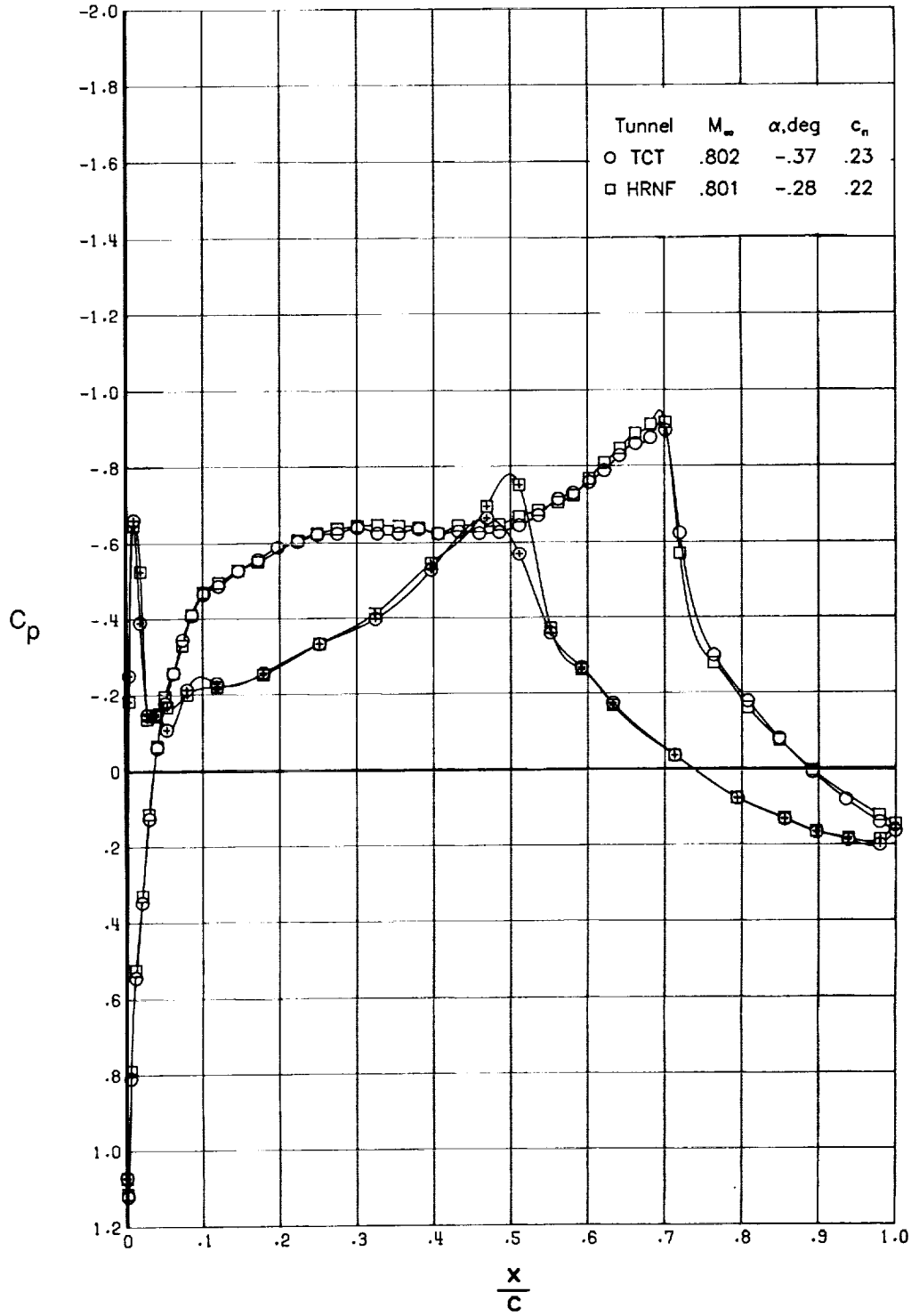

(c) $c_n \approx 0.23$.

Figure 7. Continued.

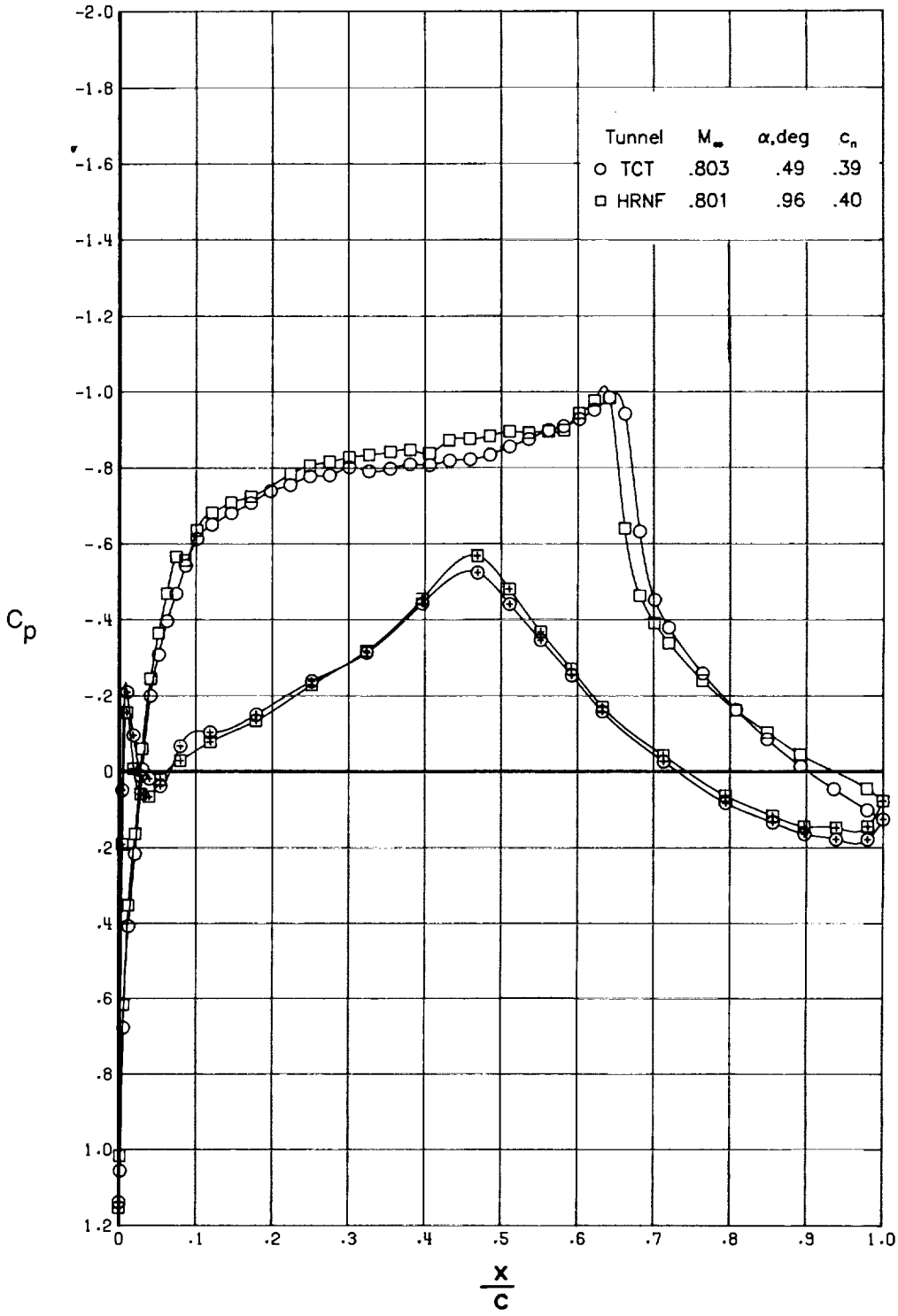

(d) $c_n \approx 0.39$.

Figure 7. Continued.

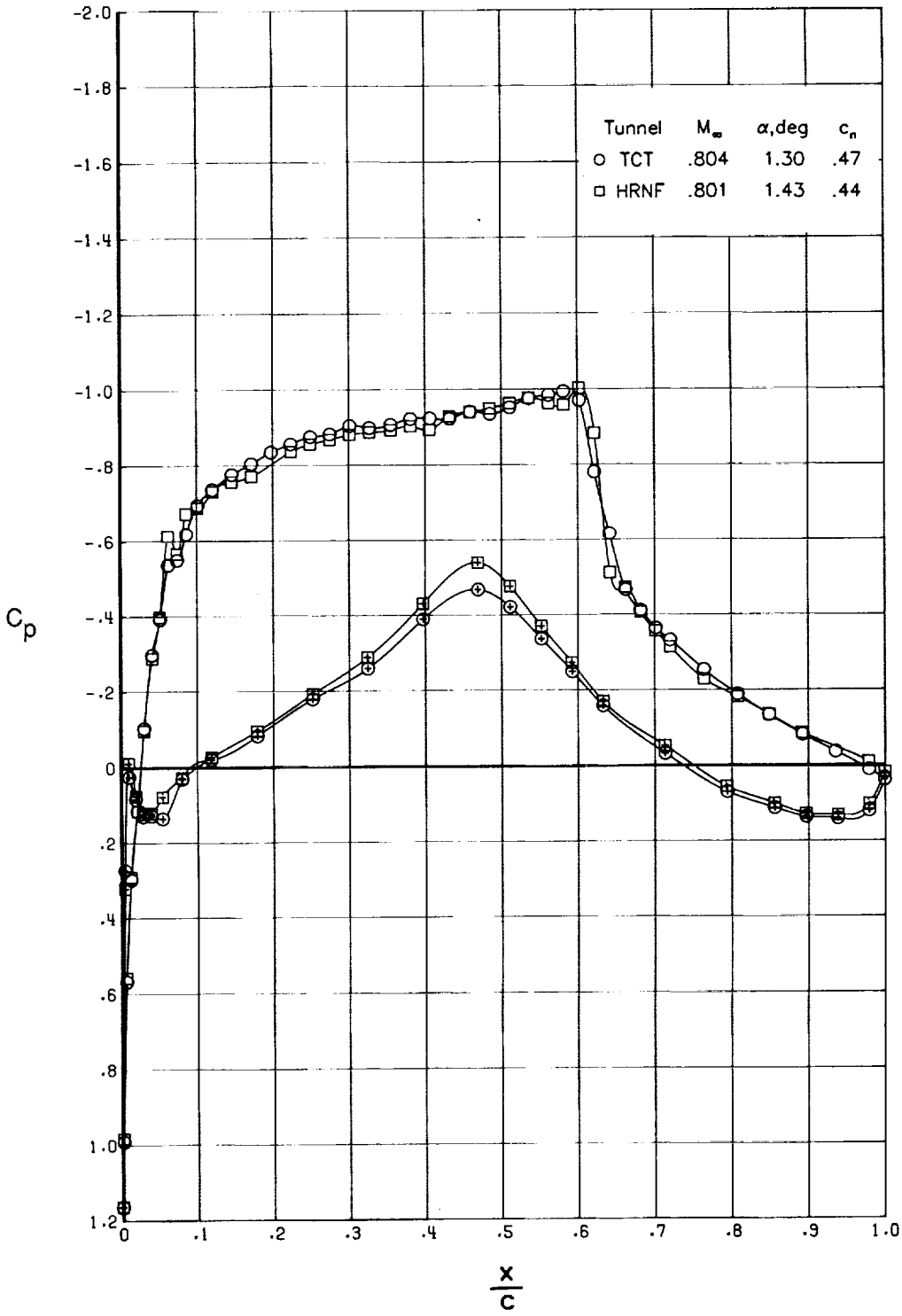

(e) $c_n \approx 0.45$.

Figure 7. Continued.

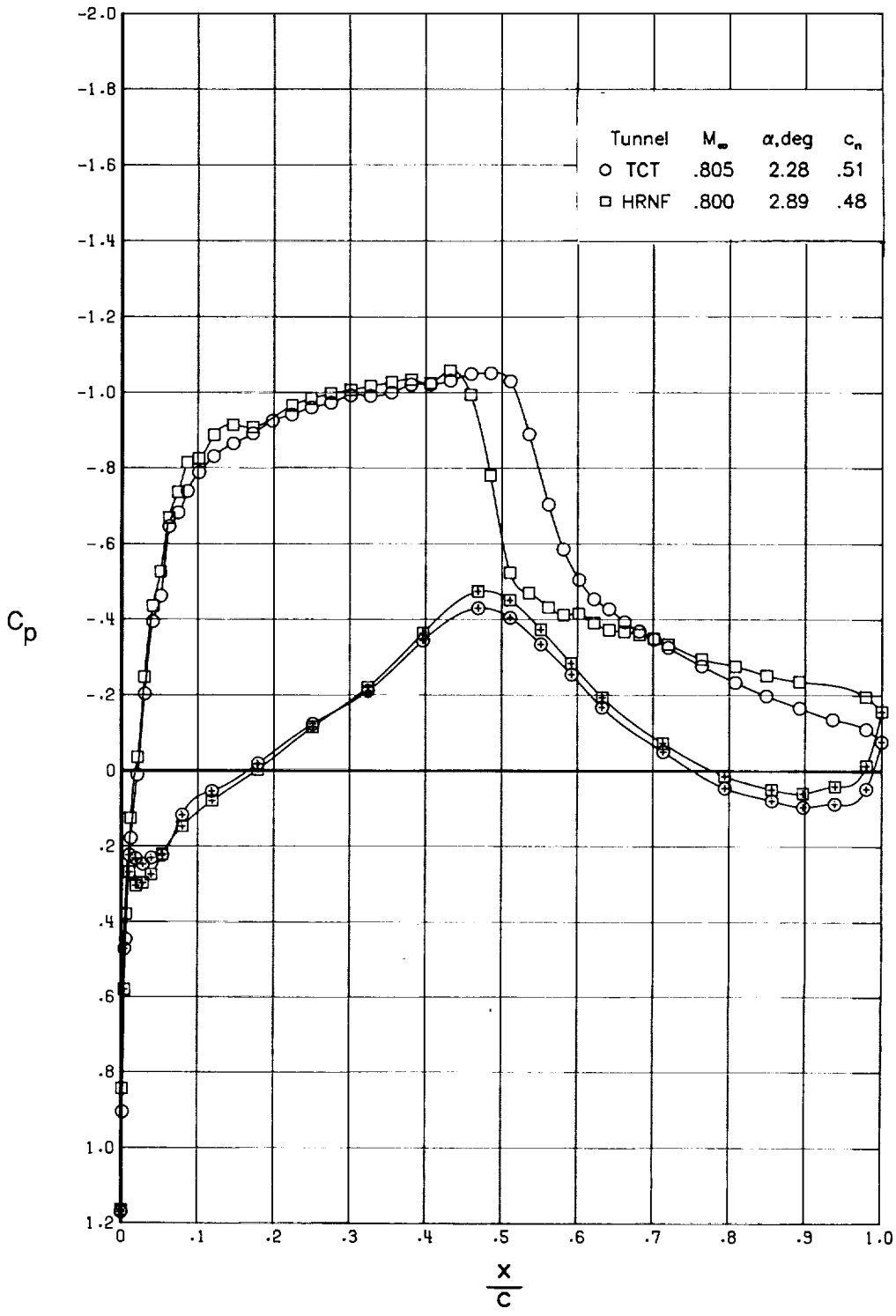

(f) $c_n \approx 0.50$.

Figure 7. Continued.

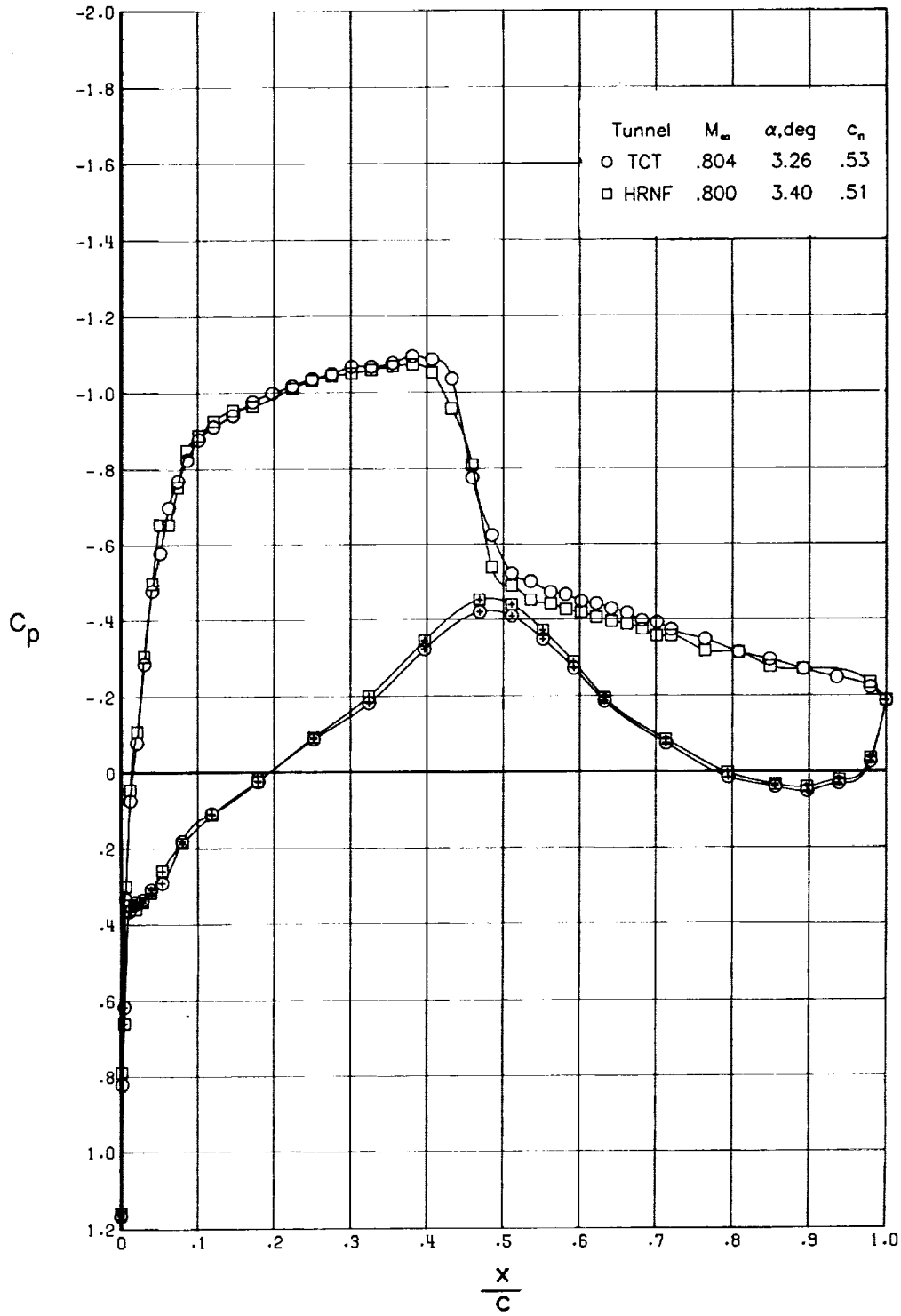

(g) $c_n \approx 0.52$.

Figure 7. Concluded.

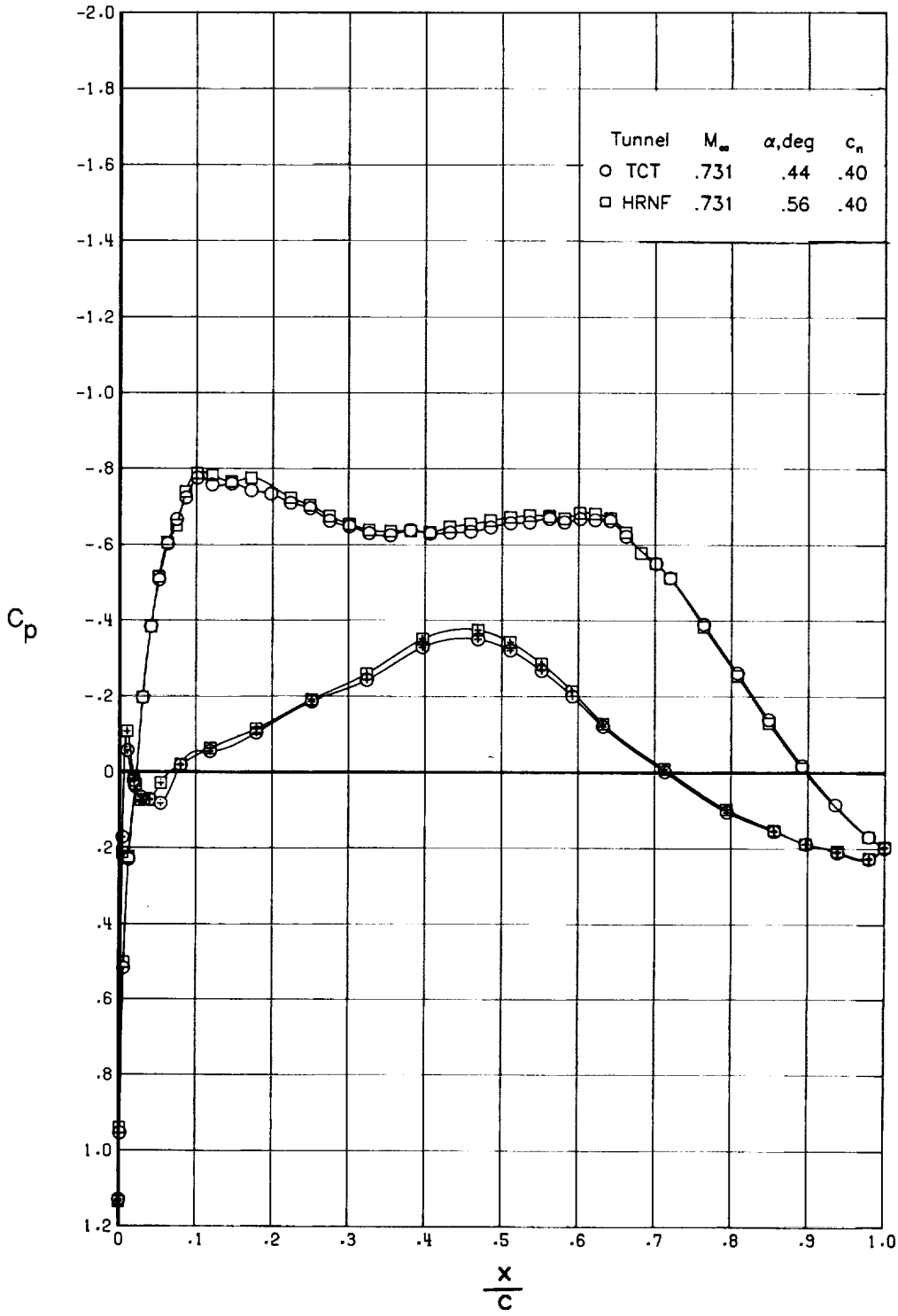

(a) $c_n \approx 0.40$.

Figure 8. Comparison of chordwise pressure distributions for $R_c = 15 \times 10^6$ and $M_\infty = 0.731$.

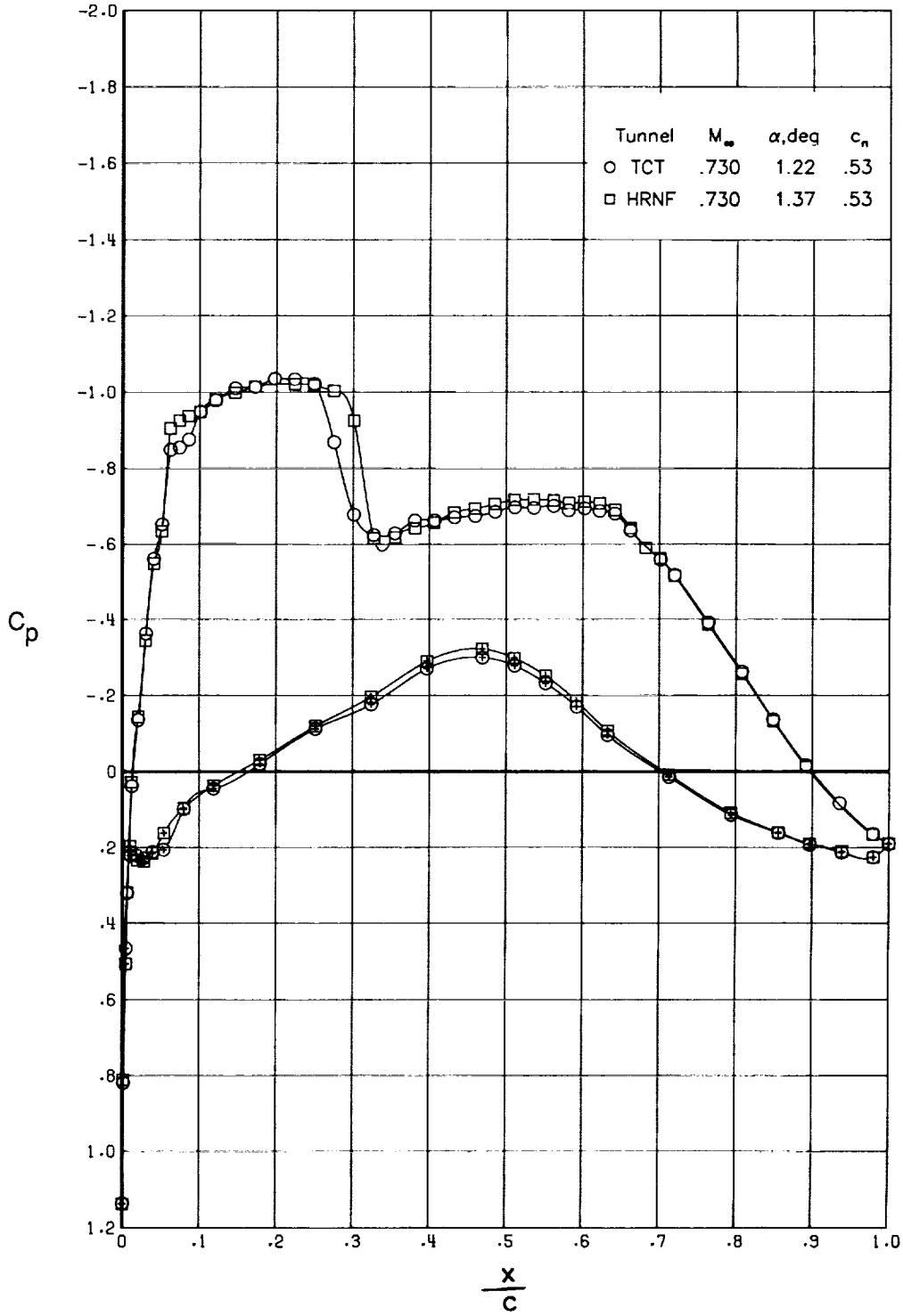

(b) $c_n \approx 0.53$.

Figure 8. Concluded.

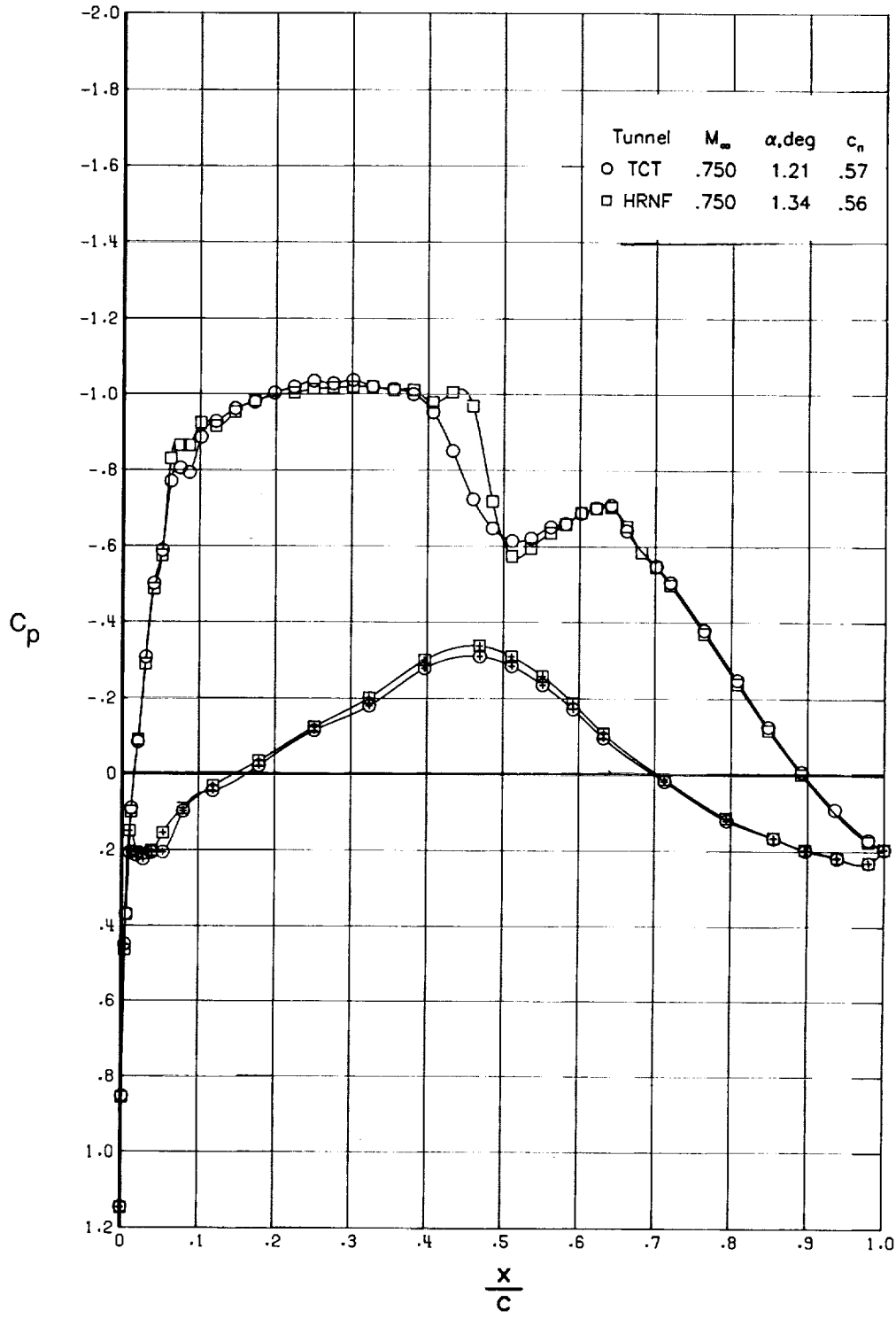

Figure 9. Comparison of chordwise pressure distributions for $R_c = 15 \times 10^6$, $M_\infty = 0.750$, and $c_n \approx 0.56$.

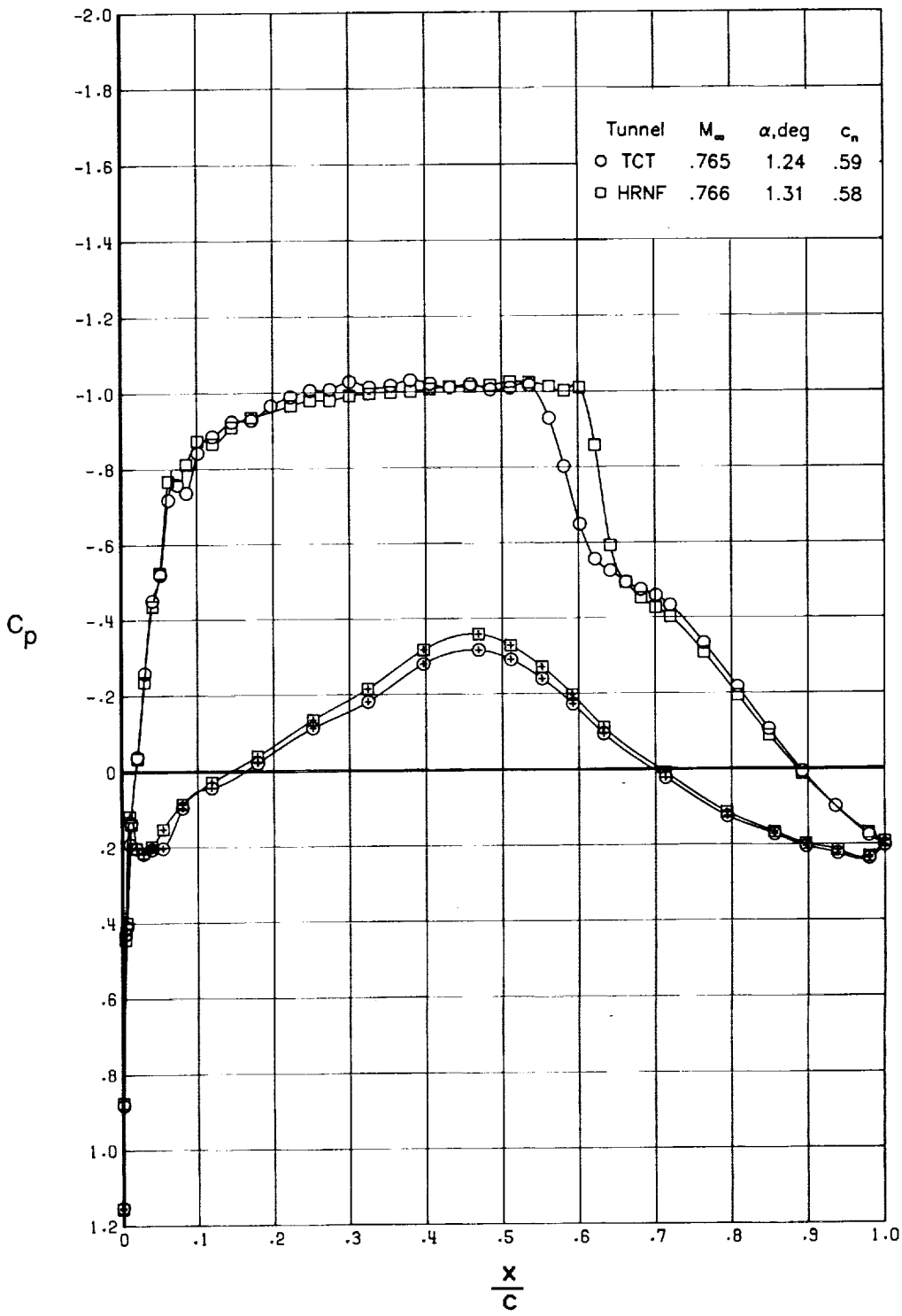

Figure 10. Comparison of chordwise pressure distributions for $R_c = 15 \times 10^6$, $M_\infty = 0.765$, and $c_n \approx 0.58$.

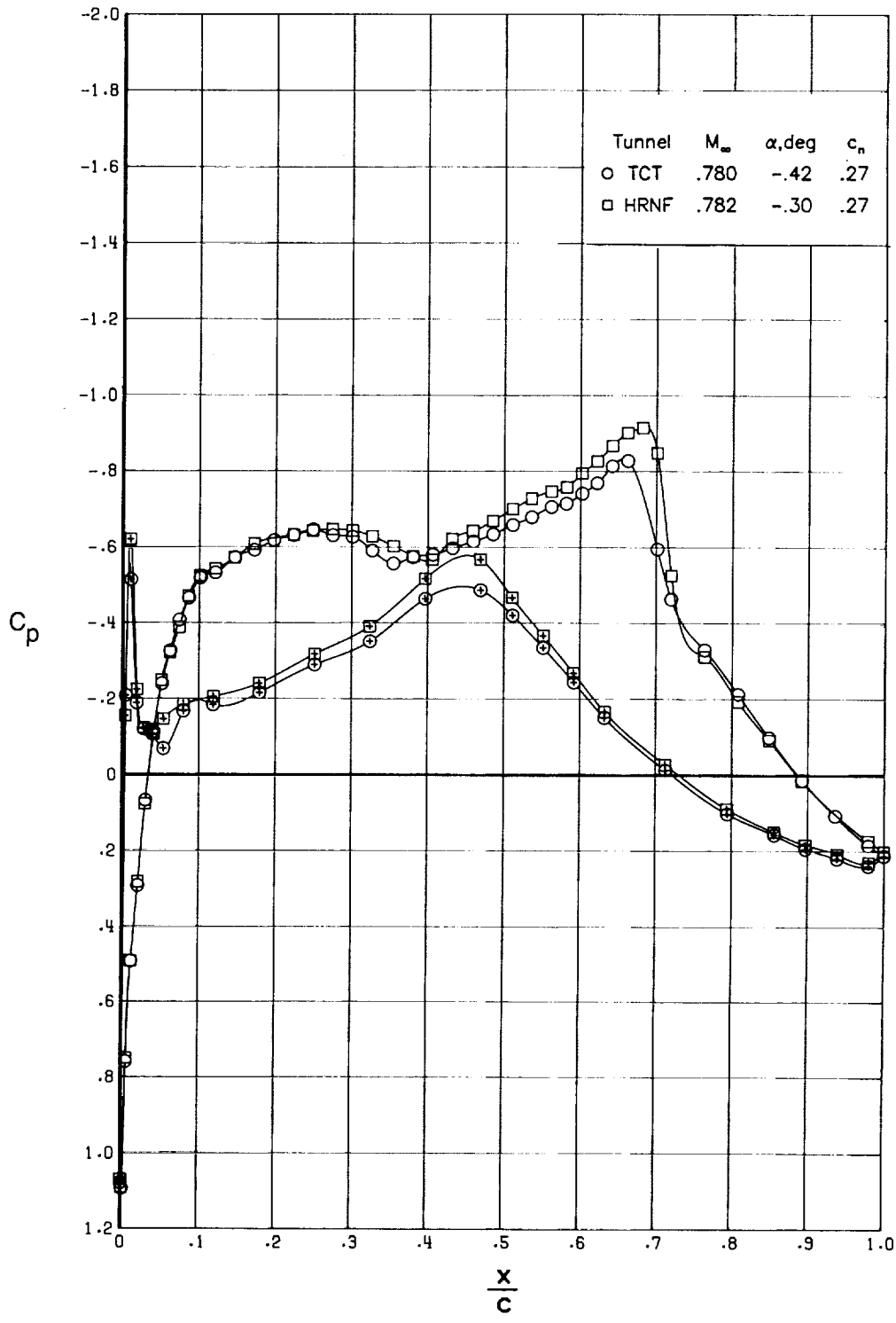

(a) $c_n \approx 0.27$.

Figure 11. Comparison of chordwise pressure distributions for $R_c = 15 \times 10^6$ and $M_\infty = 0.781$.

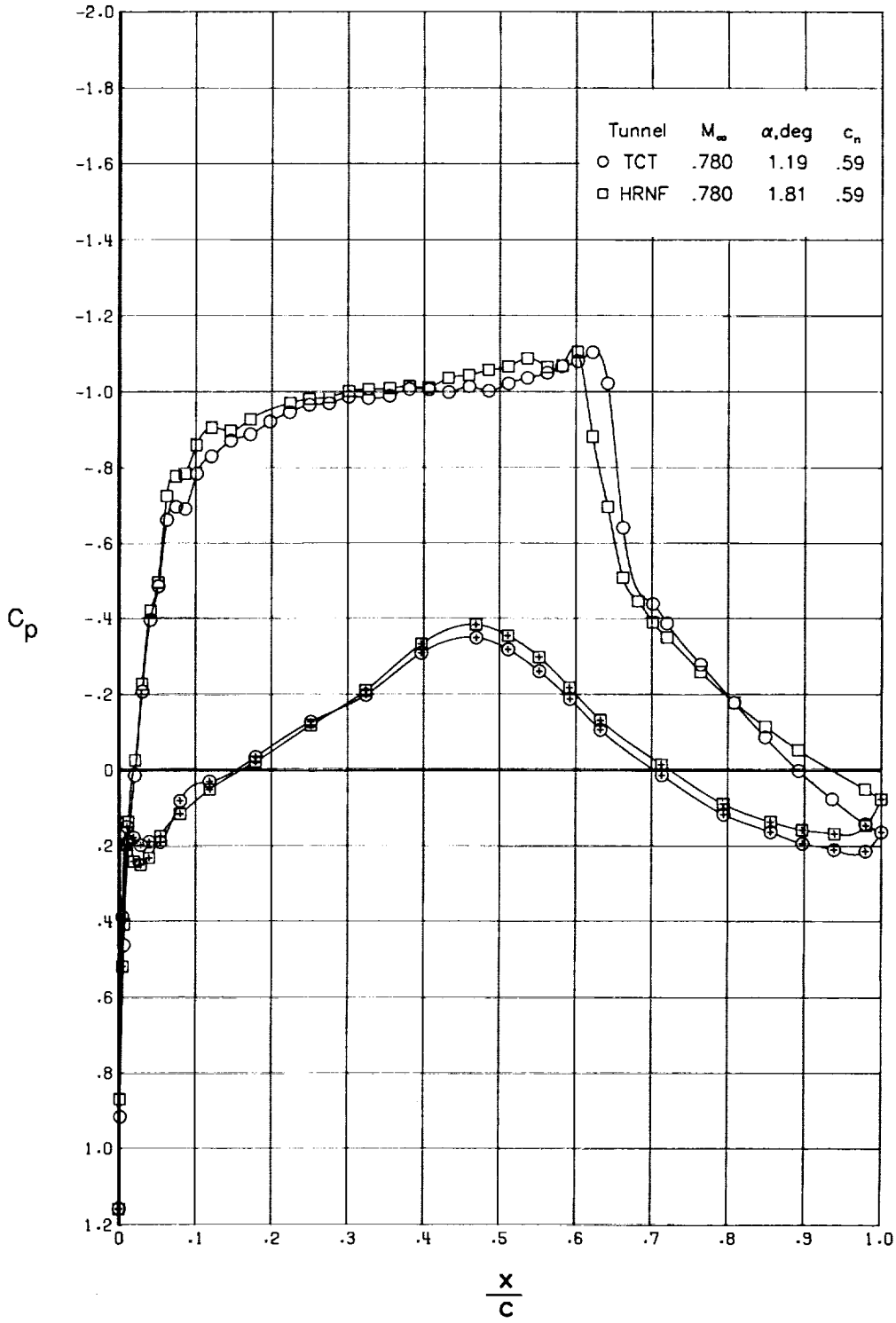

(b) $c_n \approx 0.59$.

Figure 11. Concluded.

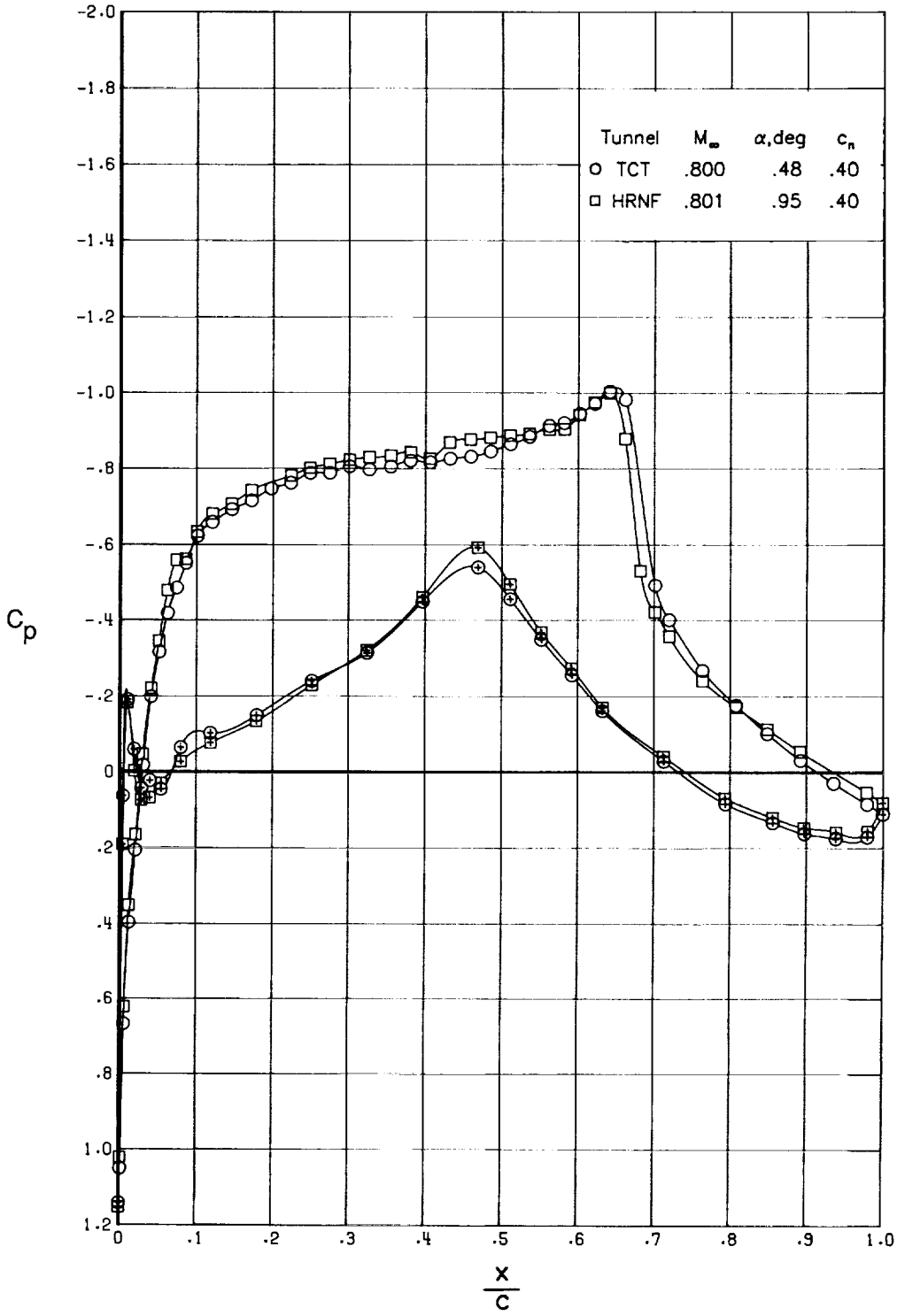

(a) $c_n \approx 0.40$.

Figure 12. Comparison of chordwise pressure distributions for $R_c = 15 \times 10^6$ and $M_\infty = 0.801$.

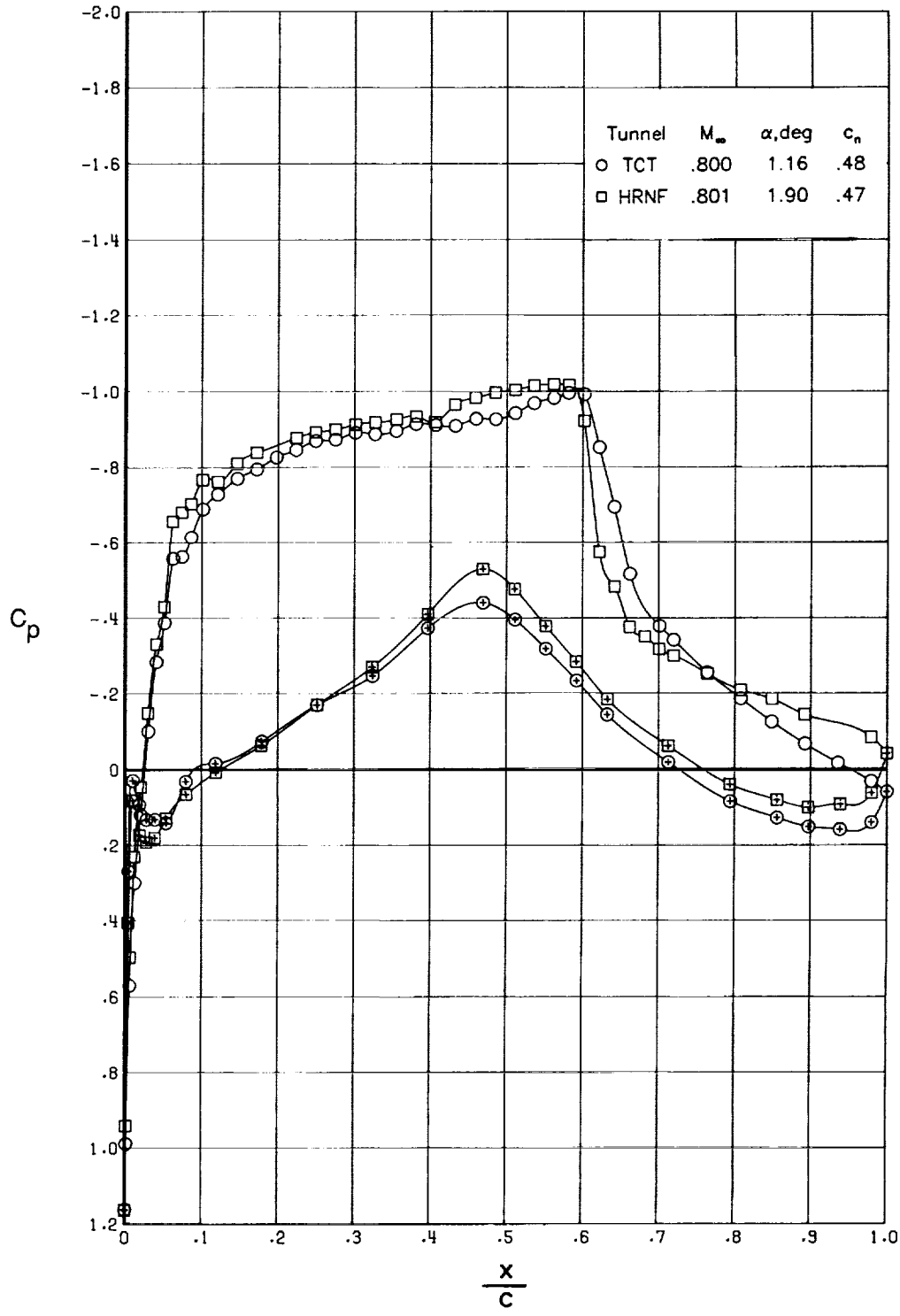

(b) $c_n \approx 0.47$.

Figure 12. Concluded.

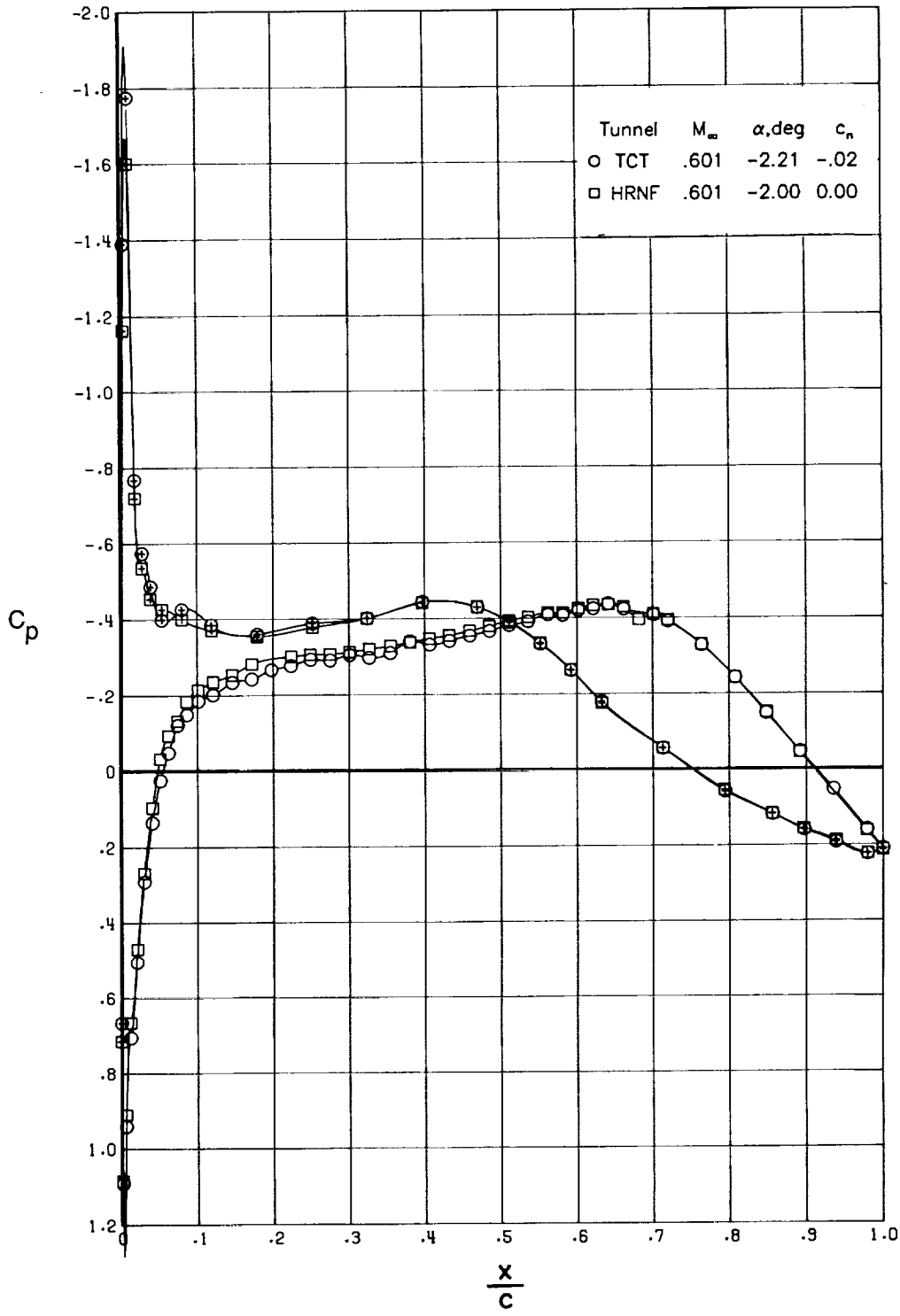

(a) $c_n \approx -0.01$.

Figure 13. Comparison of chordwise pressure distributions for $R_c = 20 \times 10^6$ and $M_\infty = 0.601$.

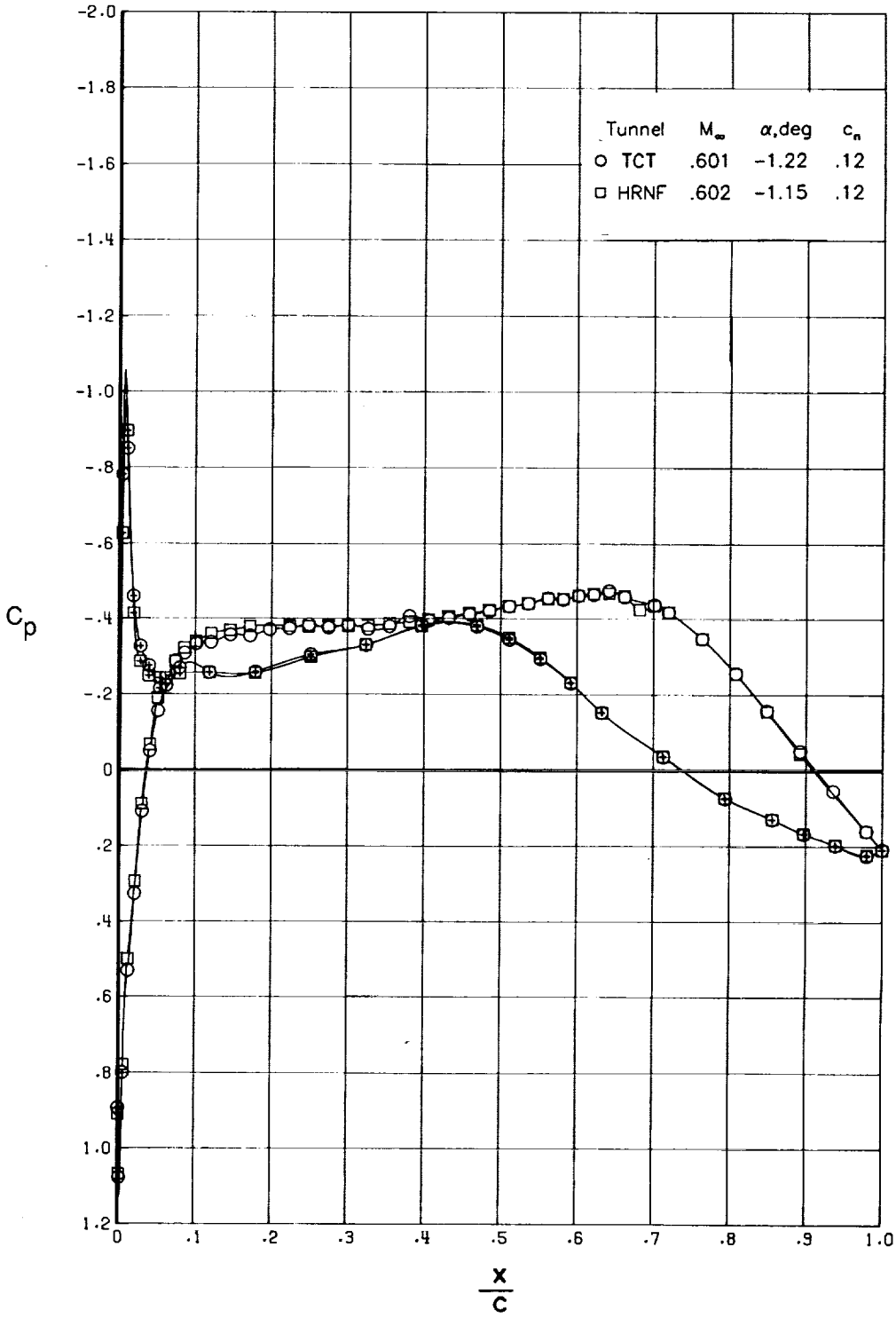

(b) $c_n \approx 0.12$.

Figure 13. Continued.

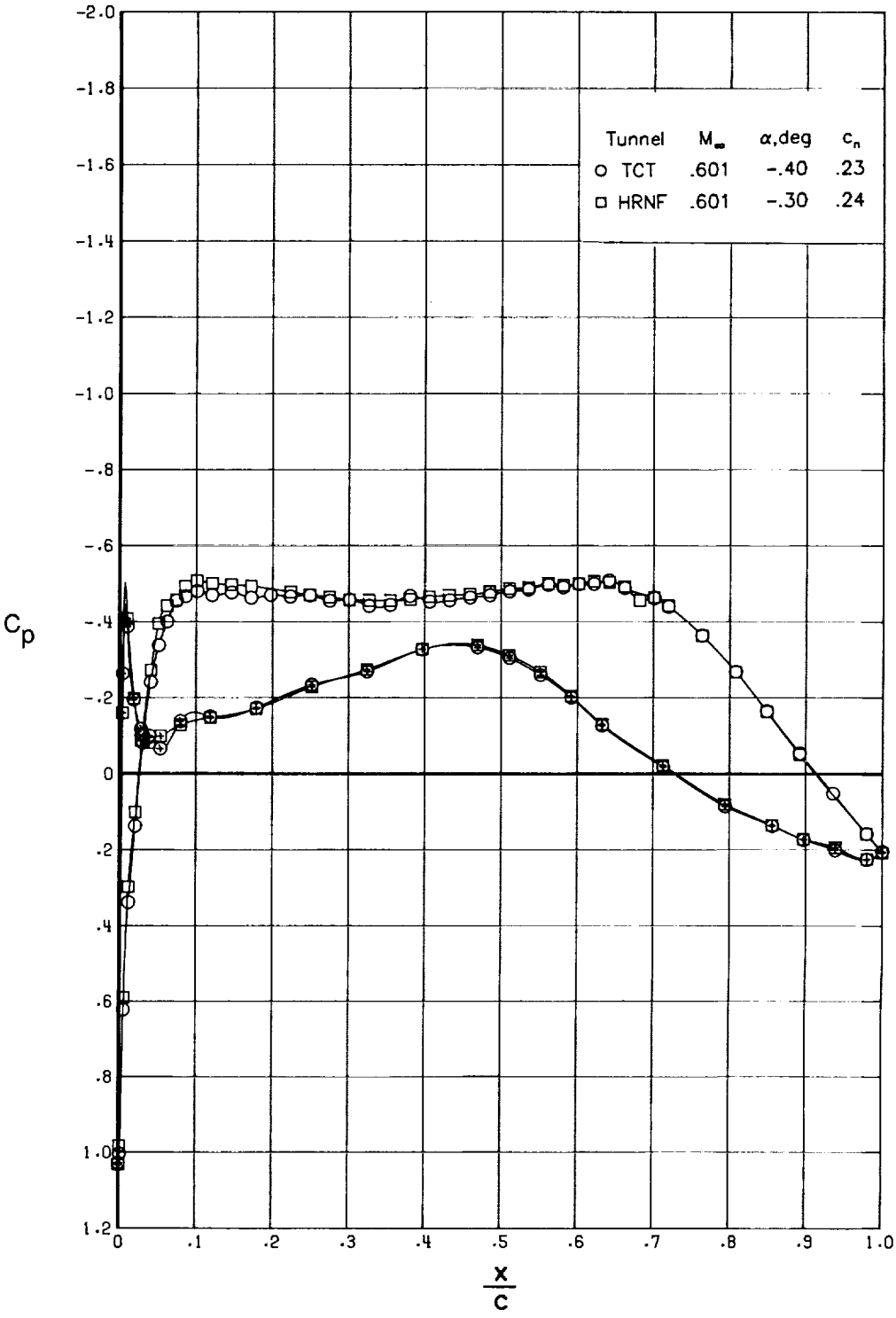

(c) $c_n \approx 0.23$.

Figure 13. Continued.

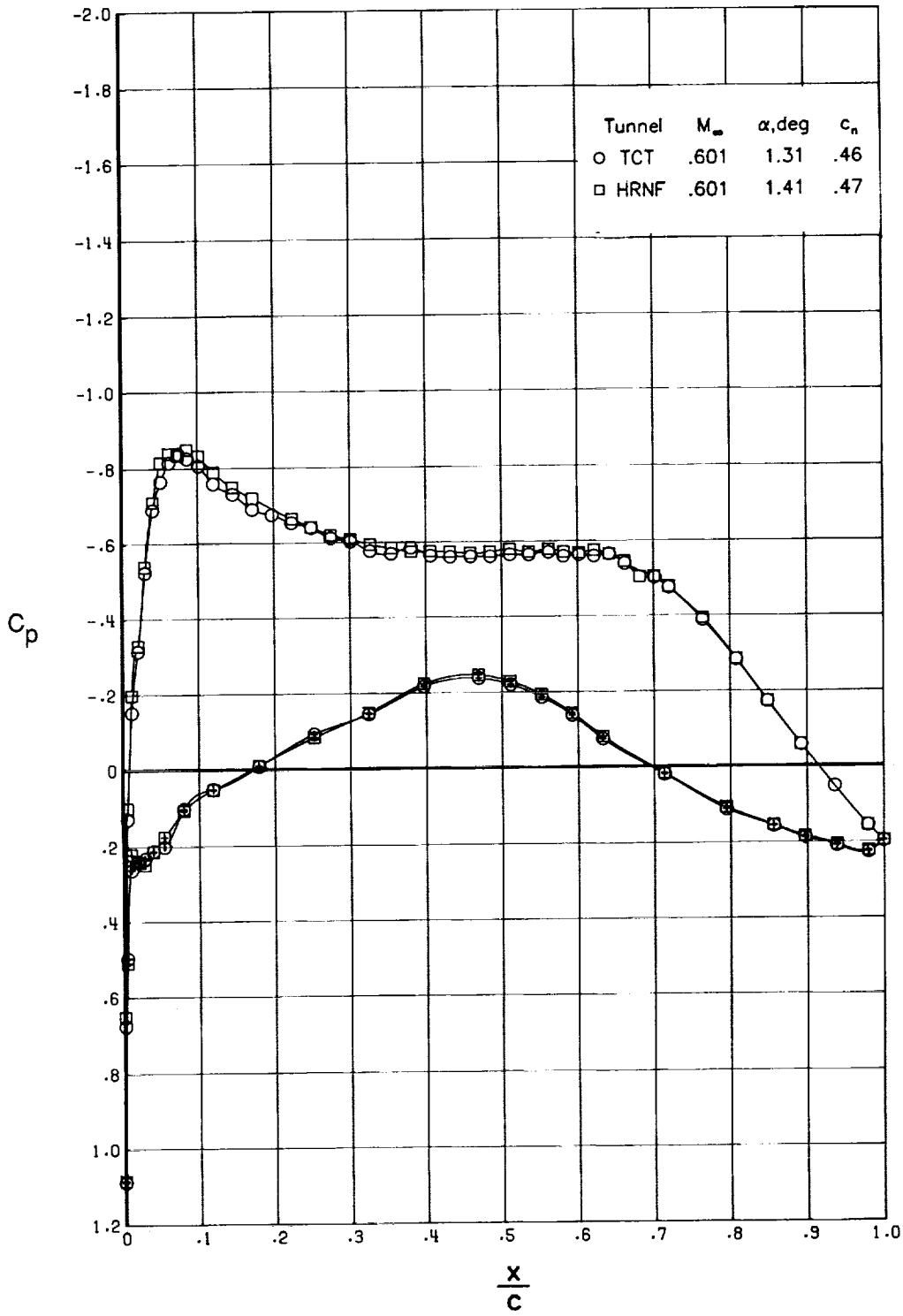

(d) $c_n \approx 0.46$.

Figure 13. Concluded.

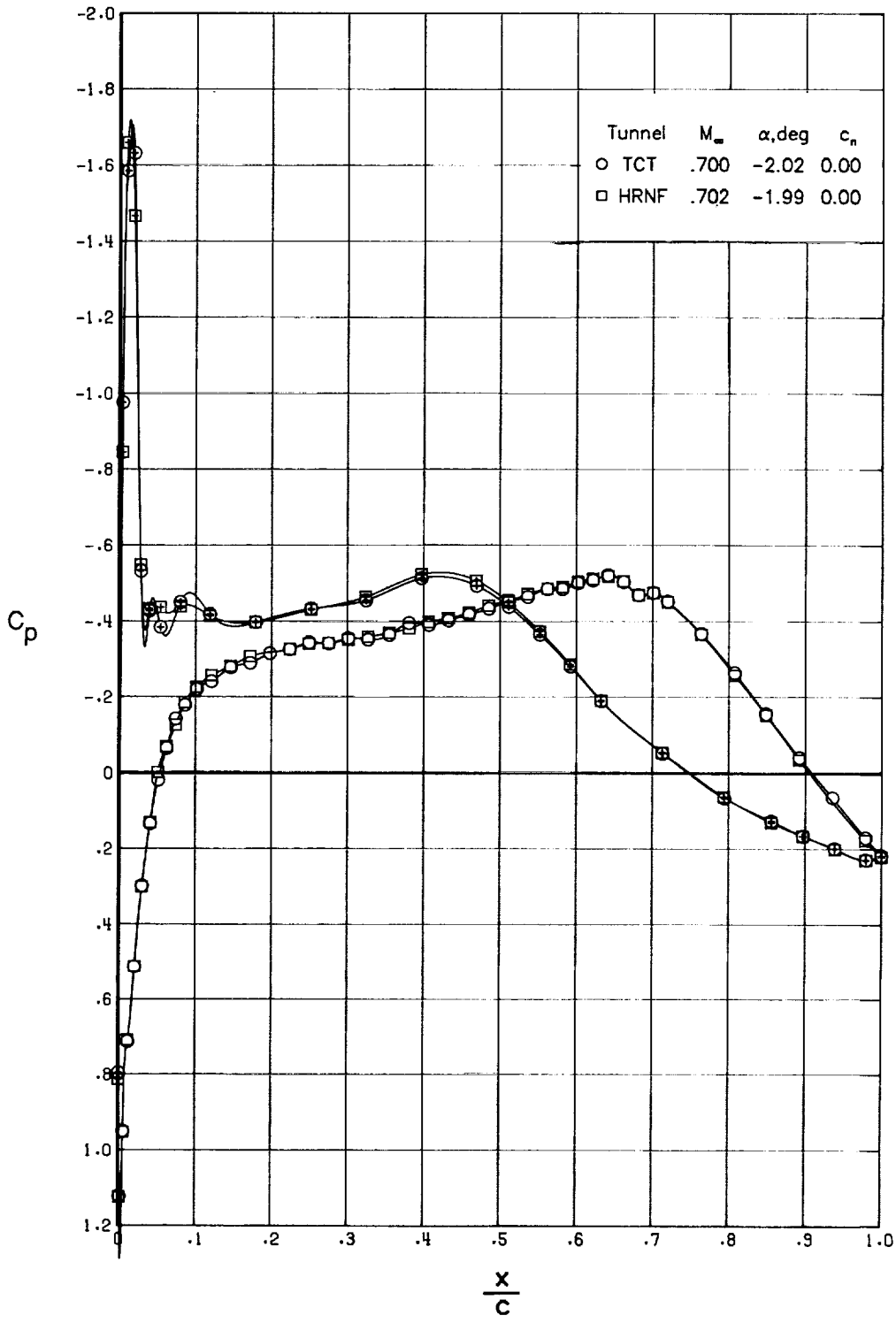

(a) $c_n \approx 0.00$.

Figure 14. Comparison of chordwise pressure distributions for $R_c = 20 \times 10^6$ and $M_\infty = 0.701$.

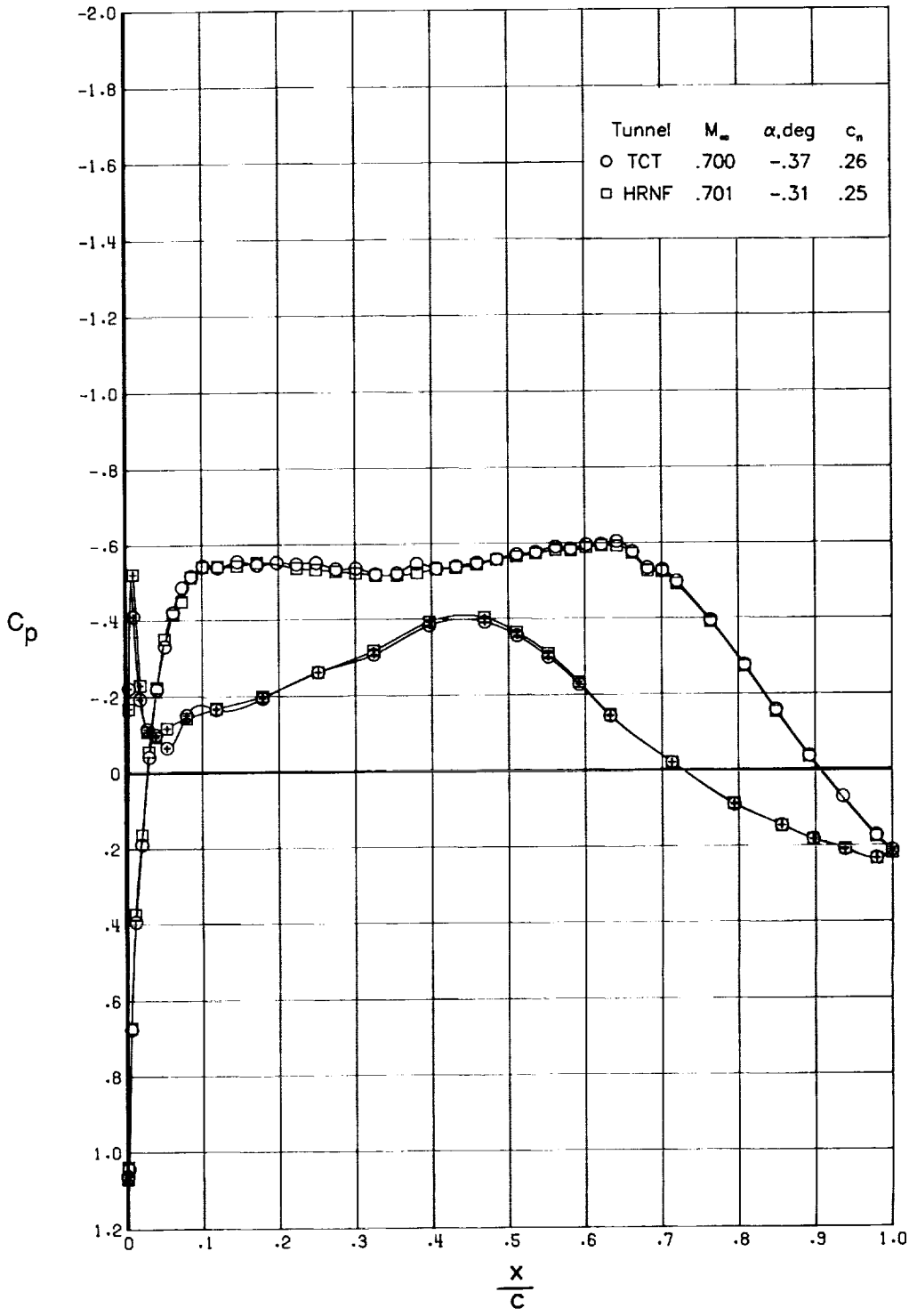

(b) $c_n \approx 0.26$.

Figure 14. Continued.

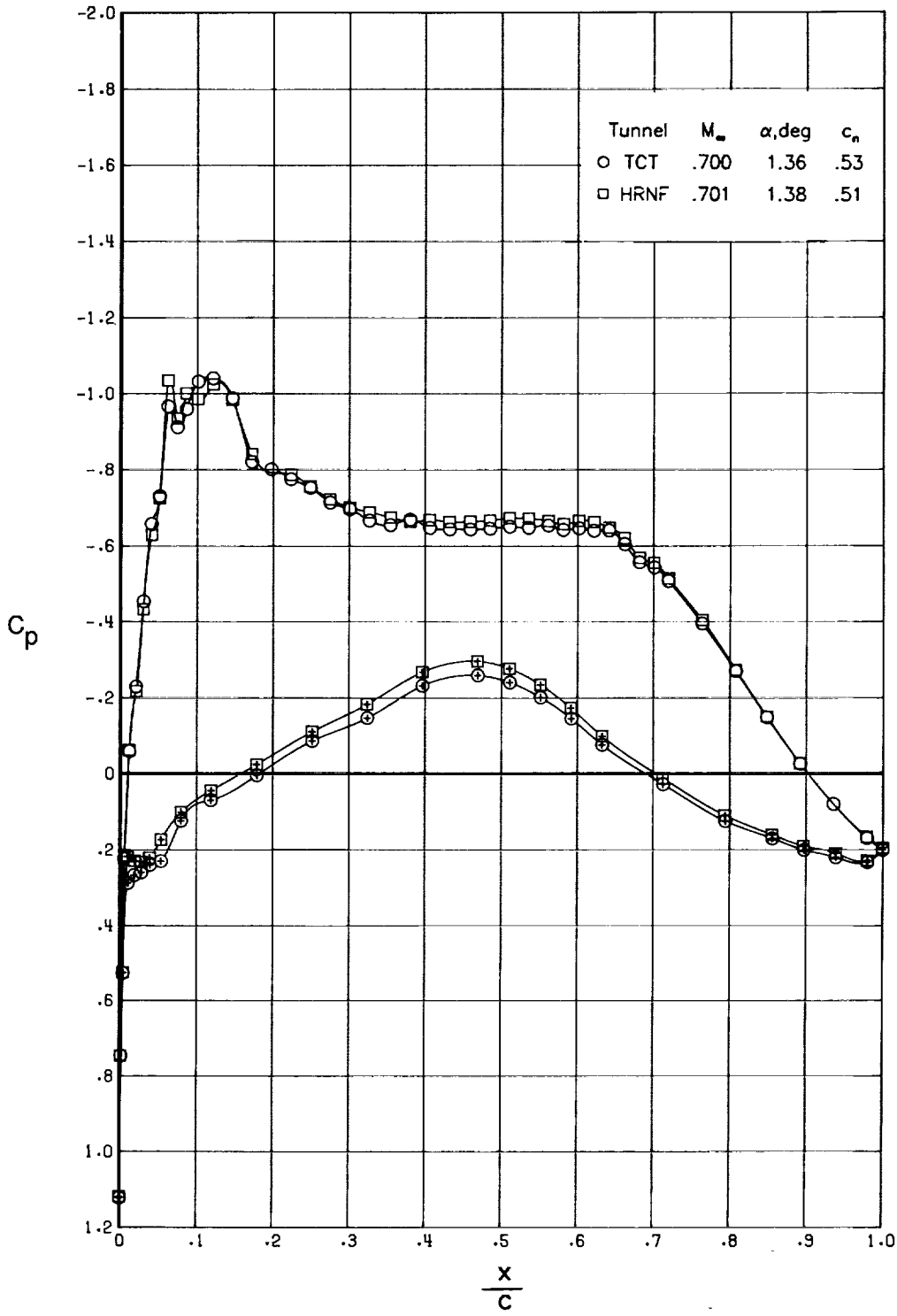

(c) $c_n \approx 0.52$.

Figure 14. Concluded.

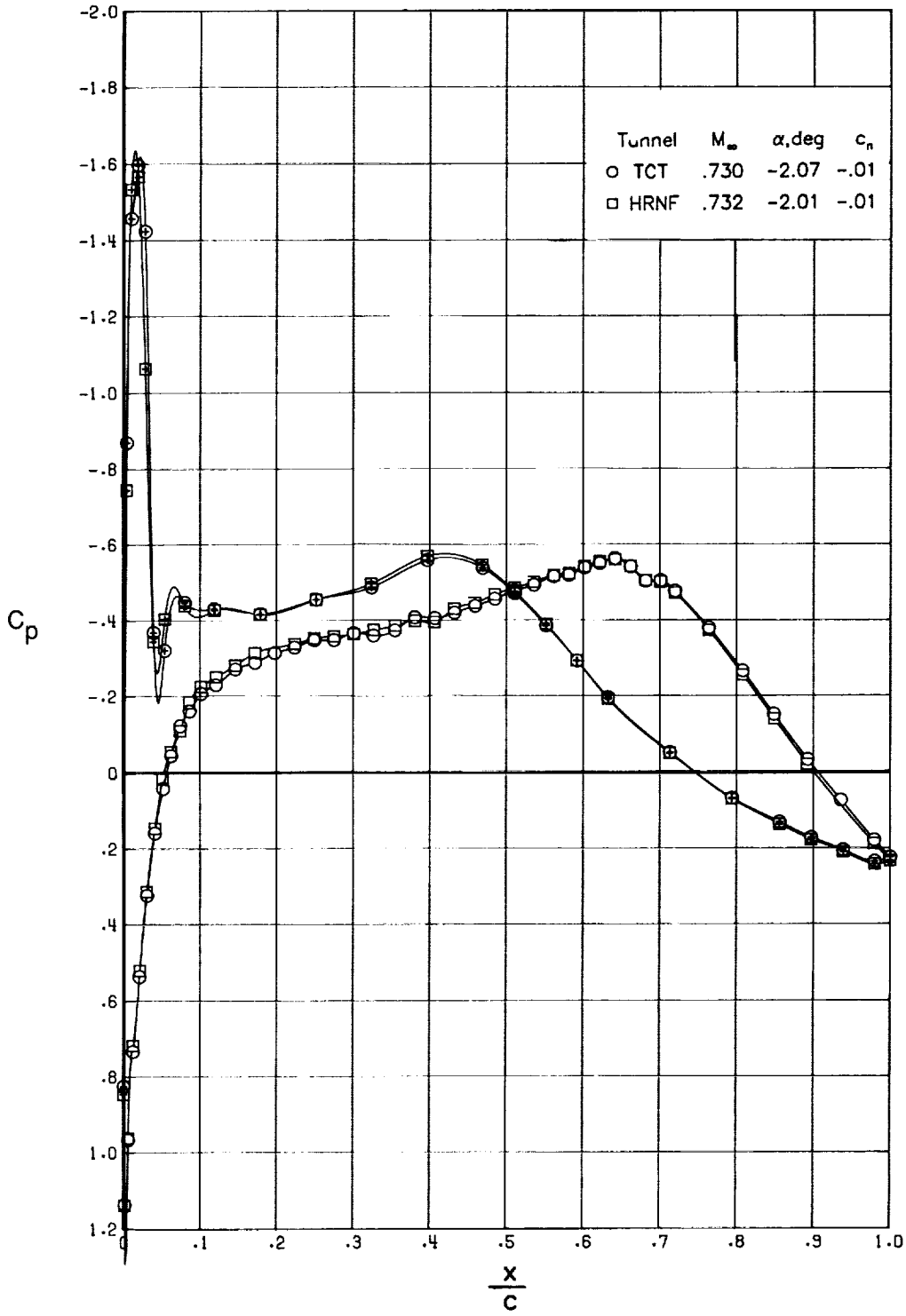

(a) $c_n \approx -0.01$.

Figure 15. Comparison of chordwise pressure distributions for $R_c = 20 \times 10^6$ and $M_\infty = 0.731$.

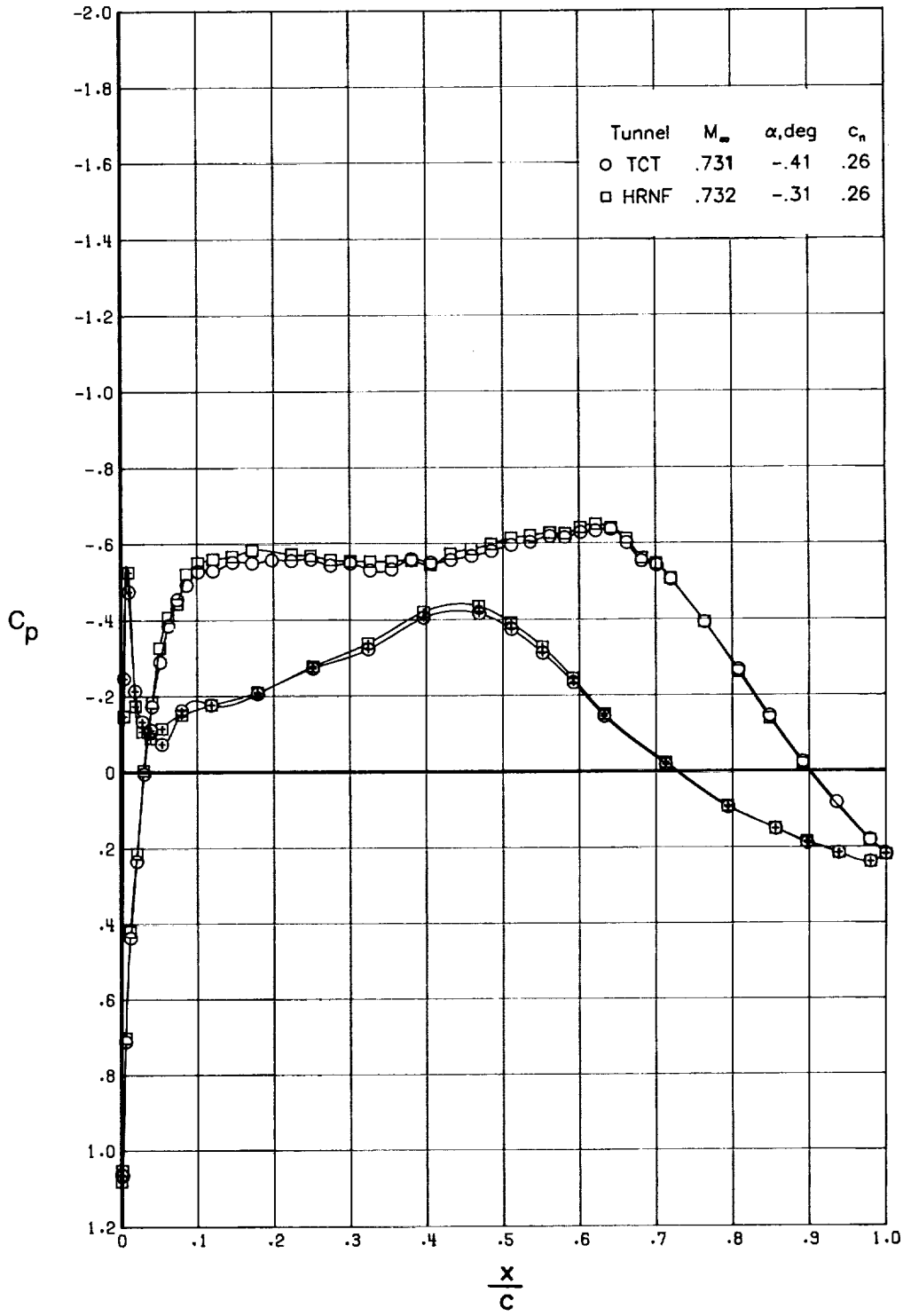

(b) $c_n \approx 0.26$.

Figure 15. Continued.

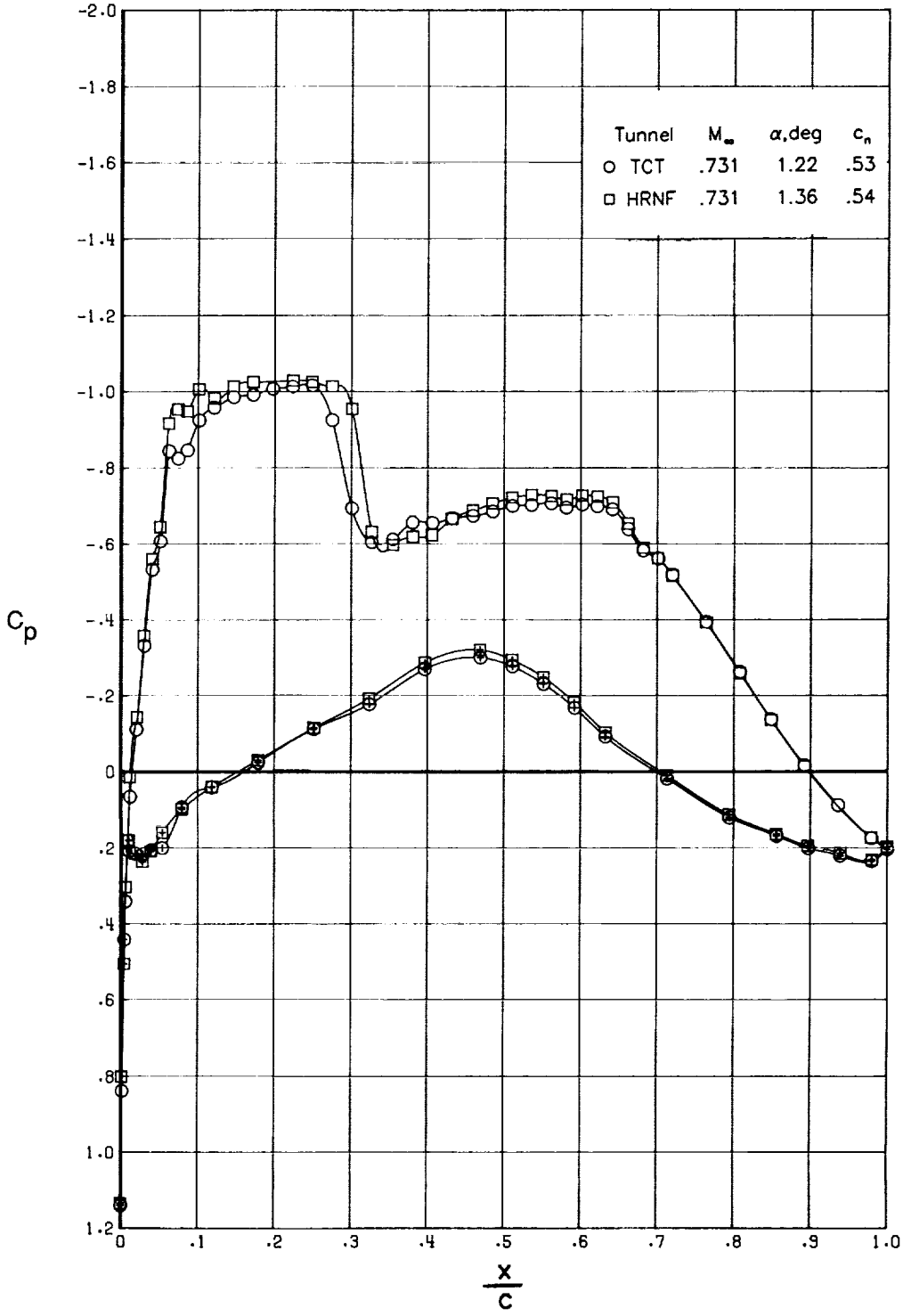

(c) $c_n \approx 0.53$.

Figure 15. Continued.

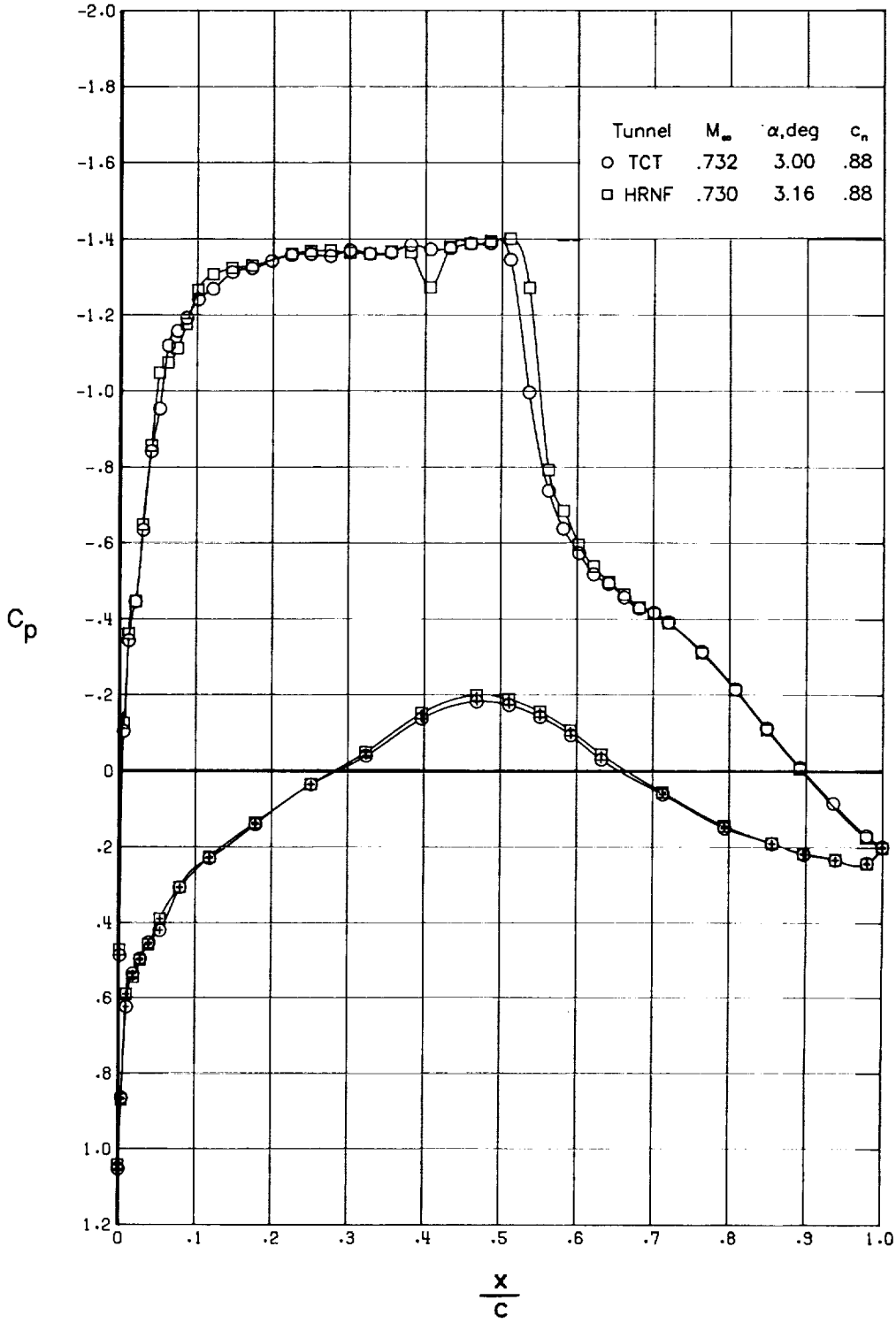

(d) $c_n \approx 0.88$.

Figure 15. Concluded.

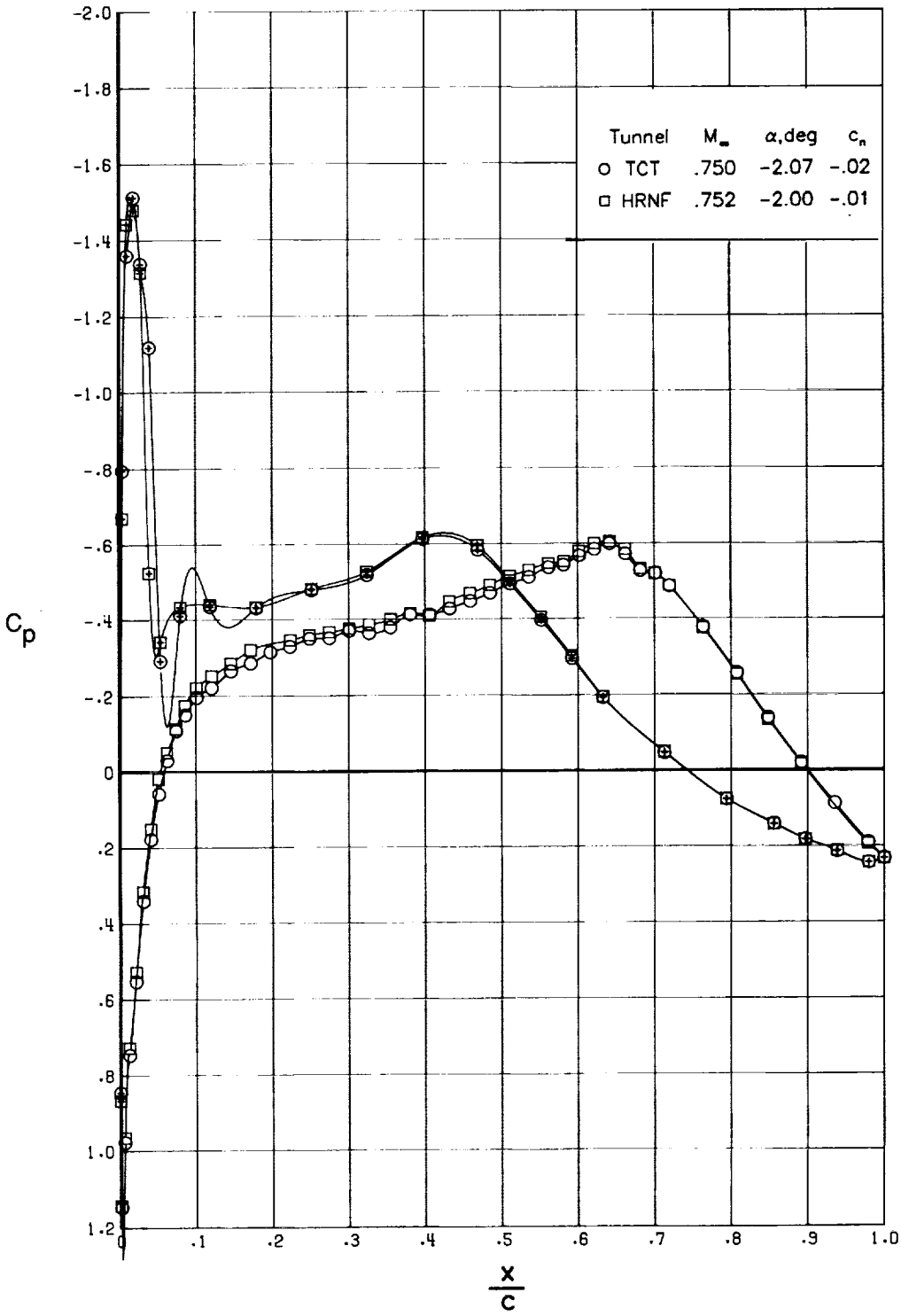

(a) $c_n \approx -0.02$.

Figure 16. Comparison of chordwise pressure distributions for $R_c = 20 \times 10^6$ and $M_\infty = 0.751$.

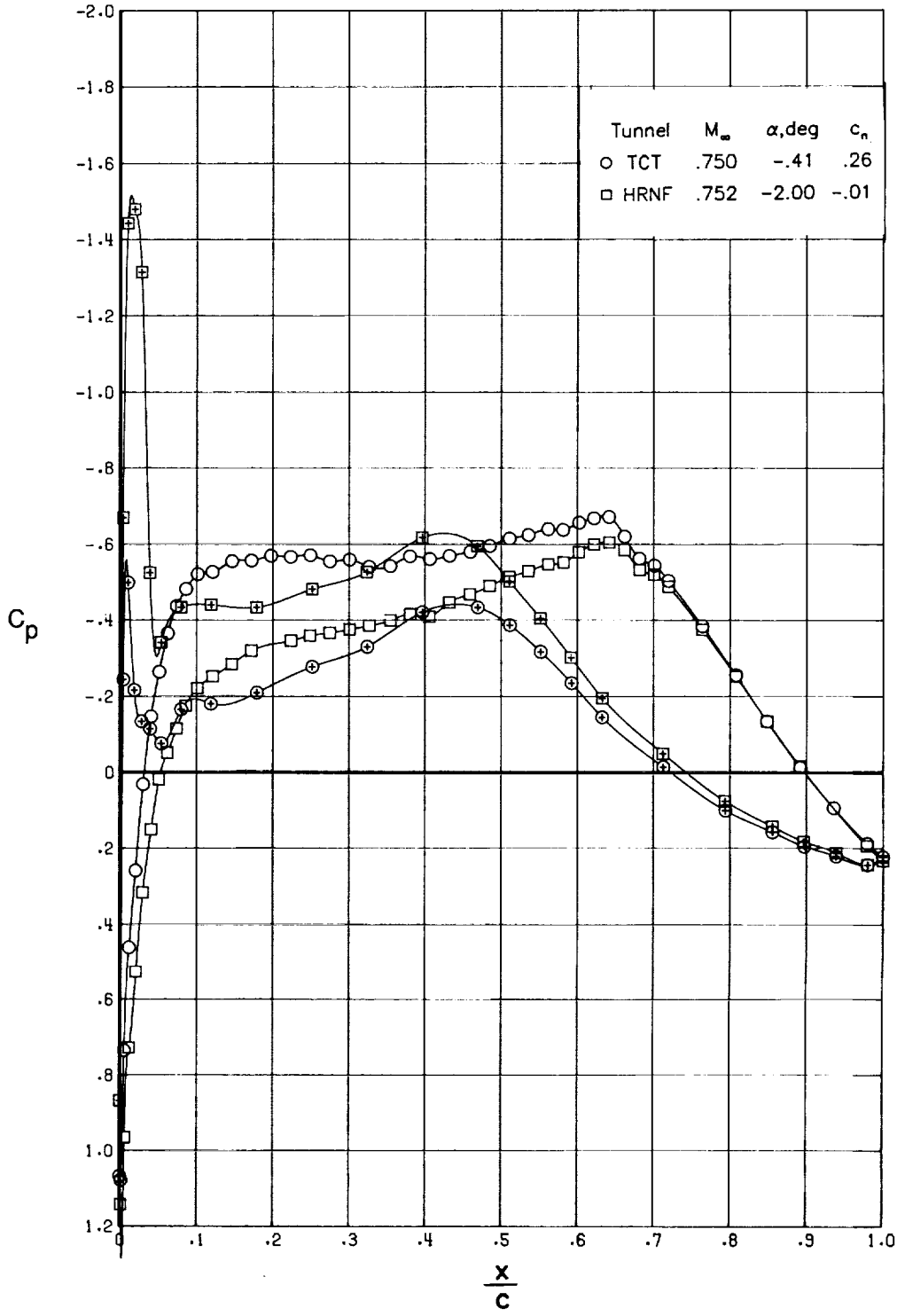

(b) $c_n \approx 0.12$.

Figure 16. Continued.

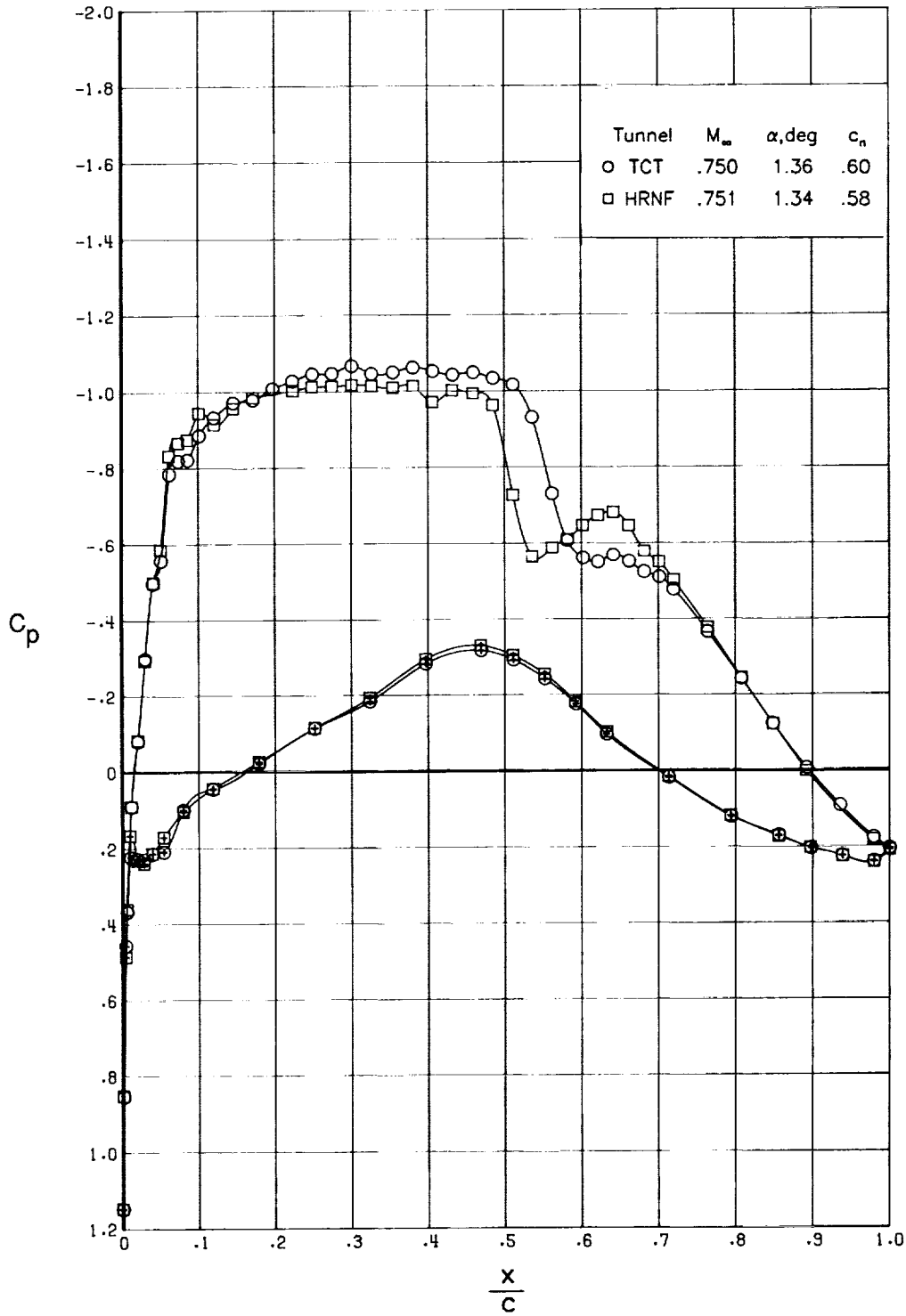

(c) $c_n \approx 0.59$.

Figure 16. Continued.

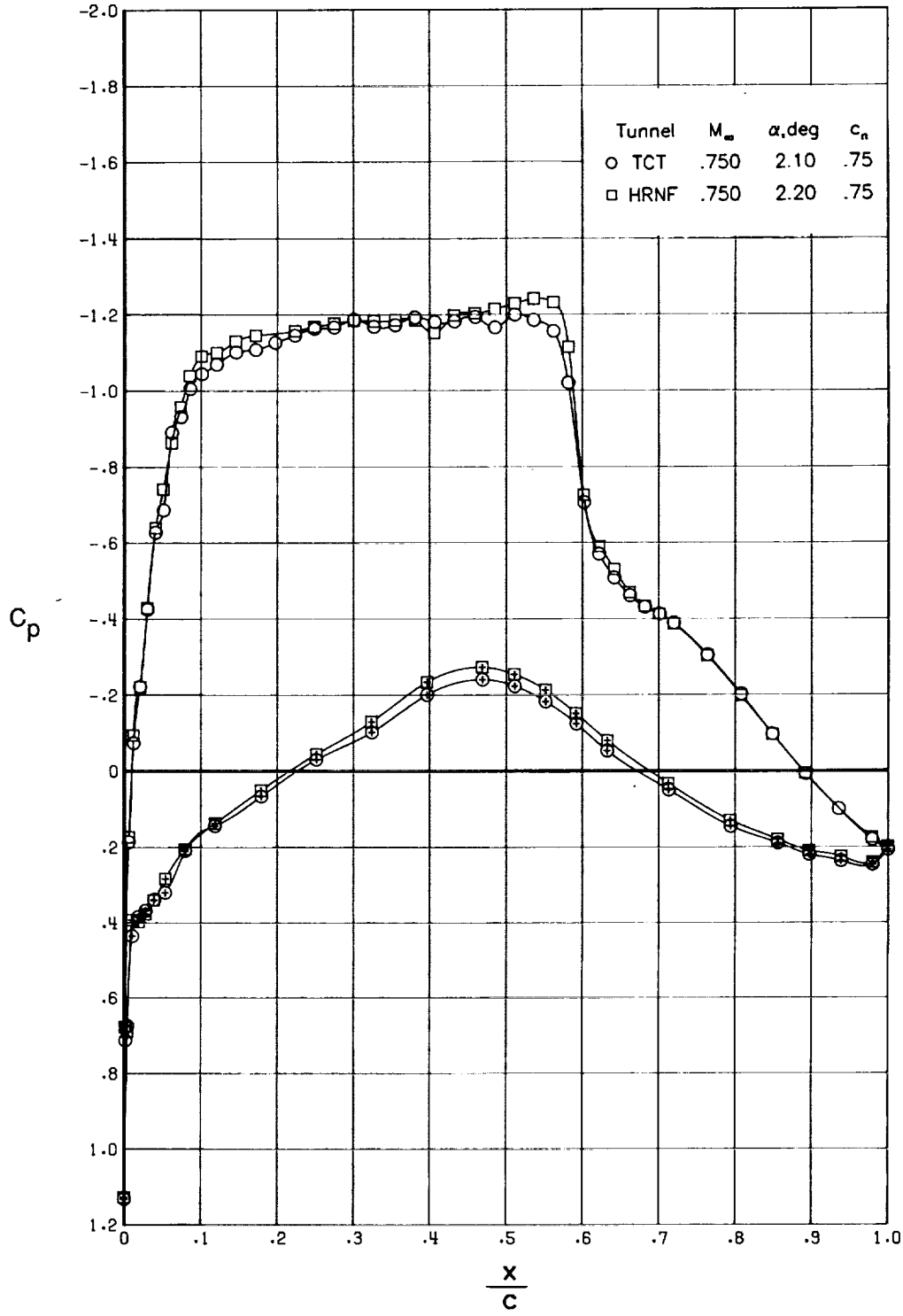

(d) $c_n \approx 0.75$.

Figure 16. Concluded.

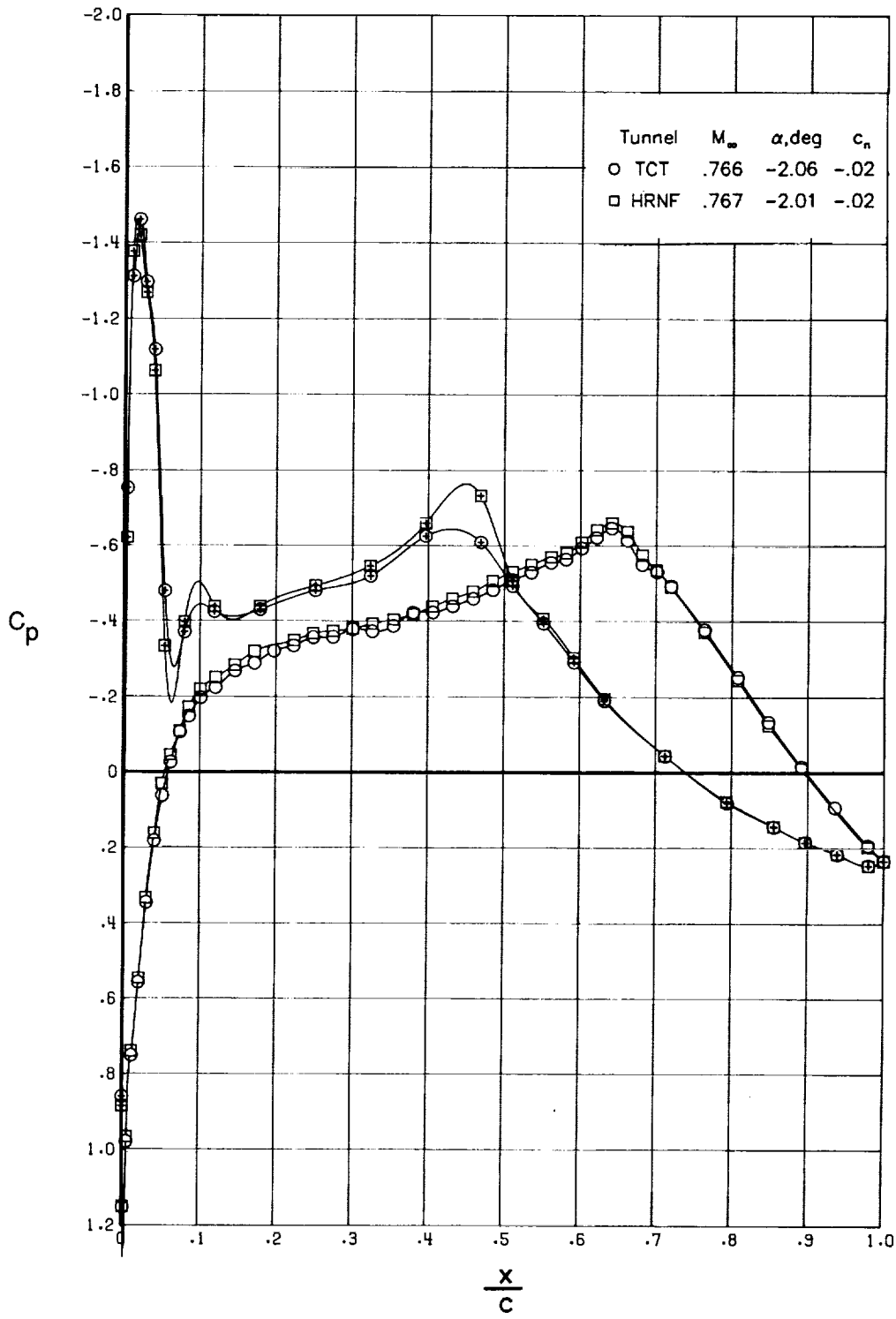

(a) $c_n \approx -0.02$.

Figure 17. Comparison of chordwise pressure distributions for $R_c = 20 \times 10^6$ and $M_\infty = 0.766$.

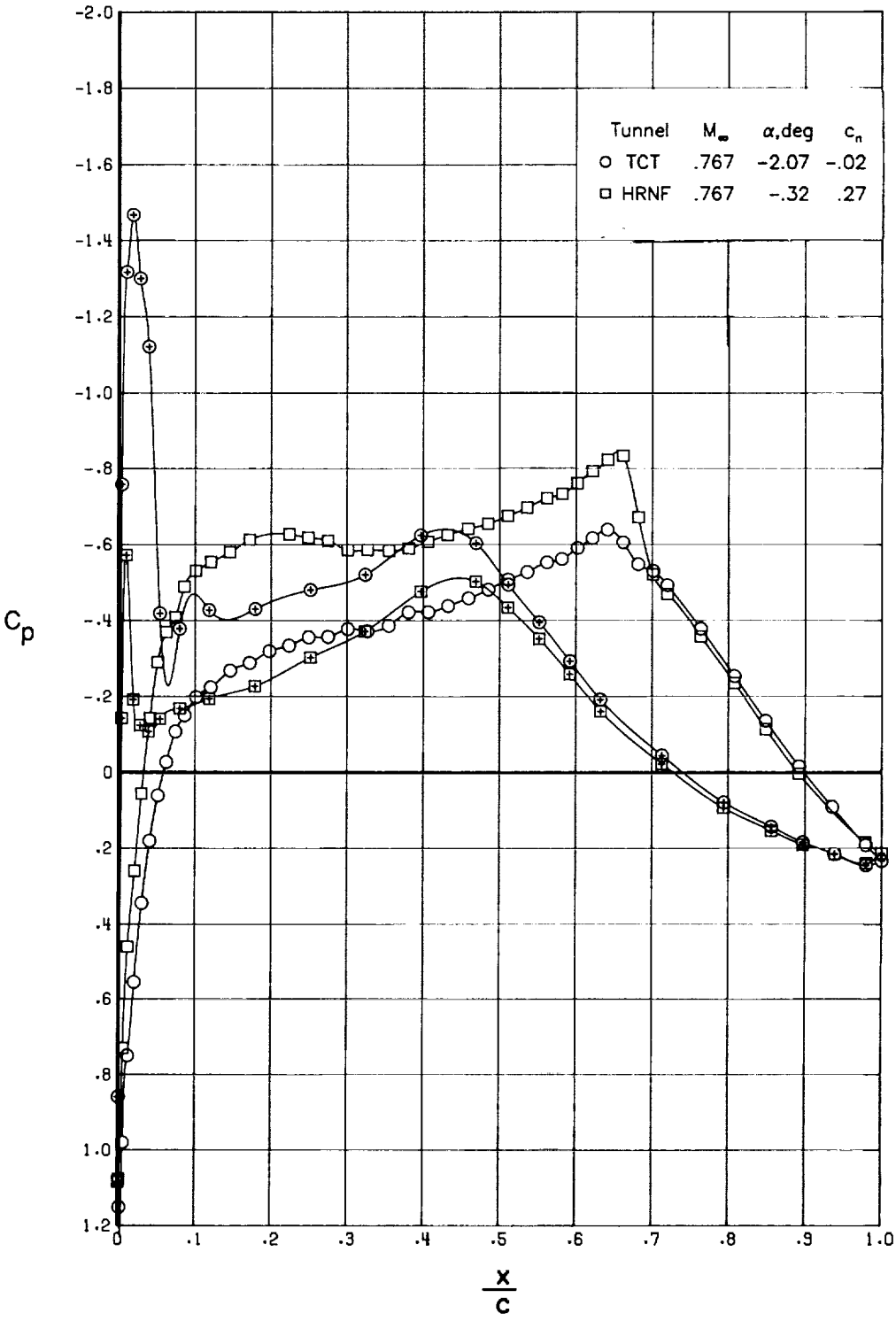

(b) $c_n \approx 0.12$.

Figure 17. Continued.

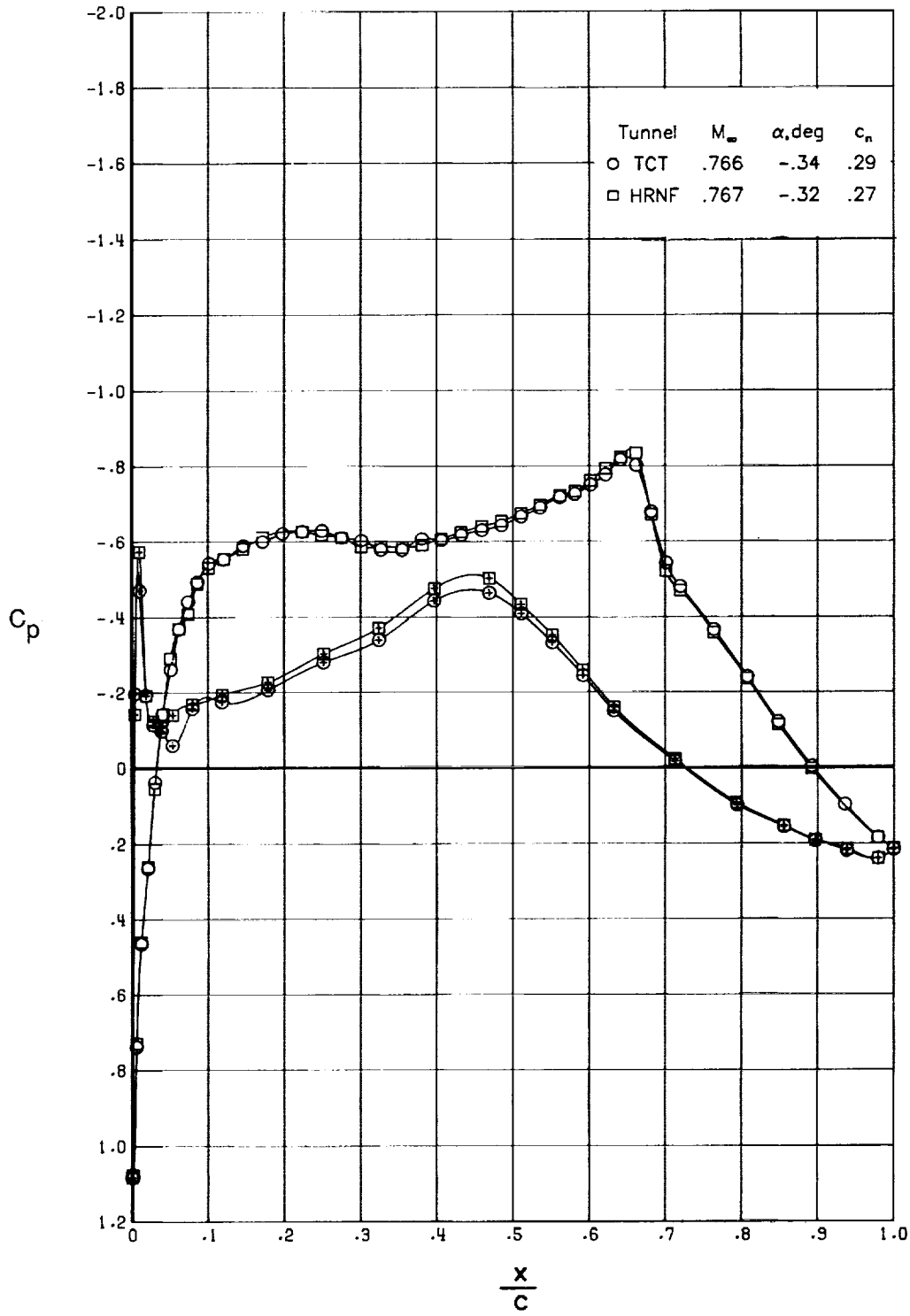

(c) $c_n \approx 0.28$.

Figure 17. Continued.

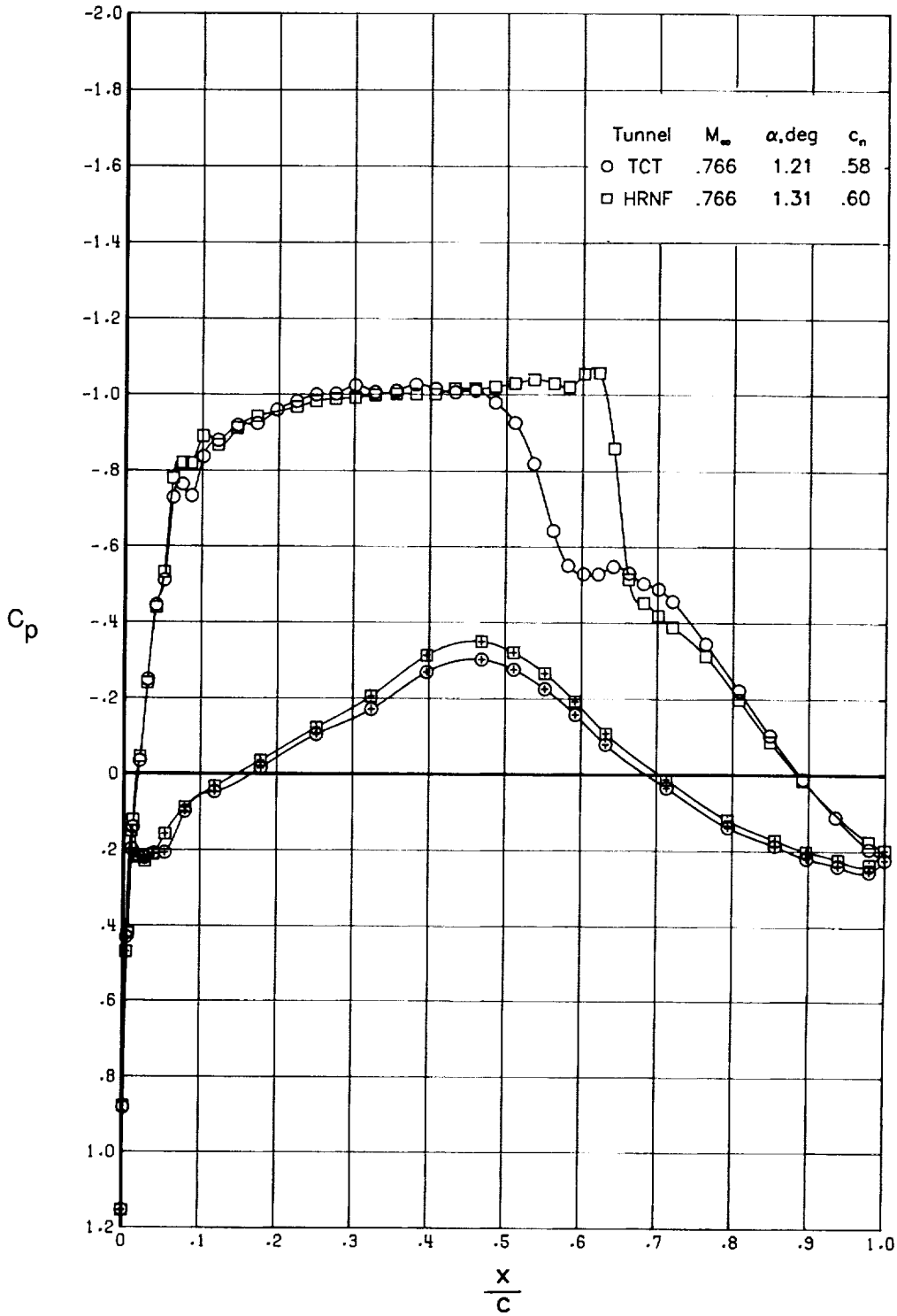

(d) $c_n \approx 0.59$.

Figure 17. Continued.

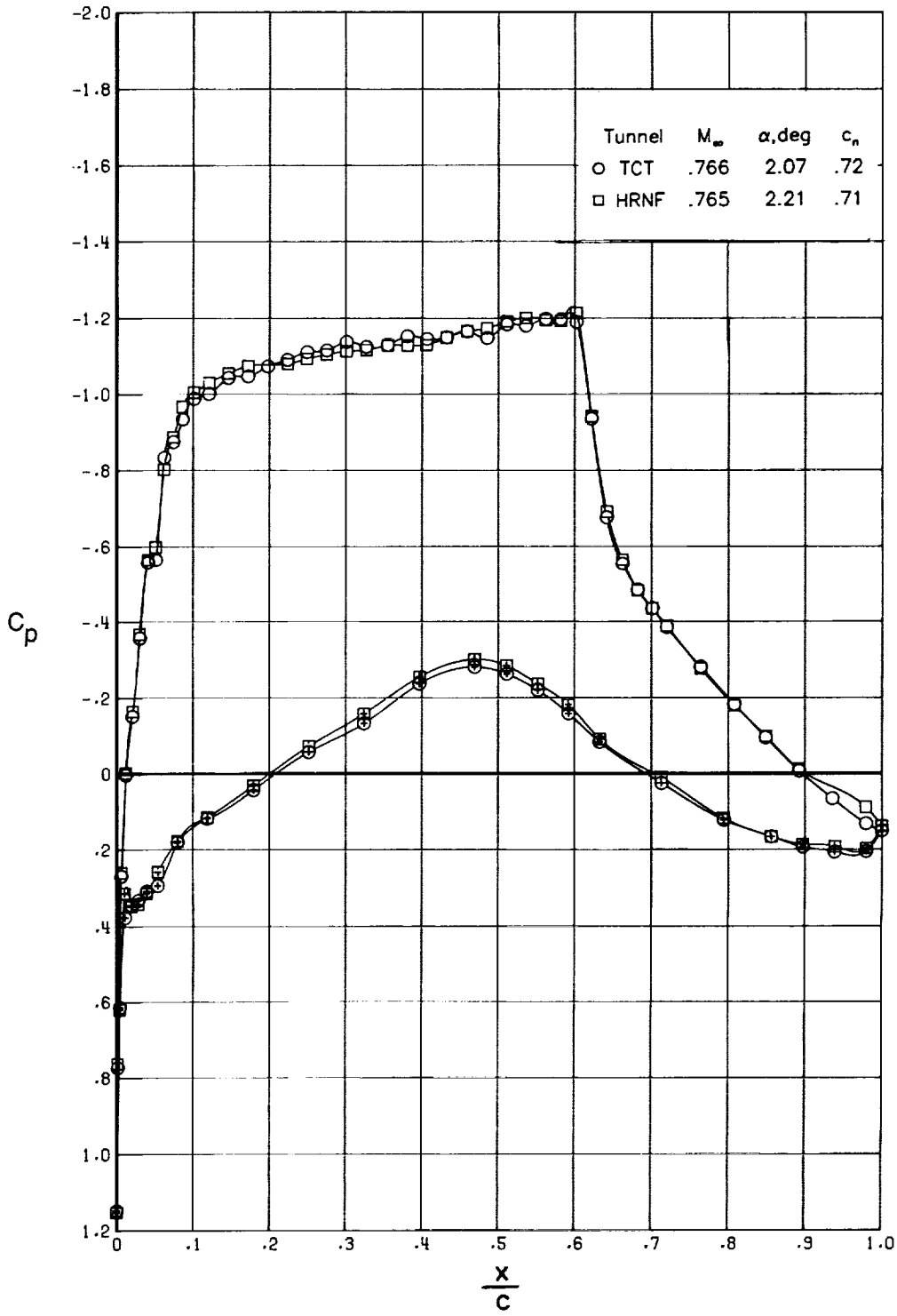

(e) $c_n \approx 0.72$.

Figure 17. Concluded.

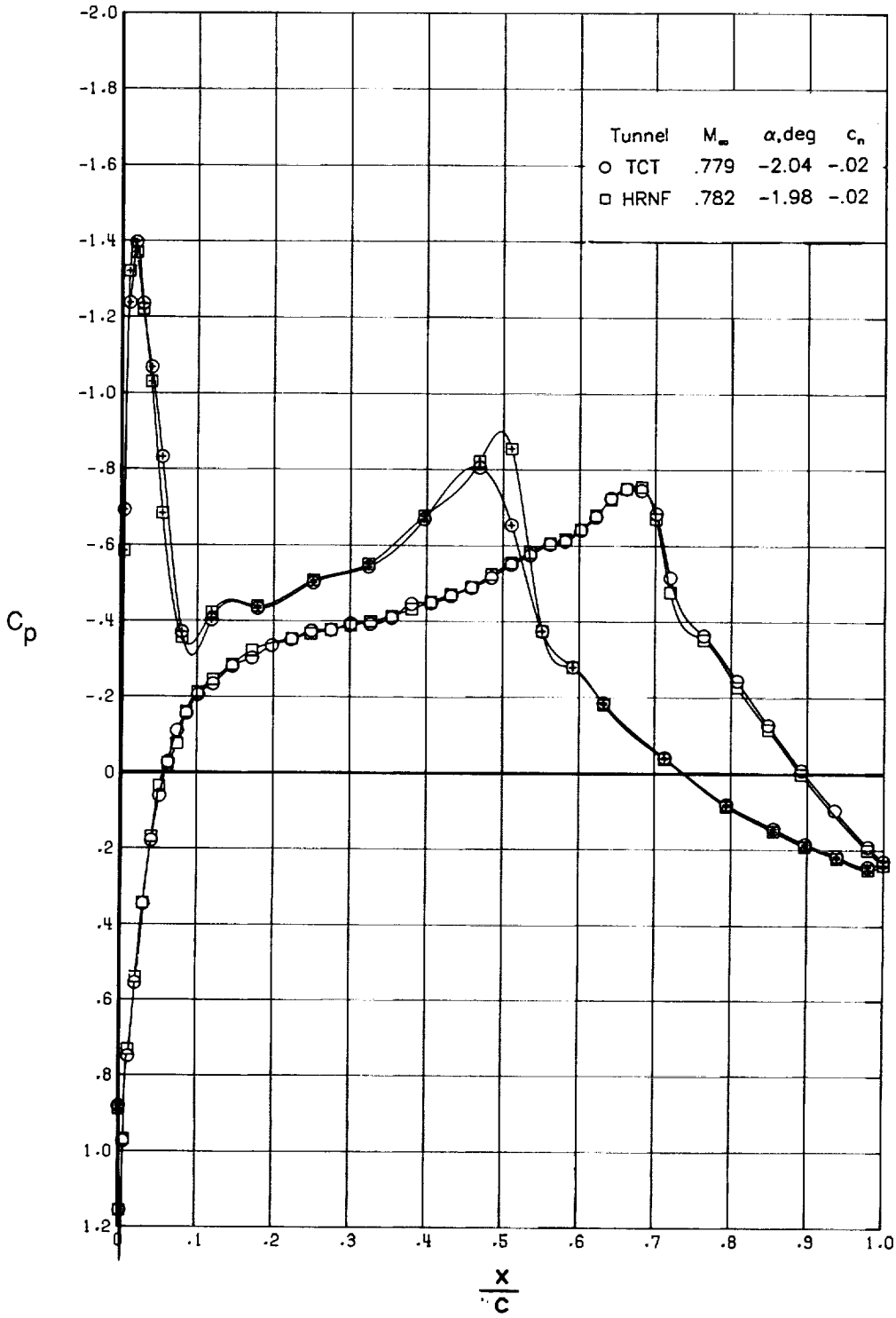

(a) $c_n \approx -0.02$.

Figure 18. Comparison of chordwise pressure distributions for $R_c = 20 \times 10^6$ and $M_\infty = 0.780$.

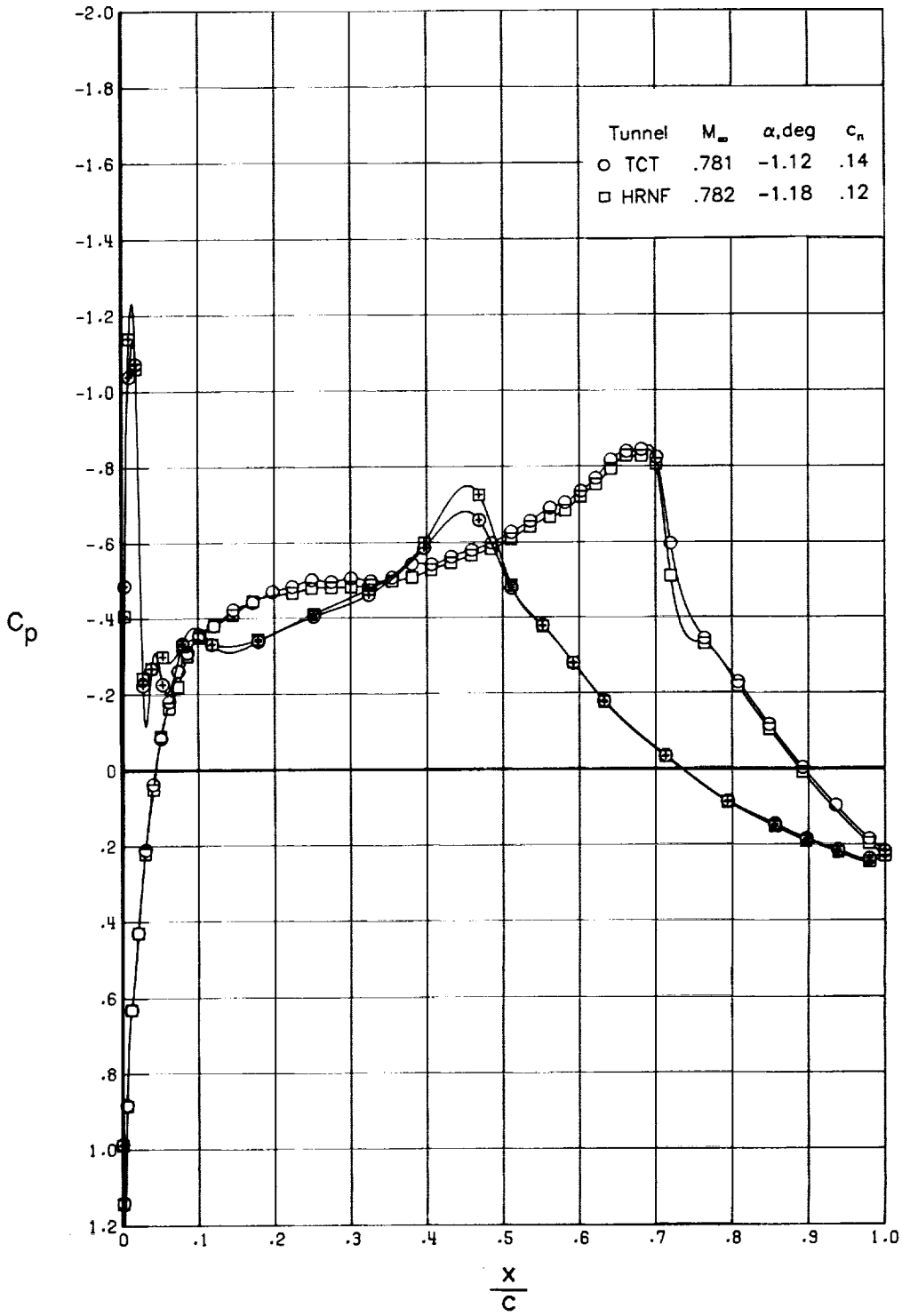

(b) $c_n \approx 0.13$.

Figure 18. Continued.

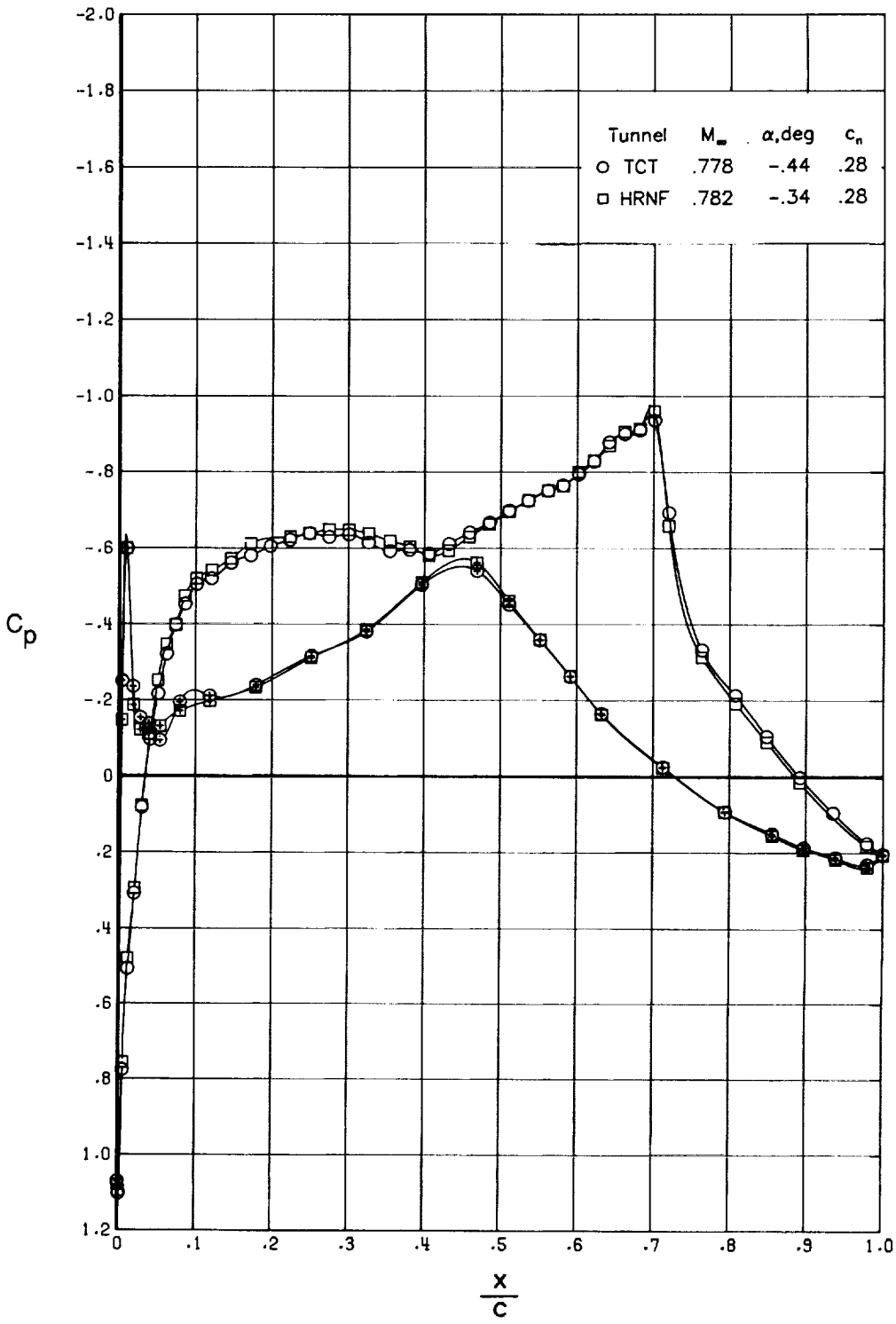

(c) $c_n \approx 0.28$.

Figure 18. Continued.

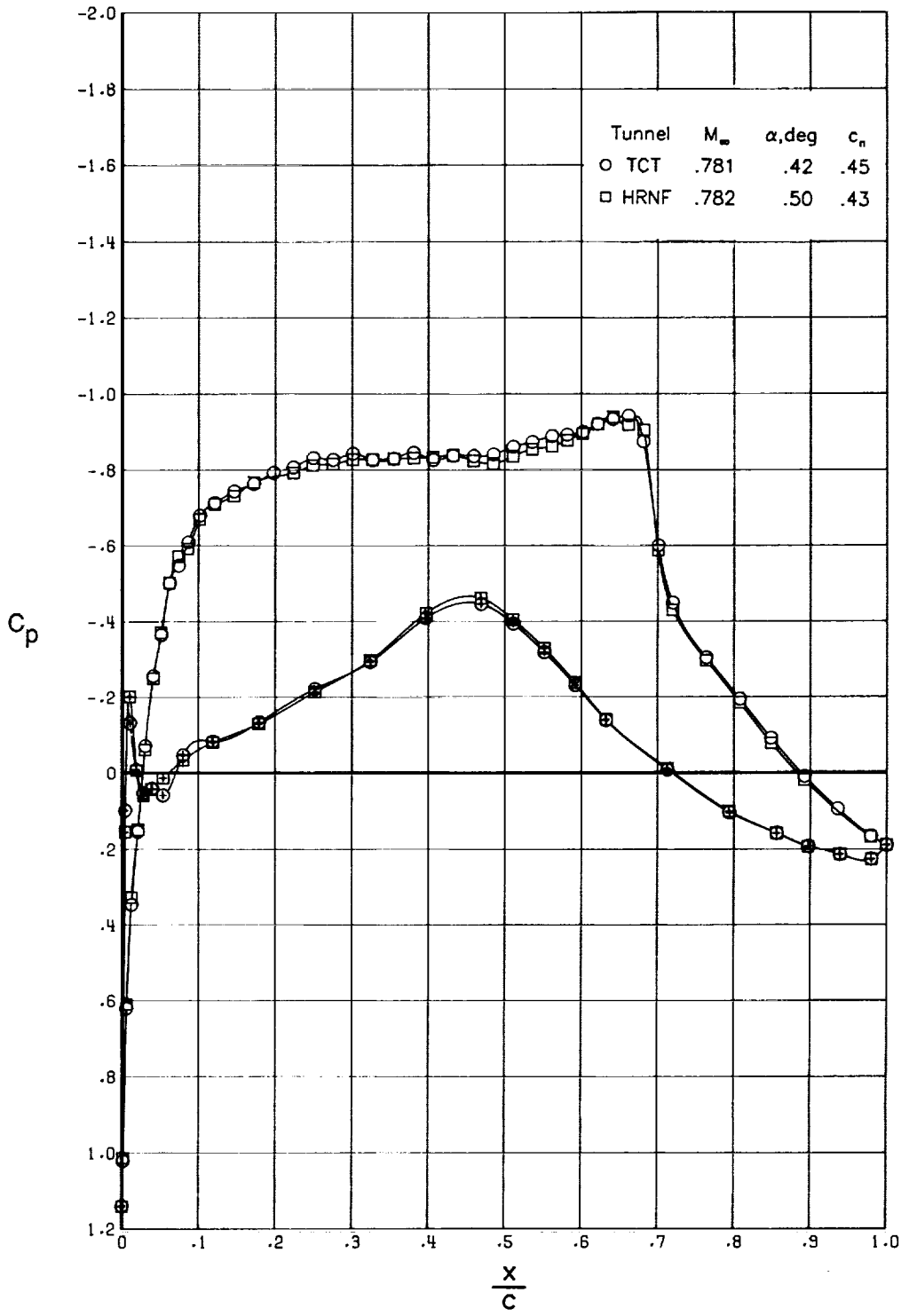

(d) $c_n \approx 0.44$.

Figure 18. Continued.

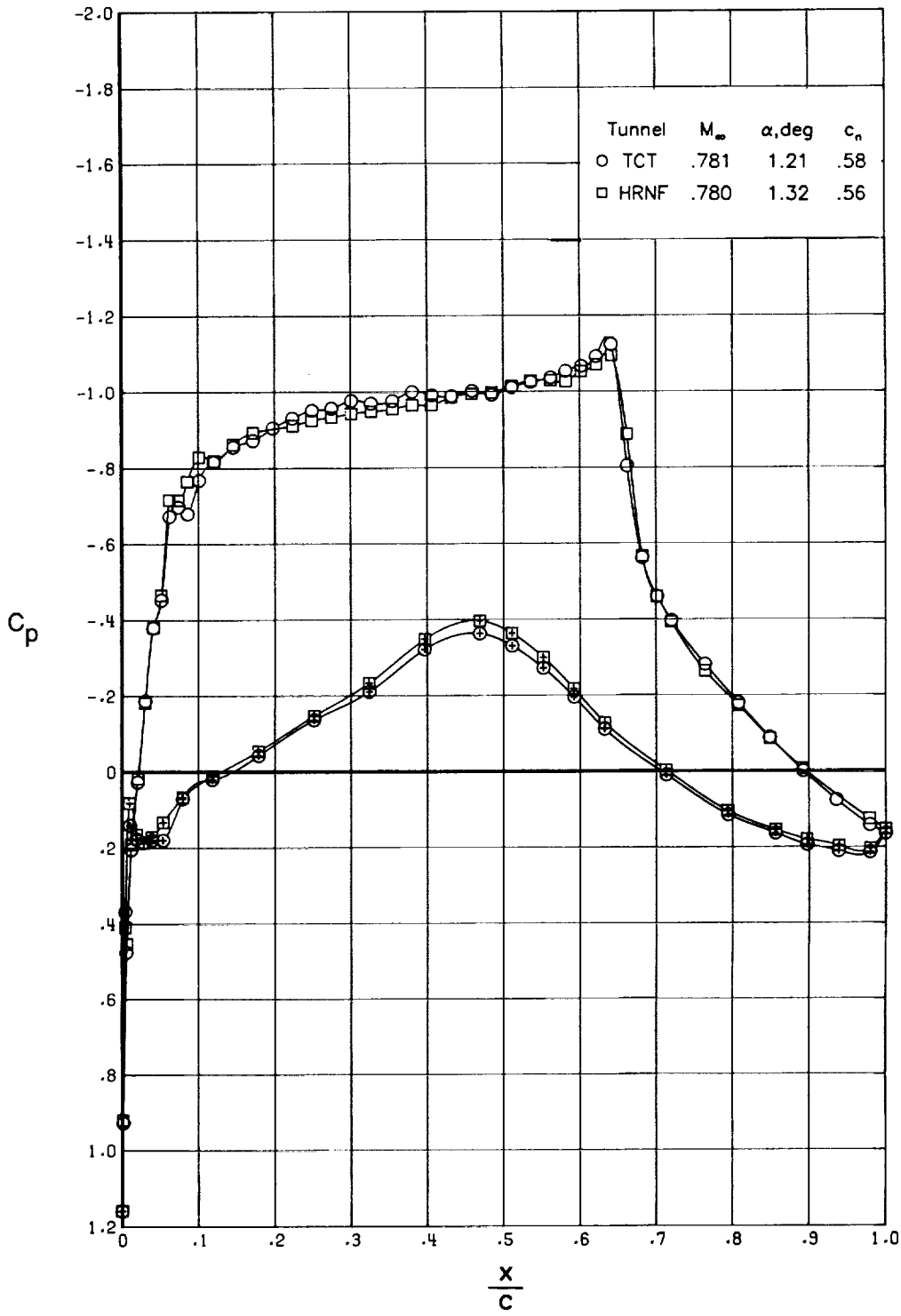

(e) $c_n \approx 0.57$.

Figure 18. Continued.

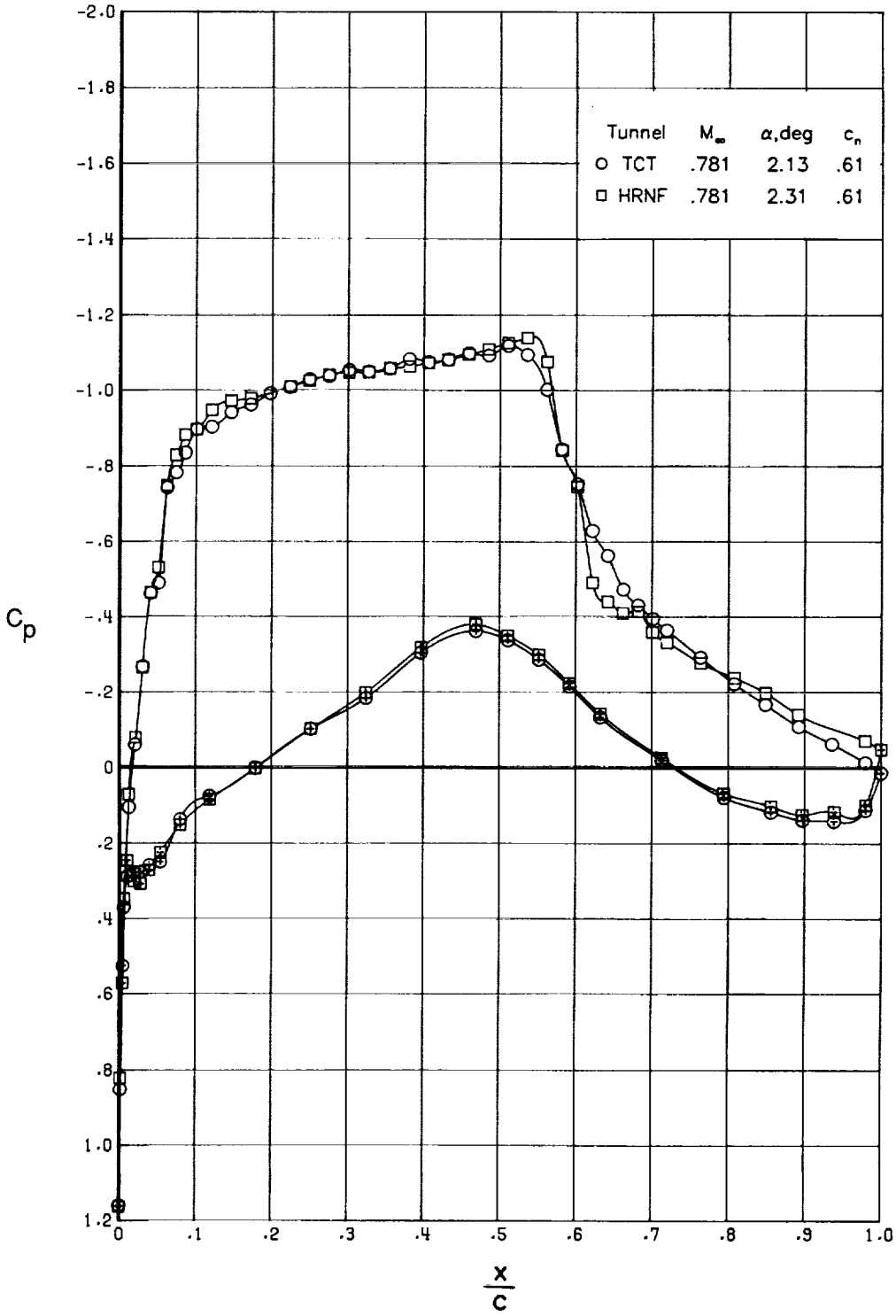

(f) $c_n \approx 0.61$.

Figure 18. Concluded.

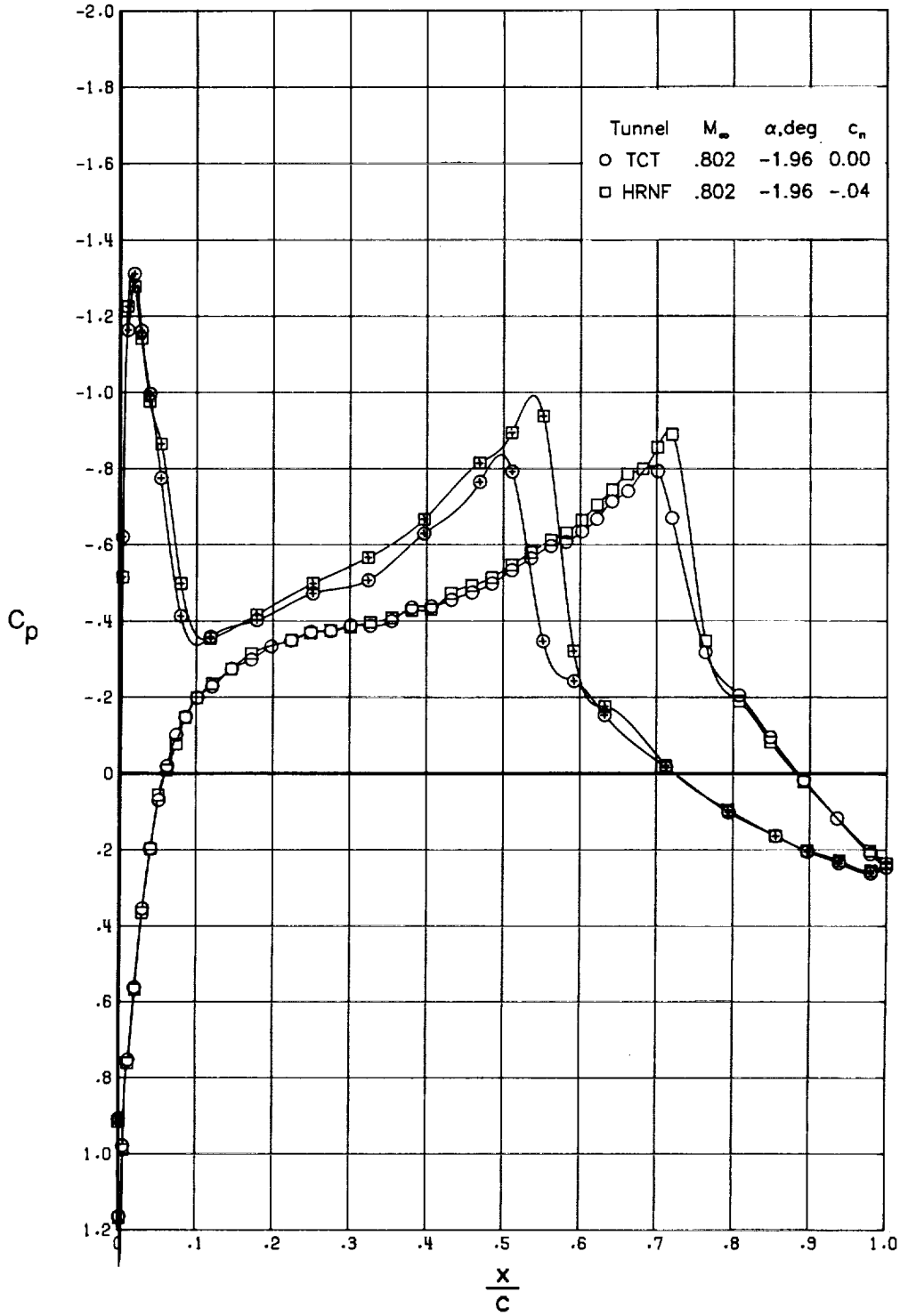

(a) $c_n \approx -0.02$.

Figure 19. Comparison of chordwise pressure distributions for $R_c = 20 \times 10^6$ and $M_\infty = 0.802$.

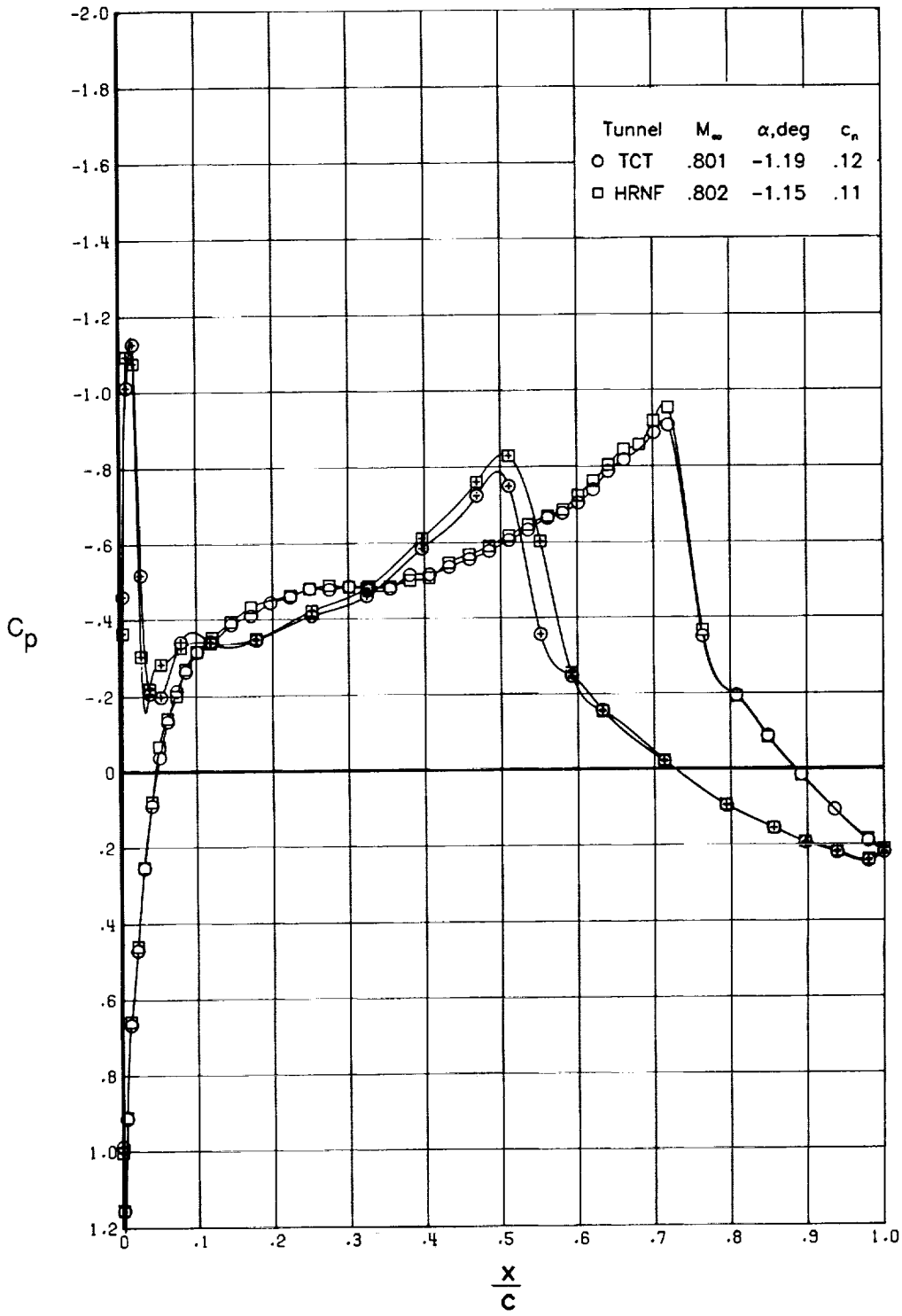

(b) $c_n \approx 0.11$.

Figure 19. Continued.

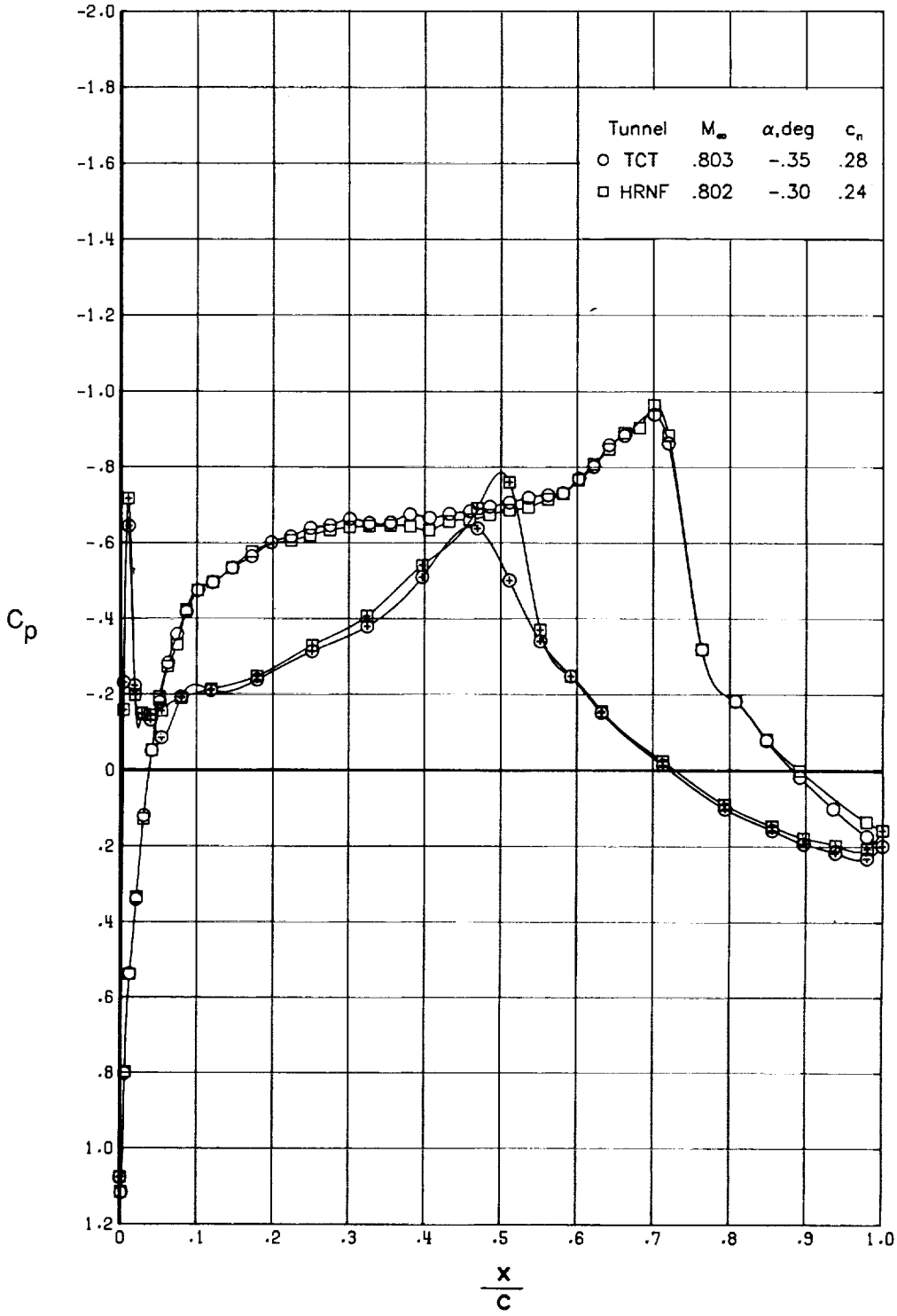

(c) $c_n \approx 0.26$.

Figure 19. Continued.

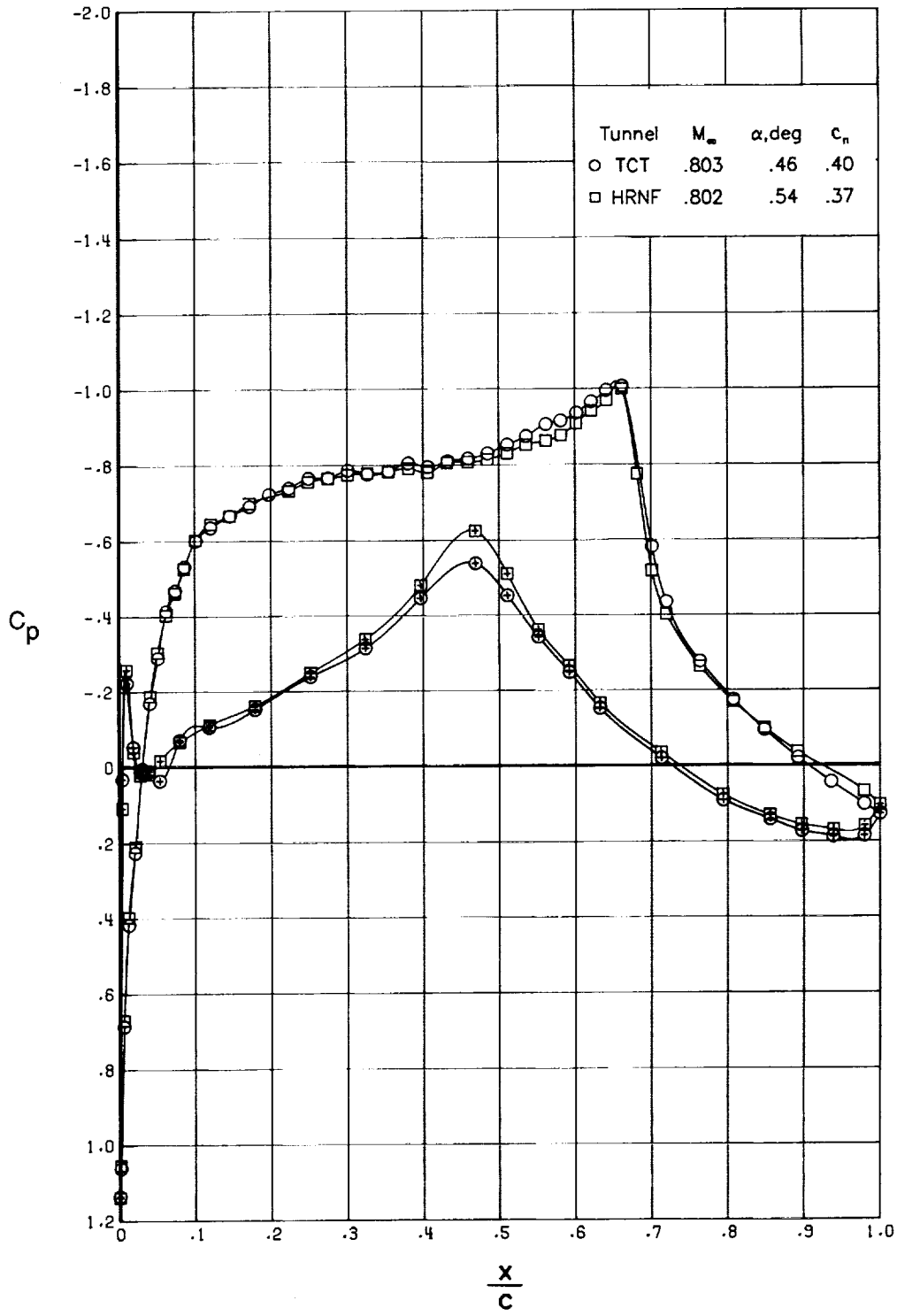

(d) $c_n \approx 0.38$.

Figure 19. Continued.

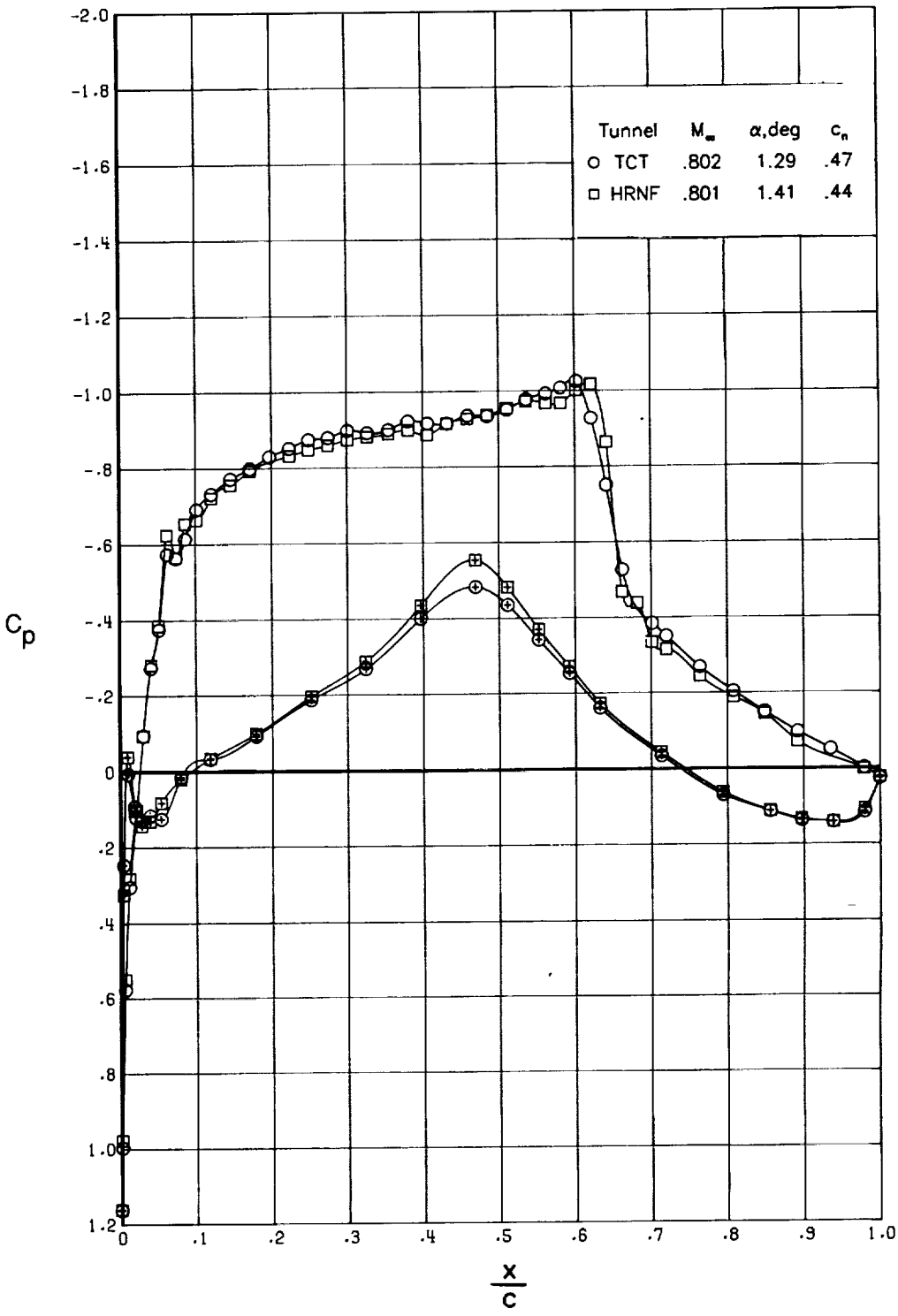

(e) $c_n \approx 0.46$.

Figure 19. Continued.

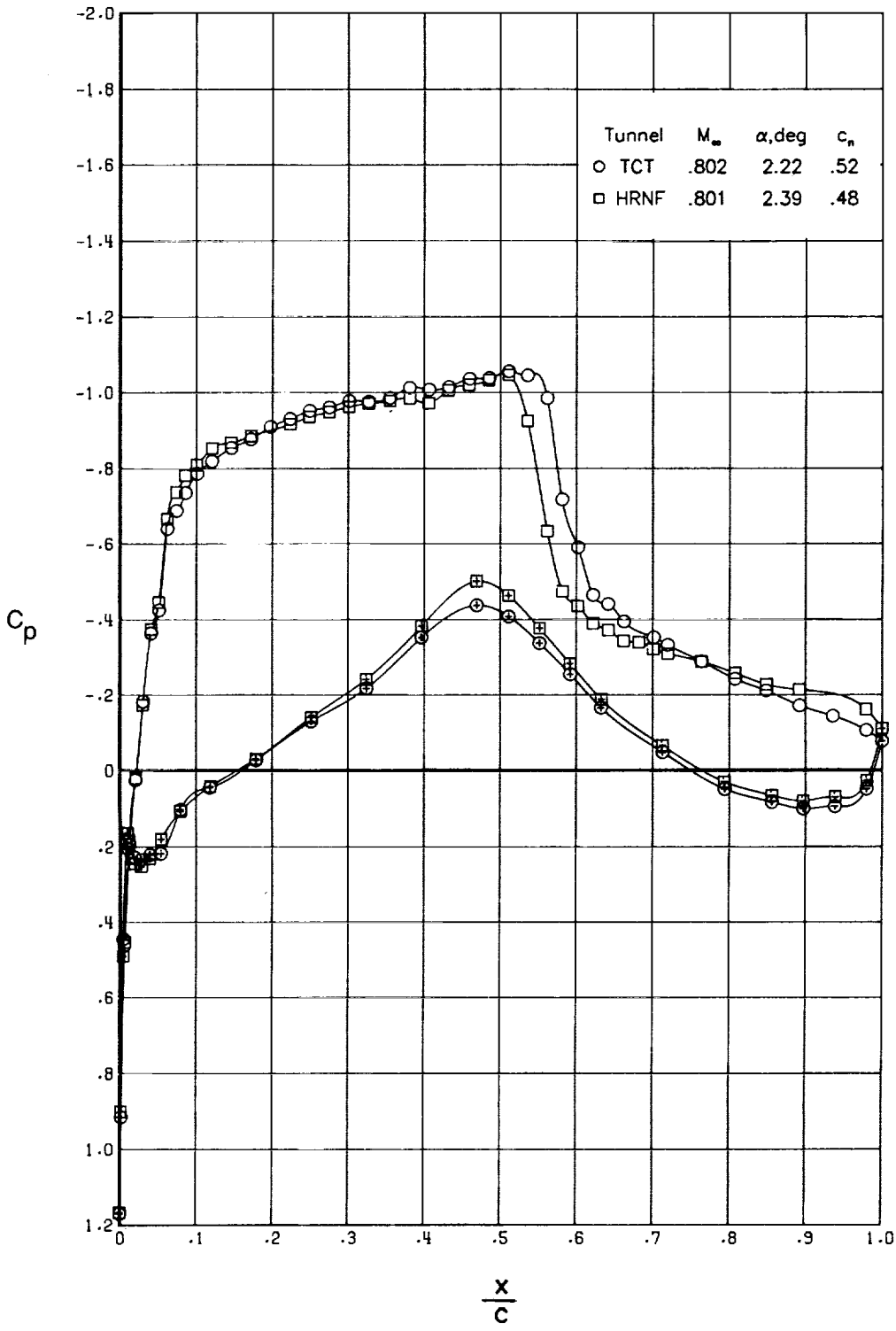

(f) $c_n \approx 0.50$.

Figure 19. Concluded.